ADVANCES IN CLASSICAL AND QUANTUM WAVE DYNAMICS ON QUASIPERIODIC LATTICES

A dissertation submitted for the degree of
Doctor of Philosophy
in
Physics

Center for Theoretical Chemistry and Physics
New Zealand Institute for Advanced Study
Massey University, Albany
New Zealand

Carlo Danieli

June 2016

Declaration

This dissertation is a presentation of the research conducted between February 2013 and June 2016 at the Center for Theoretical Chemistry Physics within the New Zealand Institute for Advanced Study at Massey University (Albany campus, Auckland, New Zealand) while enrolled in the Doctor of Philosophy degree.
The degree was carried out under the supervision of Prof. Sergej Flach, Dr. Joshua D. Bodyfelt and Dist. Prof. Gaven J. Martin.
The material reported is, at the best of my knowledge, original (except where acknowledged), and it has not been submitted in whole or in part for a degree in any university.

Carlo Danieli
June 2016

The most merciful thing in the world, I think, is the inability of the human mind to correlate all its contents. We live on a placid island of ignorance in the midst of black seas of infinity, and it was not meant that we should voyage far. The sciences, each straining in its own direction, have hitherto harmed us little; but some day the piecing together of dissociated knowledge will open up such terrifying vistas of reality, and of our frightful position therein, that we shall either go mad from the revelation or flee from the deadly light into the peace and safety of a new dark age.

H.P. Lovecraft
The Horror in Clay

Abstract

Lattices and discrete networks are cornerstones of a number of scientific subjects. In condensed matter, optical lattices allowed the experimental realization of several theoretically predicted phenomena. Indeed, these structures constitute ideal benchmarks for light and wave propagation experiments involving interacting particles, such as clouds of ultra-cold atoms that Bose-Einstein condensate. Moreover, they allow experimental design of particular lattice topologies, as well as the implementation of several classes of spatial perturbations. For example, Anderson localization being observed for the first time in atomic Bose-Einstein condensate experiments and Aubry-André localization discovered with light propagating through networks of optical waveguide.

This thesis considers different types of lattices in the presence of quasiperiodic modulations, mainly the celebrated Aubry-André potential. Particular attention will be given to spectral properties of models, localization features of eigenmodes and the transition from delocalized (metallic) eigenstates to localized (insulating) ones within the energy spectrum. We additionally discuss the relation between the model's properties and the dynamics of particles hopping along the lattice.

After introducing the linear discrete Schrödinger equation, we first discuss the spectral properties of the Aubry-André model. We then study the transition between metallic and insulating regimes of a class of quasiperiodic potentials constructed as an iterative superposition of periodic potentials with increasing spatial period. Next, we discuss the Aubry-André perturbation of flat-band topologies, their energy-dependent transition (mobility edge), which can be expressed in analytical forms in case of specific onsite energy correlations, highlighting existence of zeroes, singularities and divergences. We then discuss two cases of driven one-dimensional lattices, namely an Aubry-André chain with a weak time-space periodic driving and an Anderson chain with a quasiperiodic multi-frequency driving. We show anaytically and numerically how drivings can lift the respective localization and generate delocalization by design. Finally we discuss the problem of the possible generation of correlated metallic states of two interacting particles problem in one dimensional Aubry-André chains, under a coherent drive of the interaction.

Publications

The thesis is based on the following publications:

Published:

- H. Hatami, **C. Danieli**, J. D. Bodyfelt and S. Flach, "*Quasiperiodic driving of Anderson localized waves in one dimension*", Phys. Rev. E **93**, 062205 (2016);
- **C. Danieli**, J. D. Bodyfelt and S. Flach, "*Flatband engineering of mobility edges* ", Phys. Rev. B **91**, 235134 (2015);
- **C. Danieli**, K. Rayanov, B. Pavlov, G. Martin and S.Flach, "*Approximating metal-insulator transitions* ", Int. Journal of Mod. Phys. B **29**, 1550036 (2015);
- J. D. Bodyfelt, D. Leykam, **C. Danieli**, X. Yu and S.Flach, "*Flat bands under correlated perturbations* ", Phys. Rev. Lett. **113**, 236403 (2014);
- L.Morales-Molina, E.Doerner, **C.Danieli** and S.Flach, "*Resonant metallic states in driven quasiperiodic lattices: Aubry-Andre localization by design*", Phys. Rev. A **90**, 043630 (2014).

Selected Conference Presentations:

- **C. Danieli**, J. D. Bodyfelt and S. Flach, "*Flatband engineering of mobility edges* ",Australian and New Zealand School in Ultracold Physics, Otago University, Dunedin, New Zealand, December 2016;
- **C. Danieli**, J. D. Bodyfelt and S. Flach, "*Flatband engineering of mobility edges* ", IONS, KOALA, University of Auckland, Auckland, New Zealand, November 2015;
- **C. Danieli**, J. D. Bodyfelt and S. Flach, "*Flatband engineering of mobility edges* ", Conference on Frontiers of Nanoscience, ICTP, Triest, Italy, August 2015;
- **C. Danieli**, K. Rayanov, B. Pavlov, G. Martin and S.Flach, "*Approximating metal-insulator transitions* ", Seminar at the Center for Theoretical Physics of Complex Systems, Daejeon, South Korea, July 2015;

- L.Morales-Molina, E.Doerner, **C.Danieli** and S.Flach, "*Resonant metallic states in driven quasiperiodic lattices: Aubry-Andre localization by design*", NZIAS-MPIPKS Tandem Workshop, Nonlinear Physics at the Nanoscales: a Cross-Fertilization on Stochastic Methods, Rotorua, New Zealand, February 2015;

- **C. Danieli**, J. D. Bodyfelt and S. Flach, "*Flatband models with correlated onsite perturbation* ", INMS Postgraduate Conference, Massey University, Albany, New Zealand, September 2014;

- L.Morales-Molina, E.Doerner, **C.Danieli** and S.Flach, "*Delocalization in driven quasiperiodic lattices*", lll Dynamic Days South America, Vina de Mar, Chile, November 2014;

- S. Flach, **C. Danieli**, J. D. Bodyfelt , D. Leykam, P. Matthies and A. S. Desyatnikov, "*Perturbing flat-band*", Let's Face Chaos Through Nonlinear Dynamics, University of Maribor, Maribor, Slovenia, July 2014;

- **C. Danieli**, K. Rayanov and S.Flach, "*Approximating metal-insulator transitions* ", Dodd-Wall Symposium, Otago University, Dunedin, New Zealand, October 2013;

- **C. Danieli**, K. Rayanov and S.Flach, "*Approximating metal-insulator transitions* ", INMS Postgraduate Conference, Massey University, Albany, New Zealand, October 2013;

- **C. Danieli**, K. Rayanov and S.Flach, "*Approximating metal-insulator transitions* ", Advanced Workshop on Non-equilibrium Bosons: From Driven Condensates to Non-Linear Optics, ICTP, Triest, Italy, August 2013.

Acknowledgements

A PhD dissertation is the culmination of several years of someone's life. It means much more than just the hundred and odd pages, and between its lines one can find joy, sadness, emotions and people. People. Countless people that have been an invaluable part of this experience, which can hardly be captured in this section

Prof. Sergej Flach has not been only an extraordinary supervisor, he has been a friend and a guide. I am so grateful for the time we have spent together during these years. I thank him for the possibility to join his research within condensed matter physics, complete new subject for me, and for the freedom he gave me to approach the topics I was more interested in while minding that my projects were not losing focus from forming a coherent plot. Moreover, I want to thank him for sharing with me his love and passion for life and science. Next, I want to thank Dr. Joshua Bodyfelt. As a friend and co-supervisor, he has always been there supporting me with ideas and motivations, in particular when I was demoralized. Moreover, I want to thank all the people I had the luck and the pleasure to collaborate during these years: my co-supervisor Prof. Gaven Martin, Prof. Boris Pavlov (RIP), Dr. Xiaoquan Yu, Dr. Daniel Leykam, Dr. Luis Morales-Molina, Dr. Edoardo Doerner, Dr. Hani Hatami and Kristan Rayanov.

I found the CTCP an ideal place to grow and do science. There I have been surrounded by amazing people and phenomenal scientists, ready to help and support each other for scientific but also personal issues. The various Lukas, Krista, Jayson, Lauri, Peter, Xiaoquan, Alberto, Sasha, Sophie, Paul, Odile, Andy and everybody, thank you so much because I truly felt within a community. In particular, I want to thank Prof. Peter Schwerdtfeger for running the place with so much passion and his friendly attitude to everyone of us (you have been more that a boss, you are our godfather); and Vesna Davidovic-Alexander, I am so grateful for your constant and invaluable help and support. I want to extend these acknowledgements to those people that have hosted me as a visitor during this project, from Erica at the ICTP in Italy to Ma-Young, Yoorin, Sol, Dominika, Hwa-Sung, Jaehee, Hee-Chul, Ivan and everyone at PCS in South Korea.

Outside of science, my first thoughts go to my family back in Italy. This experience has been challenging not only for me, but also for everyone of us. During these years there have been losses, disease and grief, but also lots of joy, the arrival of new young family members, weddings and so on. Mum, dad, Luciano, Anna, Simone, all the aunts, uncles, cousins and so on, I am so grateful to you all for this. Love you all.

During this time spent in New Zealand, many friends departed for long travels or begun new experiences somewhere, each one following dreams and aspirations. Enrico, Andrea, Nevenka, Claudio, Francesco, Federica, Felix, Sabrina, Tjefa, Jakob, Matteo, Giacomo, Lorena, Tommaso, Celeste, Luca; this list can go ahead endlessly. Even if keeping in touch with everyone is not easy, you all have been with me during this time. But from friends left, new friends were expecting me along my journey. After the positive experiences of Padua and Berlin, I was hoping to again meet good people to spend time with and share interests starting from the domestic environment. This happened from the very first day I arrived in New Zealand. Russell, Shannon, Kelsie, Caitlin, Michael, Jack, Dave, Cloud, Jenna, Steven, young Manu, when I stepped for the first time in that flat and met you all, I immediately felt home. During this years you have been more than a family for me; therefore I thank you so much for welcoming me and for this awesome time together.

New Zealand didn't only gave me the opportunity to move my first steps within the scientific research, but it also gave me the opportunity to grow some personal passions. Heaps of DIY projects, house concerts organized and attended, the amazing experiences of the Off The Radar and the Chronophonium festival; moments where the enthusiasm for the projects gave rise to overwhelming atmosphere and strong connections between the people involved. Among these experiences, I would like to particularly highlight the Worn Out collective, as an undeniable evidence that even the most disorganized group of lazy people can create something great. Benny, Rory, Junior, Fluffy, Anhand, Grant, Ritchie, Glenn, Cyprian, we had such a great time and amazing experiences together, thank you so much!

Not every single moment of this project have been easy and pleasant. A bunch of people taught me to do not be afraid of pain and stress, both mental and physical, but instead to try to accept them, since they can uncover energies and motivations that you were not even thinking to have. I am so deeply grateful to Eden and Kyrsten, two wonderful human beings that have welcomed me and guided through this magical adventure. With them, I would like to thank the Skindependent family. Josh, Christopher, Fran, Betty, Travis, Scott, Martin, you guys are incredible. So are the people met during this three years in various locations and conventions. Too many to be mentioned, but none forgotten, from practitioners to enthusiastics like myself. Alice, Snow, Kat and Clay, Alan, June, Marita, Havve, Bruno. I love you my friends.

Music is, has been and will be a fundamental part of my life, and even the smallest detail of this dissertation is laced with the music I was listening while it was conceived, developed and formalized. At last then, I would like to thank all those bands, and in a broader way, all those musicians, performers and independent artists I have met and enjoyed their music and performances between Europe, New Zealand and South Korea. Also, to all the artists I haven't met but that I have deeply relished and enjoyed their art, even though we do not know each other I am so grateful to you all for all the emotions and experiences you let me have in these years, because they made this dissertation the way it is and myself the way I am.

Contents

List of Figures

CHAPTER 1

Motivations and Outline

The concept of waves, the study of their properties, and their behavior in time is at the very foundation of modern physics. From the differential equations of classical mechanics to modern techniques of quantum mechanics, waves have always played a central role in practically every branch of the fundamental sciences. One of the most notable example concerns the study of light waves. From the first experiments that cemented the foundation of quantum mechanics to the latest achievements in photonics, light propagation has always been an exemplar development of the natural sciences. As a result, optics found applications in a vast range of fields, yielding technologies that play a vital role in our lives, for example in telecommunications, medicine, surgery, renewable energy.

The study of waves can be traced through the various periods of human history, from ancient times towards the Renaissance until our modern era. Pythagoras (c.560-480 BC) studied the relation of pitch and length of strings in musical instruments. Essential concepts such *frequency* and *fundamental harmonic* were introduced by Benedetti (1530-90), Beeckman (1588-1637) and Galileo (1564-1642). Newton (1642-1727) was the first to calculate the speed of sound in air in his *Principia* [1]. Leonardo da Vinci (1452-1519) portaited and discussed the flow patterns produced by water flowing, introducing a few centuries in advance the concepts of *turbulence* and *chaos*, as well as their relations with wave transports.

From all the studies developed during the centuries, it appeared clear that properties of the wave and their transport are deeply connected with the media where the phenomena are taking place. A particular aspects, present in any physical system, assumed more and more importance: the *presence of alterations* in the media. Impurities, imperfections and defects are naturally present in any material or element. In the past many underestimated the importance, the physical relevancy, and the amount of outcomes that could have been obtained by including irregular and chaotic perturbations in their models. Disordered systems still nowadays is an incredibly prolific research field, with applications ranging from condensed matter physics to material science.

One of the highlights of the twentieth century was obtained in 1958, when Anderson predicted the complete localization of waves along a one dimensional lattice under the pres-

ence of uncorrelated random potentials [2]. At that time, other studies had already been performed in spatially perturbed periodic models, highlighting unusual scattering phenomena of the conduction of electrons in metallic structures due to the presence of magnetic impurities [3–5]. However, Anderson's prediction was a breakthrough that put the study of waves in disordered media (or, generally, aperiodic) at the very core of condensed matter physics.

Anderson himself was probably motivated in his research from the practical interests of understanding the conductance properties of semiconductors, a field under huge expansion at that time. Practical interest extended the research towards more complicated disordered systems, with respect to a one-dimensional chain. Since the 1958, a huge number of achievements followed, from higher dimensional structures [6, 7] to systems of many interacting particles [8–12] and non-linear chains [13–18]. Optics have been an ideal benchmark for the observations and the experimental measurements of the wave localization phenomena [19, 20]. Several experimental observations of Anderson localization have been realized in a number of different physical systems, from light and sound waves, to electronic gases and microcavities [21–29]. Recently, Anderson theory has found application in the study of lasers and their dynamic [30–35], biological systems [36, 37], and material science [38–41].

Several of the natural models where Anderson theory has been tested exhibit certain type of recurrence in their spatial perturbations, making clear that the uncorrelated uniformly distributed disorder was not the only case worth considering. Studies involved systems with correlated disorder [42, 43], correlated spatial perturbation in optical lattices [44] and metamaterial [45], and lattices with off-diagonal correlated disorder [46–48]. Among these, a particular class of spatially correlated perturbation became important in the study of wave localization: the class of *quasiperiodic* potentials. The *quasiperiodicity* belongs to a the set of *quasi-concepts*, that represents systems where a characterization, a property is not satisfied, but instead it is approximated. Within the scientific community, names like *quasiparticle* or *quasicrystal* have become commonly used, but in general the *quasi-concepts* still lacks mathematical definition. The major focus of this work, the *quasiperiodic* case, aims to consider those physical systems that exhibit an approximated periodicity along either the spatial or the temporal coordinate.

Chapter 2 will introduce basic concepts, while results will be presented throughout the thesis. Starting from introducing photonic lattices, optical lattices and the tight-binding approximation, we will move towards the Schrödinger equation. We then discuss the effects of breaking the periodicity, with a focus on specific cases of localizing potentials. The second part of the chapter will be devoted to the quasiperiodic case, in particular the Aubry-André model. We will discuss in detail the features of its spectral and dynamical properties.

Chapter 3 will continue discussing features of the Aubry-André model. However in this chapter we intent to understanding a specific property of the model, namely the topological Cantor structure of the spectrum and its self-similar fashion. In doing so, we construct a new class of quasiperiodic potentials. We will show the existence of an approximated transition between metallic and insulating regimes for our new model. For one case of the class, we will also computationally obtain the energy dependent transition (called mobility edge).

Chapter 4 will focus onto the implementation of the Aubry–André quasiperiodic potential in very specific one-dimensional lattices, the *flat-band* lattices. First we will introduce the concept of flat-band in crystalline lattices, reviewing properties, effects and classification. We will also introduce a Fano rotation method of the unit cells, that explains the existence of the flat-band. Then we will discuss the presence of quasiperiodic potential, and the appearance of an energy dependent mobility edge. Making use of the rotation formerly introduced, we will obtain analytical expressions of the mobility edge for specific energy

correlations.

Chapter 5 will discuss two examples of a driven one-dimensional chain. The first is an Aubry-André chain under a driving, that is spatially quasiperiodic and periodic in time, while the second is an Anderson chain under a multi-frequency quasiperiodic driving. We will see how the former will generate metallic states by resonant coupling of groups of localized ones. The second driving instead will substantially increase the localization length of the models, needing an infinite number of frequencies to generate complete delocalization.

Chapter 6 will discuss two interacting particles in a one-dimensional Aubry-André chain. We first overview the topic of the Many-Body Localization. Then we will focus on the case of two interacting particles in disordered and quasiperiodic chains. We will at last discuss the introduction of certain classes of external driving, and present some preliminary results, from both the analytical and the numerical point of view.

We then summarize our results and discuss open issues to be tackled. At last in the appendices, we will refer to most of the technical details (analytical and numerical) that have been omitted from the main chapters.

CHAPTER 2

Introduction

This chapter reviews basic concepts and fundamental results of transport and localization in optical lattices. We will first introduce the Schrödinger equation and its tight-binding approximation. We then discuss the effects of periodicity breaking in the model, and its connections to natural systems. Particular attention will be given to specific two cases of localizing potentials: *random* and *quasiperiodic*. From Anderson localization, we will shift focus to the Aubry-André model as the main example of quasiperiodicity, discussing its analytical properties. We will finish the chapter by presenting recent experimental realizations of the Aubry-André model.

2.1 Wave Propagation in Continuous and Discrete Systems

Although electromagnetic waves are unique in that they can propagate in a vacuum, in general any type of wave (*e.g.*, sound wave) cannot propagate through a vacuum. Instead, a transmission medium must exist. The nature and characteristics of the medium is of fundamental importance for the properties of the waves themselves, as well as their propagation. There exists several classes of differential equation that describe the propagation of waves in media, each of them describing different phenomena and setting - for example, the *wave* equation, the *diffusion* equation or the *heat* equation. The main differential equation class of this work is the *Schrödinger* equation. Based on the works of Einstein, Bohr, and DeBroglie, it is a particular wave equation about the relations between light, particles and energy quantization. This particular equation was introduced in 1926 by Erwin Schrödinger, with the intention of finding a wave equation for electrons [49]. Schrödinger derived this celebrated equation starting from Maxwell's equations for classical electrodynamic on a continuous medium, under the assumption of a small particle velocity with respect to the speed of light in vacuum, obtaining

$$i\frac{\partial}{\partial t}\psi(\mathbf{r},t) = \Delta_{\mathbf{r}}\psi(\mathbf{r},t) + V(\mathbf{r})\psi(\mathbf{r},t)\ . \tag{2.1}$$

where i is the complex unit, and the wave function $\psi(\mathbf{r}, t)$ depends on the variable $\mathbf{r}$, which is a positional vector of dimension D, and the time variable t. The operator $\Delta_{\mathbf{r}}$ is the Laplacian operator, while the symbol $\frac{\partial}{\partial t}$ denotes the time derivative. The potential term $V(\mathbf{r})$ is of fundamental importance for the type of systems represented by Eq.(2.1), and it is a key element for the develop of this dissertation.

Let's now refer to the one-dimensional case $D = 1$. The continuous equation Eq.(2.1) can be discretised with a *tight-binding approximation*, which is obtained approximating the continuous field $\psi(\mathbf{r}, t)$ with the sum $\psi(\mathbf{r}, t) = \sum_l \psi_l(t)\omega_l(\mathbf{r})$ of the single site mode $\omega_l(\mathbf{r})$, for the vector of complex numbers $\{\psi_l(t)\}_l$

$$i\frac{\partial}{\partial t}\psi_l(t) = \epsilon_l\psi_l(t) + \sum_{m\neq 0} W_{l-m}\psi_{l-m}(t) \ . \tag{2.2}$$

This approximation holds in the limit of weakly coupled modes. The real sequence $\{W_{l-m}\}_{m\neq 0}$ discretizes $\Delta_{\mathbf{r}}$, and it describes the strength of the hopping. Typically, only the coupling between the nearest neighbouring sites is significant hopping ($W_{l-m} = 1$ for $l - m = \pm 1$ and 0 elsewhere), yielding to the classical version of the discrete Laplacian operator. The real sequence $\{\epsilon_l\}_l$ is the onsite potential. A detailed derivation of Eq.(2.1) and Eq.(2.2) could be found in [50].

Although it is not in the interests of this dissertation, it is worth recalling that the Schrödinger equation have been generalized in several ways. Here we recall one case of the *discrete nonlinear Schrödinger* equation

$$i\frac{\partial}{\partial t}\psi_l(t) = \epsilon_l\psi_l(t) + \psi_{l-1}(t) + \psi_{l+1}(t) + \beta\psi_l(t)|\psi_l(t)|^2 \ . \tag{2.3}$$

where the real number β controls the strength of the nonlinearity. This cubic nonlinear term represent the propagation of light through the Kerr media [51]. Nonlinear problems have been studied since the pioneer work by Fermi, Pasta and Ulam in 1955. Together with M. Tsingou, they analyzed the phenomenon of the energy equipartition in a finite chain of nonlinearly coupled oscillators [52]. This problem has been under investigation for more than 50 years, and it has inspired many problems in condensed matter physics [53–57]. One notable example where Eq.(2.3) has been used goes back in 1989, when Peyrard, Bishop [58] and Yakushevich [59] introduced two nonlinear tight binding chains in order to describe the DNA double-helix structure and its duplication/transcription processes. A number of works followed since, involving the nonlinearity [60–62], the 3D helicoidal geometry of the DNA chains [63], and the relation between nonlinearity and the spatial distribution of the nucleobases (Adenine, Cytosine, Guanine and Thymine) [64, 65].

Here follows the time-dependent one-dimensional discrete Schrödinger equation

$$i\frac{\partial}{\partial t}\psi_l(t) = \epsilon_l\psi_l(t) + \psi_{l-1}(t) + \psi_{l+1}(t) \ . \tag{2.4}$$

This equation can be expanded using *amplitude-phase* coordinates

$$\psi_l(t) = A_l e^{iEt} \ , \tag{2.5}$$

for the system energy E. It follows the associated time-independent eigenvalue problem

$$EA_l = \epsilon_l A_l + A_{l-1} + A_{l+1} \ . \tag{2.6}$$

From here on, we drop the notation (t) in the time dependent equation Eq.(2.4). For the various models considered in following chapters, the analysis will be focused on the computation of the time evolution of Eq.(2.4) and the diagonalization of the associated

eigenvalue problem Eq.(2.6). We will report the numerical schemes used for the studies in every chapter. A detailed report on the numerical techniques can be found in Appendix A. In the linear case, a key element of the spectral and dynamical properties of the model becomes the onsite perturbation $\{\epsilon_l\}_l$. According to its nature, the model's features may change drastically. We will focus on a particular case of correlated disorder, the *quasiperiodic* perturbation. Before introducing this class of onsite perturbation, we will first discuss the periodic and the uncorrelated cases.

2.2 Periodic Structures

Periodicity is a fundamental concept in mathematics and fundamental science. In nature, periodic patterns can be easily spotted, from flower petal arrangements to animal fur marking. Even though these patterns are usually altered by the presence of imperfections, defects and minor alterations, the identification of periodicities and symmetries in a system is generally a great achievement, allowing drastic simplification in the complexity of a problem by applying certain mathematical tools. One of these is the *Bloch decomposition*.

This decomposition consists in expressing the solution of crystalline or periodic structures in *Bloch* waves [66]. This kind of solution, in general, holds for any wave-like phenomenon in a periodic medium, for example a periodic dielectric in electromagnetism (which leads to photonic crystals) or a periodic acoustic medium. In the case of the continuous Schrödinger equations - Eq.(2.1) - the Bloch solution exists in the periodic case (there exists $\mathbf{T}$ such that $V(\mathbf{r}+\mathbf{T}) = V(\mathbf{r})$ for every $\mathbf{r}$). In this case, first we obtain the time-independent eigenvalue problem with the expansion $\psi(\mathbf{r},t) = \phi(\mathbf{r})e^{iEt}$, in analogy with Eq.(2.5). This expansion turns Eq.(2.1) into

$$E\phi(\mathbf{r}) = \Delta_{\mathbf{r}}\phi(\mathbf{r}) + V(\mathbf{r})\phi(\mathbf{r}) \ . \tag{2.7}$$

In the case of periodic potential $V(\mathbf{r})$, the Bloch theorem states that the energy spectrum is made of a discrete set of bands $E = E_n(\mathbf{k})$, where n is the band index and $\mathbf{k}$ the *wave vector*, that lives in the Brillouin zone [66]. The eigenmodes are instead *Bloch wave* $\phi(\mathbf{r}) = u_n(\mathbf{r})e^{i\mathbf{k}\cdot\mathbf{r}}$, where $u_n(\mathbf{r})$ have the same periodicity of the potential $V(\mathbf{r})$. The Bloch waves, substituted in Eq.(2.7), yields to an eigenvalue problem for the *Bloch function* $u_n(\mathbf{r})$

$$E_n(\mathbf{k})u_n(\mathbf{r}) = \left[\Delta_{\mathbf{r}} + 2i\mathbf{k}\nabla_{\mathbf{r}} - \mathbf{k}^2 + V(\mathbf{r})\right]u_n(\mathbf{r}) \ , \tag{2.8}$$

where $\nabla_{\mathbf{r}}$ is the gradient operator. The *Bloch* wave expansion is a useful tool for the study of a periodic model, since the decomposition in energy bands of the spectrum allows, for example, the understanding of linear wave-packet dynamics, or the understanding of certain nonlinear phenomena (band transitions). We will use the spectral decomposition in band structure $E = E_n(\mathbf{k})$ in Chapter 4 for flat-band lattices. Before introducing non-periodic models, we shall describe two topological structures that can be represented with the discrete linear Schrödinger equation Eq.(2.2). These have been used to experimentally benchmark the localization phenomena discussed in this thesis: *photonic* lattices and *optical* lattices.

Photonic lattices are families of coupled optical waveguides arranged according to specific topologies. Since each waveguide emits an evanescent field (an oscillating field spatially concentrated in the vicinity of the guide), the waveguides in close proximity then couple through phase coherent transfer. This coupling is called *evanescent coupling*. The spatial coordinate $\mathbf{r}$ describes the arrangement of the waveguides according to a periodic potential $V(\mathbf{r})$, from which follows a traslation invariance on a smaller section of the waveguides. The time coordinate t becomes the spatial propagation along each waveguide [67]. Specific coupling arrangements of the waveguides yield emulations of various physical systems [68, 69]. Experimentally these lattices are realized using waveguides etched in semiconductiors [70], and lattices induced optically in photorefractive media [71, 72].

Optical lattices are instead structures consisting of microtraps that are created by interfering optical laser beams. Due to interference, the overlap of two counter-propagating laser beams form an optical standing wave, which can trap atoms or particles in the equispaced wells. Varying the lasers' intensities changes the wave's amplitudes, and with that the hopping strength of the model. By interfacing more lasers higher dimensional lattices can be formed [73]. The resulting structure is called an *optical lattice*, and they act as discrete structures to trap ultracold quantum gases of bosons and fermions. Additionally the particle-particle interactions are easily controlled via Feshbach resonance, therefore they form an ideal benchmark for quantum many-body systems, strongly correlated quantum phases and nonlinear wave dynamics.

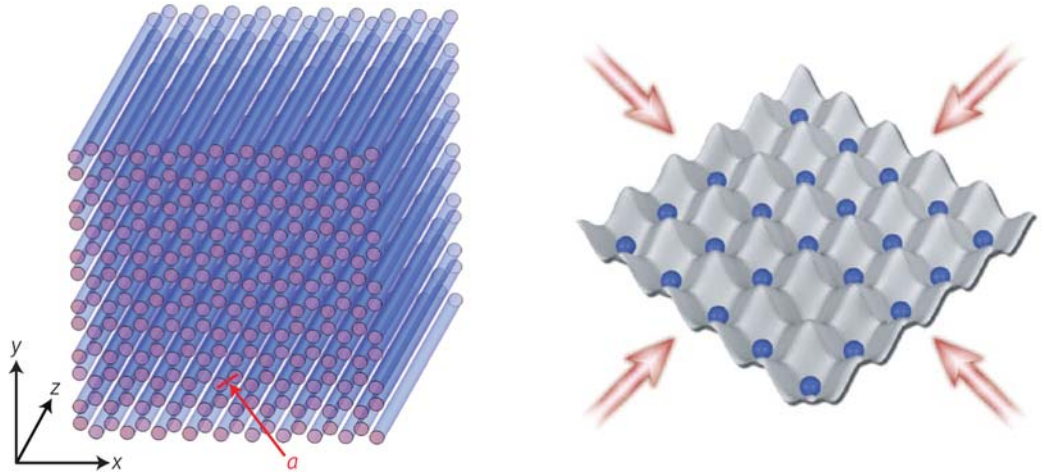

Figure 2.1: Left: Photonic Lattice that form the Honeycomb lattice profile. The parameter a is the nearest-neighbor distance. Figure taken from [74]. Right: Two-dimensional optical lattice formed as the overlap of several standing waves, each generated by superimposing two laser beams. Figure taken from [75].

2.3 Periodicity-Breaking and Localizing Potentials

Having introduced systems exhibiting spatial translation invariances, a natural phenomenon generally present in physical systems is the *breaking of the periodicity*. One effect of the periodicity breaking is the presence of defects and alterations on the spatial domain of the lattices. The presence of these entities usually makes the lattice's fundamental elements (site, cavities or guides) non-indistinguishable, and since the perturbations are distributed according to non periodic distributions, the models lose their translation invariance. In the remainder of the chapter, we will discuss causes and effects of the presence of disordered and correlated onsite perturbations.

In nature perfectly crystalline media do not exist, and instead every structure posses imperfections and defects. The influence of the presence of impurities on a periodic medium can lead to very rich physics. From certain types of semiconductor to the metastable states of the charge-density wave systems, it has been shown that presence of impurities pins dynamics around the defects [76–78]; in particular, unusual scattering phenomena of the conduction of electrons in metallic structures due to the presence of magnetic impurities. In 1934, de Haas, de Boer and van den Berg observed a resistance alteration in gold dependent on the temperature, and they hypothesized in some additional scattering mechanism giving an anomalous contribution to the resistivity [3]. Other examples of metals and heavy

fermions showing a resistance minimum were later observed [79]. In 1957, Landauer proposed a formula relating the electrical resistance of a quantum conductor to the scattering properties of the conductor [80–82]. In 1964, van den Berg showed the reciprocity between resistance minima and the number of magnetic impurities in gold [4]. In the same year, Kondo described how certain scattering processes are generated from the presence of magnetic impurities, and how they could give rise to a resistivity contribution depending logarithmically of the temperature [5]. Kondo's explanation of the observed resistance alteration was considered a highly satisfactory solution to this longstanding puzzle. The phenomenon has since been given his name (*Kondo effect*). From the study of the scattering effects of metallic structures with sparse impurities, the step towards systems with impurities scattered everywhere along the spatial domain was short.

During the studies of these phenomena of resistance alterations and absence of transport related to presence of irregularly scattered impurities, the analysis of the model's spectrum and the related eigenstates has revealed to be a fruitful effort. This followed from the understanding of the relation between the vanishing of the model's conductivity and the amplitude decay in the space of the eigenmodes. This introduced a separation between those modes whose amplitude decays along the spatial coordinate, called *localized*, and those where instead the decay does not occur, called *extended* - see Fig.2.2. The understanding of the decay law of the eigenmodes (if any) and the nature of the energy spectrum fully describes the dynamics of a single particle in an optical lattice. This constitutes a step of fundamental importance for the understanding of many-body problems.

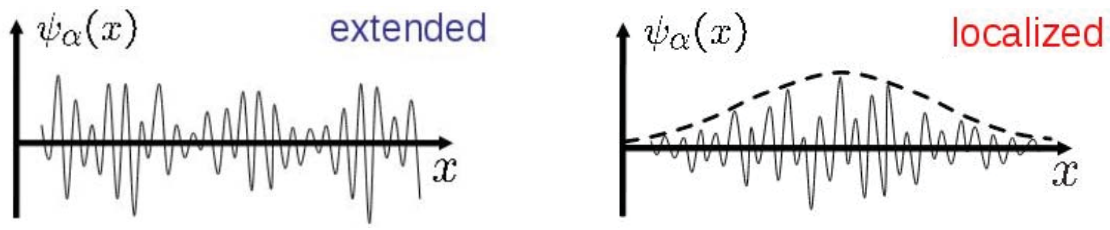

Figure 2.2: Example of extended (left plot) and localized waves (right plot). In the extended case we do not expect any regularity of the wave amplitude (as with the Bloch waves), however the wave profile does not exhibit any decay law, which instead it is shown in the localized case, here represented from the dashed curve. Figures courtesy of Boris L. Altshuler.

In 1958, Anderson predicted that one-dimensional waves localize in the presence of uncorrelated random potentials [2]. By obtaining the exponential decay of every eigenstate of a disordered class of one-dimensional linear wave equations, Anderson proved the localization of a single quantum particle, within a finite volume of the chain, due to disorder. Since then, disordered systems have been of large interest within the condensed matter community, especially in the study of transport phenomena. Anderson localization has been well studied analytically and several features are now common knowledge. We recall here the major ones, since they will be used throughout the thesis.

Anderson localization occurs in a one-dimensional lattice of Eq.(2.4). With the phase amplitude expansion $\psi_l = A_l e^{iEt}$ we obtain the eigenvalue equation Eq.(2.6), here recalled

$$EA_l = \epsilon_l A_l + A_{l-1} + A_{l+1} \ . \tag{2.9}$$

The onsite potential is an uncorrelated sequence $\epsilon_\nu \in [\, -\frac{W}{2}, +\frac{W}{2}]$ uniformly distributed over an interval of width W (parameter called *disorder strength*). The energy spectrum is a dense and discrete set with the eigenenergies E_ν uniformly distributed within the interval

$E_\nu \in [-2-\frac{W}{2}, 2+\frac{W}{2}]$. The width of the spectrum is then $\Delta = 4+W$. The eigenvector's amplitudes $\{A_l^\nu\}_l$ corresponding to the energy E_ν exhibits spatial decay $A_l^\nu \sim e^{-|l|/\xi(E_\nu)}$ for $|l| \to +\infty$. The decay rate $\xi(E_\nu)$ is called *localization length*, and it depends of the energy value E_ν and on the disorder strength W. An approximation for $W \leq 4$ is $\xi(E_\nu) \approx 24(4-E_\nu^2)/W^2$ [83]. In general, the analytical and numerical calculations of ξ are a highly useful tool in the study of disordered systems (or, generally, systems with modes exhibiting exponential decay). Alongside the localization length, others measures that describe the finite behavior of the eigenmodes $\{A_l^\nu\}_l$ are usually calculated which focus on the region of strongly excited sites before the exponential decay (called *localization volume*, V_ν). For a renormalized mode, $\sum_l A_l^\nu = 1$, the *participation number*

$$P_\nu = \frac{1}{\sum_l (A_l^\nu)^4} \ , \tag{2.10}$$

counts the number of non-negligibly excited sites. The *second moment*

$$m_2^\nu = \sum_l \left(l - \sum_{l'} l' |A_{l'}^\nu|^2 \right)^2 |A_l^\nu|^2 \tag{2.11}$$

approximates the distance between the exponentially decaying tails. The ratio between the two is called *compactness index*, and is defined as $\zeta_\nu = P_\nu^2/m_2$ (parameters true only for the one-dimensional case). From numerical arguments, the localization volume is of the order $V_\nu \approx 3\ \xi_\nu$, and it converges to unity $V_\nu = 1$ in the limit of strong disorder. We refer to Appendix A for further details.

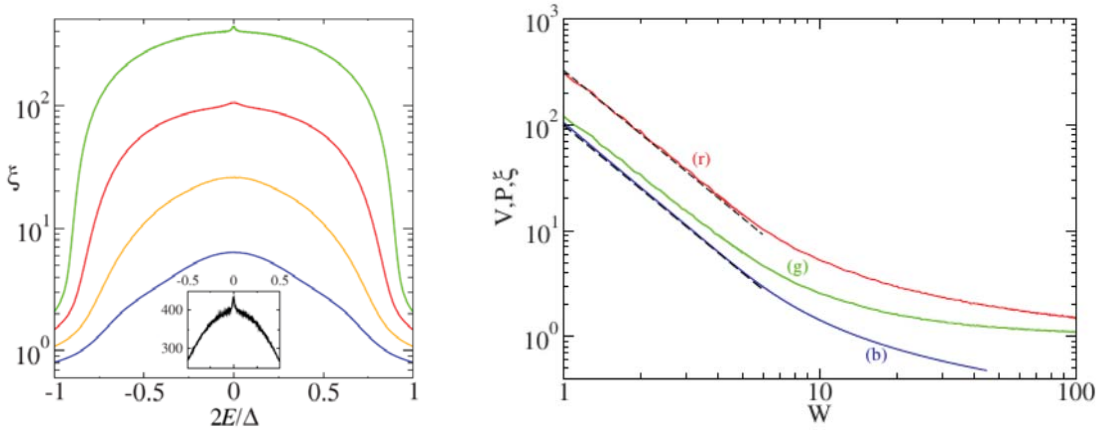

Figure 2.3: Left: Localization length *zeta* versus normalized eigenvalue for $W = 0.5$ (green), $W = 1$ (red), $W = 2$ and $W = 4$. Inset: zoom for $W = 0.5$ around the band-width center. Right: Averaged localization volume V (red), participation number P (green) and localization length ζ (blue) of normal modes with eigenmodes $E \approx 0$ versus the disorder strength W. The dashed lines estimates the asymptotic behaviors of V and ζ at weak disorder. The dashed lines have equations $330/W^2$ and $100/W^2$ respectively. Both figures taken from [84].

Beyond Anderson's pioneering work, theoretical studies have been performed on higher dimensional lattices in random potentials, showing absence of diffusion in the two dimensional case [6], and mobility edges between the insulating and the metallic phase in the three dimensional case [7]. A few and many body problems in disordered lattices have been extensively studied [8–12] as well as the case of non-linear disordered chains, reporting a loss of the Anderson localization [13–18]. Experimentally, Anderson localization has been

observed in a number of experiments. In the remaining part of the section we briefly recall two experiments: atomic Bose-Einstein condensates (BEC) in a one dimensional optical lattice [19] and one with light waves on disordered photonic lattices [25]

In the first experiment [19], a BEC formed by 1.7×10^4 atoms of rubidium-87 is trapped in an anisotropic opto-magnetic hybrid trap in an optical lattice. A weak disorder potential is applied using an optical speckle produced by shining a laser beam through a diffusive-detuning plate. Fig.2.4 - left (a) portraits the trapped BEC. The longitudinal magnetic confinement is released and the BEC starts expanding but the expansion rapidly stops due to the disorder perturbation. Fig.2.4 - left (b) the BEC expanding after the release and exhibiting exponential localization.

In the second experiment, the system consists in a one-dimensional set of waveguides, and light is injected into one of the guides, Fig.2.4 - right (a). The onsite potential is introduced by changing the width of each waveguide, and light can tunnel to the other guides as it propagates longitudinally. Light intensity is measured at the output. Fig.(b) and (c) correspond to lights propagating in two different periodic potential, and both images show a final extended state. Fig.(d) instead corresponds to light propagating through a disorder lattice, showing absence of light propagation between the waveguides.

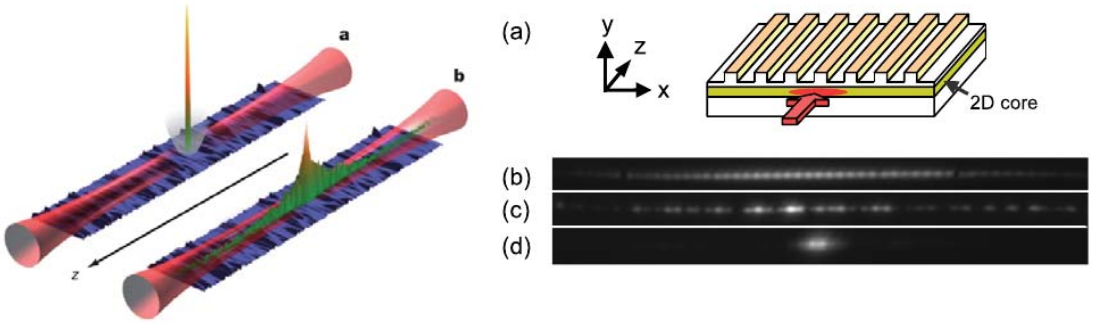

Figure 2.4: Left: Anderson Localization in Optical Lattices. (a) magnetically trapped BEC in a weakly disordered optical lattice. (b) the BEC expanding after the release and exhibiting exponential localization. Figure taken from [19]. Right: Anderson Localization in Photonic Lattices. (a) Schematic view of the experimental setting. (b)-(d) Light amplitude along the lattice over a few sites: (b) periodic lattice; (c) in disordered lattices, with a large value of localization length ξ; (d) in disordered lattices, when the localization is clearly observed. Figure taken from [25].

2.4 The Quasiperiodic Class

From the case of uncorrelated random potential, other classes of aperiodic potentials found interest within the condensed matter community. In this section we will discuss one particular case of correlated disordered sequences, the class of *quasiperiodic* potentials. The property of *quasiperiodicity* is deeply connected with the concept of *incommensurability*, which is the impossibility to compare objects using integer multiples. In general, quasiperiodic objects are characterized by the presence of two or more periodic structures which are incommensurate with each other, *i.e.*, the ratios of their periodicities are irrational numbers. Therefore, quasiperiodicity is related to the field of irrational numbers.

The property of quasiperiodicity can be found in several mathematical and natural objects. One of the most important and renown example is the family of *quasicrystals*, which yielded the Nobel Prize in Chemistry to Shechtman in 2011 for a work published in 1984 [87]. Quasicrystals are crystalline structures characterized by the lack of spatial translation invariance (or symmetry) and the existence of an infinite set of translations which leave the network almost invariant [87–89]. Related to the quasicrystal is another notable example of quasiperiodic structure, the *Penrose tiling* [90]. Moreover, quasiperiodic objects have been studied and found applicability in several areas of mathematics [91–93], computer science [94, 95], and cryptography [96].

In mathematics it is well known the class of *quasiperiodic* functions of a single real variable. Moreover, there exists the *quasiperiodic* sequence. Both of these two cases will be studied in this thesis, with particular focus on the latter. We recall here the definition of the former case, however it will be discussed in greater details within Sec.5.3 and Appendix B.1. We introduce here the latter case, since it will be the major focus of this work.

The case of quasiperiodic continuous functions of a single real variable $\varphi : \mathbb{R} \longrightarrow \mathbb{R}$ is of great importance in the whole field of mathematical physics; for example, the quasiperiodic oscillations on D-dimensional tori for the Kolmogorov-Arnol'd-Moser (KAM) theorem [97, 98]. The definition of a quasiperiodic continuous functions is

Definition. *Let $\varphi : \mathbb{R} \longrightarrow \mathbb{R}$ be a real continuous one-dimensional function. For φ being quasiperiodic implies that there exists continuous function $F : \mathbb{R}^D \longrightarrow \mathbb{R}$ with $D \geq 2$ periodic in every component with period 2π such that*

$$\varphi(t) = F(\omega_1 t, \ldots, \omega_D t) \ , \quad t \in \mathbb{R} \ , \tag{2.12}$$

for D frequencies $\Omega = (\omega_1, \ldots, \omega_D)$ incommensurate between each other

$$\mathbf{k} \cdot \Omega = k_1\omega_1 + \cdots + k_D\omega_D \neq 0 \ , \quad \forall \ \mathbf{k} \ \in \mathbb{Z}^D \ , \quad \mathbf{k} \neq 0 \ . \tag{2.13}$$

More technical details about this function will be given in Appendix B.1, while in Sec.5.3 we will consider a particular case of this function class as the driving of the Anderson chain. Spatially quasiperiodic sequences are defined as following

Definition. *A real sequence $\{\epsilon_l\}_{l\in\mathbb{Z}} \subset \mathbb{R}$ is quasiperiodic if for every $\delta > 0$, there exists $T = T(\delta) > 0$ such that for all $l \in \mathbb{Z}$ we have*

$$|\epsilon_{l+T} - \epsilon_l| < \delta \ . \tag{2.14}$$

We call the sequence of vectors $\{\epsilon_\ell\}_{\ell\in\mathbb{Z}^D} \subset \mathbb{R}$ quasiperiodic if for $i = 1, \ldots, D$ and for every $\delta > 0$, there exists $T_i = T_i(\delta) > 0$ such that for all $\ell \in \mathbb{Z}$

$$|\epsilon_{\ell+T_i\cdot\mathbf{e_i}} - \epsilon_\ell| < \delta \ . \tag{2.15}$$

where $\mathbf{e_i}$ is the i-th element of the canonical basis of $\mathbb{R}$.

The incommensurability is not explicitly contained in this definition. Instead, the definition highlights the approximated translation invariance Eq.(2.14). However, the incommensurability appears in the general construction of such potentials. Let's consider a real periodic continuous function f of period T restricted to the lattice $\mathbb{Z}$, renormalized to period 1, and then modulate with an irrational parameter $\alpha \in \mathbb{R} \setminus \mathbb{Q}$

$$f(\cdot) \longmapsto f(T\cdot) \longmapsto f(T\cdot)_{|l\in\mathbb{Z}} \longmapsto f(\alpha T\cdot)_{|l\in\mathbb{Z}} \ , \tag{2.16}$$

Since the function f is continuous and periodic, it is bounded $|f(x)| \leq M < +\infty$ for every $x \in \mathbb{R}$. The sequence generated in Eq.(2.16) is therefore bounded and of a given strength.

It naturally follows to include a parameter $\lambda > 0$ to control this strength the sequence amplitude

$$\epsilon_l = \lambda f(\alpha T l) \ , \quad l \in \mathbb{Z} \ , \quad \alpha \in \mathbb{R} \setminus \mathbb{Q} \ . \tag{2.17}$$

Due to the density of the irrational numbers in the real numbers and the continuity of the real function f, the inequality Eq.(2.14) holds and the sequence defined in Eq.(2.16) is quasiperiodic. The key ingredient for the quasiperiodicity of this potential is the irrational number α: since the period of the potential $1/\alpha$ is irrational and therefore incommensurate with the lattice spacing $\Delta l = 1$. Other quasiperiodic sequences are the *Cantor* sequence [99], the *Fibonacci* sequence [100–102] or the *Rudin-Shapiro* one [103, 104].

Let's consider the linear Schrödinger model Eq.(2.4), with an onsite energy sequence of the form Eq.(2.17). For the crystalline case $\lambda = 0$, the energy spectrum obtained from the associated eigenvalue problem Eq.(2.6) consists of a single band. For $\lambda \neq 0$, if the parameter α is rational $\alpha = p/q$ (p and $q \neq 0$ integers), the lattice is periodic and the energy spectrum splits into q sub-bands. In the incommensurate limit $|q| \longmapsto +\infty$, the number of sub-bands increases and, since the total spectral width is not increasing, the sub-band lengths decay to zero. Consequently, the spectrum becomes more and more fragmented. For α irrational, it is then legitimate to expect a discrete spectrum, though not dense in any interval as for the disordered case, since the gaps opened are, in general, sets of a non-empty interior. For specific choices of the function f, spectral properties and features of the dynamics of the single particle have been analytically and numerically studied. We will now introduce one particular case, also discussed in the next chapter.

One of the most important cases of this class of potentials is defined by choosing the *cosine* function in Eq.(2.16). This specific case, also called *Harper* or *Aubry-André* potential is then defined as

$$\epsilon_l = \lambda \cos(2\pi(\alpha l + \theta)) \ , \tag{2.18}$$

where $\alpha \in \mathbb{R} \setminus \mathbb{Q}$ is the *incommensurate parameter*, $\theta \in \mathbb{R}$ is a phase shift and the parameter $\lambda > 0$ controls the potential strength. This onsite potential has been introduced by Harper in 1955 [85]. It came as a surprise that in 1980 Aubry and André predicted that such quasiperiodic model allowed a Metal-Insulator transition (MIT) between metallic and insulating regime through a critical value [86]. This MIT is tuned by the strength λ of the cosine function and separates a metallic phase for $\lambda \in]0, 2[$ from an insulating phase for $\lambda \in]2, +\infty[$. This analytical result has been introduced thanks to a duality principle, relating states and spectrum in direct and Fourier space. This very principle prevents the appearance of mobility edges. The transition between extended or localized states of the Aubry-André model is not dependent on the eigenenergy but only on the potential strength λ. Much attention has been dedicated to the spectrum of this model, from topological structure [105], Lebesgue and fractal measures [106–111] and its spectral decomposition [112–114]. In Fig.2.5 we show the participation number P versus the potential strength λ in either the real and momentum spaces. The figures are mirror images of each other and reflects the Aubry–André duality.

An interesting extension of the duality principle has been proposed in [116], for an onsite potential defined as a finite sum of Aubry-André potentials of higher harmonics in a lattice with long range hopping. Other studies have been dedicated to the transition between metallic and insulating regimes in models which do not posses any self duality feature. The lack of such principle usually leads to a energy dependent metal insulator transition in the energy spectrum, called *mobility edge*. An example of mobility edge transition is a bichromatical quasiperiodic lattice [117, 118]. Moreover, the lack of self duality makes the model's analysis most likely to be exclusively numerical. Even if the mobility edge is frequent for quasiperiodic model, this is not the case for every quasiperiodic lattice. For

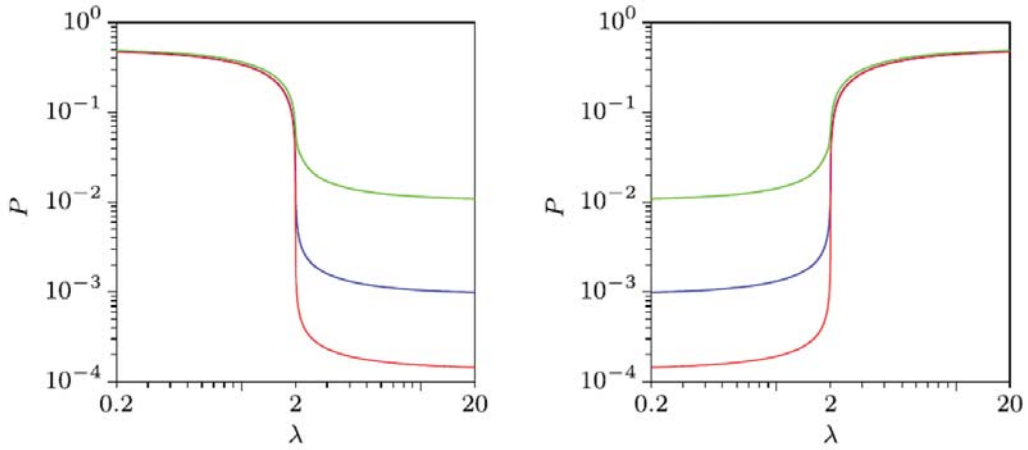

Figure 2.5: Left: participation number P versus the potential strength λ in the real space. Right: participation number P versus the potential strength λ in the momentum space. Both figures, system size is $N = 144$ (green), $N = 1597$ (blue) and $N = 10946$ (red). Figure taken and re-elaborated from [115].

example, a Fibonacci sequence based quasiperiodic potentials kept the system at the critical point [119, 120]. Another quasiperiodic chain shows that the localized regime could be maintained irrespective of the potential strength [121,122]. In this regard, an extended dual transformation, based on Aubry duality principle, allowed to show the dynamical localization (localization in the momentum space) for a particle evolving in a rotor. Quasiperiodic potentials have been proposed for the study of chains that aimed to described the dynamics of the DNA chains [65]. A recent study of two interacting particles in the Aubry-André model established the appearance of metallic correlated bound states deep in the insulating regime for a single particle [123].

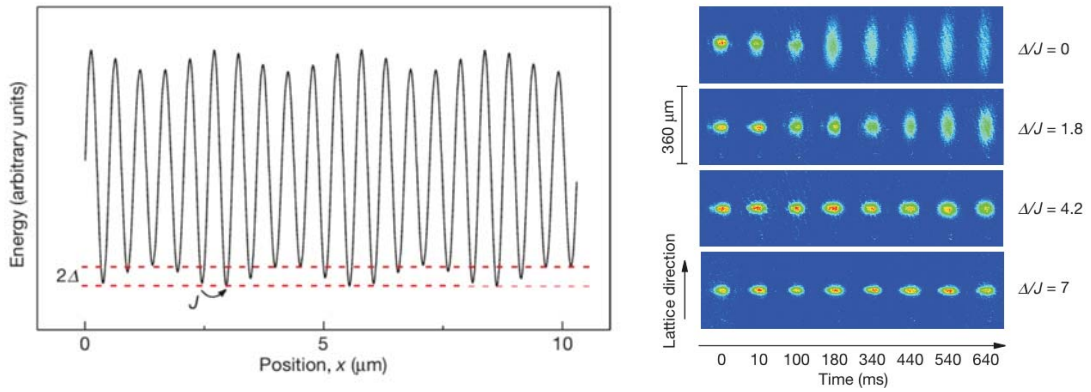

Figure 2.6: Left: the quasiperiodic potential experiemntally realized. J is the hopping strength between nearest-neighbor sites while Δ is the onsite energy shift induced by the secondary lattice. Right: time evolution of the BEC after the release of the harmonic confinement. We observe diffusion for the first two cases and localization for the third and the fourth cases. Figure taken from [20].

Experimental studies on light propagating through optical waveguide networks [124] and ultracold atomic clouds expanding in optical potentials [20] successfully tested the MIT within the Aubry-André model. The experiment shown in Fig.2.6 refers to [20], and it consists in a cloud of cold potassium-39 atoms with the s-wave scattering length turned to

(almost) zero by the use of the Feshbach resonance [125, 126]. It results a non-interacting BEC kept confined in a subregion of the optical lattice by a harmonic confinement. The quasiperiodic potential is created by the superposition of two counter-propagating lasers of wavelength respectively of $\lambda_1 \approx 1.032$ nm and $\lambda_2 \approx 862$ nm. In Fig.2.6 - right, the time evolution of the BEC after the release of the harmonic confinement is shown for four different settings. The first two ($\Delta/J = 0$ and $\Delta/J = 1.8$) belong to the metallic regime $\Delta/J \leq 2$, while the the last two ($\Delta/J = 4.2$ and $\Delta/J = 7$) belong to the insulating regime. Localization is observed for the latter cases, while for the former ones spread along the lattice, confirming the MIT transition of the Aubry-André chain. The flexibility in the choice of potentials makes these optical lattices ideal benchmark for the experimental realization of other quasiperiodic potentials. Discussion about possible experimental observation of the mobility edge in the bichromatical lattice can be found in [118]. At the same time these systems have finite size, and have unavoidable precision limitations on the generated potentials [127, 128]. Desired effects like the MIT or mobility edges are therefore needed only up to that precision, and only to be observable on these length scales.

2.5 Summary and Discussions

In this introductory chapter we discussed basic notions and fundamental results we will use along the thesis. We first introduced the wave propagation in continuous and discrete systems. We introduce the tight-binding model and the discrete Schrödinger equation and the Bloch waves for waves in periodic media. We then focus on the breaking of spatial periodicity and the arising of wave localization phenomena. After an overview of Anderson localization, we have introduced the main concept of the thesis: the *quasiperiodicity*. The last part of this introduction has been dedicated to discussing fundamental knowledge and applications of this class. The beginning of the next chapter naturally continues this introduction, since there we will discuss one of the most renown quasiperiodic model: the *Aubry-André* model.

CHAPTER 3

Wave Localization in Quasiperiodic Potentials

In this chapter we first discuss more in detail certain properties of the Aubry-André model mentioned in the former section. In order to reproduce the self similar nature of the Aubry-André spectrum, we propose an iterative construction of quasiperiodic potentials from sequences of potentials with increasing spatial period. At each finite iteration step the eigenstates reflect the properties of the limiting quasiperiodic potential properties up to a controlled maximum system size. We then observe approximate metal-insulator transitions (MIT) at the finite iteration steps. We also report evidence on mobility edges which are at variance to the celebrated Aubry-Andre model. The dynamics near the MIT shows a critical slowing down of the ballistic group velocity in the metallic phase similar to the divergence of the localization length in the insulating phase.

This chapter is based on the following publication:

- **C. Danieli**, K. Rayanov, B. Pavlov, G. Martin and S. Flach, "*Approximating metal-insulator transitions*", Int. Journal of Mod. Phys. B **29**, 1550036 (2015).

3.1 Introduction

In the introduction we have reviewed several fundamental concepts of the field of wave localization in localizing potentials, with main focus on Anderson localization, quasiperiodic lattices and the Aubry-André model. The topic is still very open and unrestrained of new results. As an example, we discuss the construction of localizing potentials which offer designable localization properties. In this chapter we propose a recursive construction of a new class of quasiperiodic potentials that exhibit an approximated energy dependent metal insulator transition. However, in the first part of the chapter we discus more in detail the Aubry-André model.

This Hamiltonian model, the tight-binding model Eq.(2.6) defined with the quasiperiodic potential Eq.(2.18) that we call Aubry-André model, has been introduced by Harper in the 1955 to study the problem of crystal electrons in the presence of a magnetic field [85]. In the scientific community, this system is also renown as the *Ten Martini* problem [105] and the *Almost Mathieu* operator [110, 112, 113]. Several works and significant progresses have been recently made in the study of this model, from the analytical to the numerical point of view. Nowadays, the Aubry-André model can be considered one of the main example in the condensed matter theory where several properties could be exhaustively stated and proved analytically.

One of the main Aubry and André contribution to the understanding of the Harper model is the so called *duality principle* [86]. Such fundamental principle allowed to show the Metal-Insulator transition between insulating and metallic regime in the energy spectrum via a critical value. Several other quasiperiodic models show a similar transitions between insulating and metallic regimes. However their transition consist in an energy dependent transition (called mobility edge) and in general these models lack of a duality principle. Of course the feature of the transition is not necessarily connected to the quasiperiodicity, since there exists examples of quasiperiodic chains that are kept at the critical transition value [119, 120], or localized irrespective to the potential strength [121, 122]

Several analytical studies have been done on the Aubry-André model during the last years. Particular attention has been given to the model's spectral properties. Its spectrum has indeed revealed to be a very intriguing mathematical object, where a number of its properties have been showed analytically. Among these properties, it has been showed that, for any potential strength λ and incommensurate parameter $\alpha \in \mathbb{R} \setminus \mathbb{Q}$ of Eq.(2.18), the energy spectrum of the Aubry-André model is self-similar, meaning that it is formed by a finite number of bands that are gaped, and each sub-bands is gaped, and this process follows *ad infinitum*, similarly to the celebrated Cantor set.

The self-similarity of the spectrum of the Aubry-André model inspired the project discussed in this chapter. Here we present a systematic and constructive way to approximate a quasiperiodic potential by a periodic one. Each approximation is defined both by its period and by the convergence criteria of the amplitude sequence of higher harmonics. This flexibility allows us to obtain a wide variety of quasiperiodic potentials which can be expected to exhibit the above phenomena. In addition the experimentally relevant length scale can be easily taken into account by the corresponding periodic approximation of a quasiperiodic potential.

The chapter is structured as follows: in Sec.3.2 we discuss more in depth the Aubry-André model, we will introduce the duality principle and list and briefly comment on its properties, specifically about spectral properties and wave packet spreading. In Sec.3.3 we introduce the construction principle for the new class of quasiperiodic potentials. We discuss the main properties of localized and extended states for particular amplitude sequences. Finally in Sec.3.4 we conclude and summarize the results.

3.2 Aubry-André model

Consider the $D = 1$ dimensional discrete Schrödinger operator $H : \ell^2(\mathbb{Z}) \longrightarrow \ell^2(\mathbb{Z})$, also known as Aubry-André model, defined by

$$(H\psi)_l := \epsilon_l \psi_l + \psi_{l+1} + \psi_{l-1} \ , \quad l \in \mathbb{Z} \ ; \tag{3.1}$$

discussed in Sec.2.4 of the introduction defined with a quasi-periodic potential

$$\epsilon_l = \lambda \cos(2\pi(\alpha l + \beta)) \ , \quad \alpha \in \mathbb{R} \setminus \mathbb{Q} \ , \tag{3.2}$$

with a positive real strength $\lambda > 0$, $\beta \in \mathbb{R}$, and irrational α. As formerly introduced, one property very unique of this model is the *self duality*. This principle is based on the idea of mapping the model from the real space to the momentum space via the Fourier expansion. The expansion

$$\psi_l = e^{i2\pi kl} \sum_m f_m e^{i2\pi m(\alpha l+\beta)} \tag{3.3}$$

maps the Aubry-André model equation in the real space

$$i\dot{\psi}_l = \lambda \cos(2\pi(\alpha l + \beta))\psi_l + \psi_{l+1} + \psi_{l-1} \ , \tag{3.4}$$

to the equation in the momentum space

$$i\dot{f}_m = 2\cos(2\pi(\alpha m + k))f_m + \frac{\lambda}{2}(f_{m+1} + f_{m-1}) \ . \tag{3.5}$$

The transformation Eq.(3.3) maps the hopping of Eq.(3.4) to the onsite energy of Eq.(3.5). Analogously, the onsite energy of Eq.(3.4) is mapped into the hopping of Eq.(3.5). Therefore, the transformed Aubry-André model Eq.(3.5) is of analogous form of the original one Eq.(3.4). It follows that the Aubry-André model is *self dual* under the Fourier transform.

Up to the phase shifts of the onsite energy β and k, the two equations are exactly the same when the potential strength λ is equal to 2. It is commonly called *critical value*. Aubry and André first and several other later showed analytically and numerically that at the critical value $\lambda = 2$ the model exhibits a transition between a metallic phase for $\lambda \in]0, 2[$ and an insulating phase when $\lambda \in]2, +\infty[$. In the insulating regime, the model behaves as the Anderson case. It has been shown in [86] that, for any given λ in the insulating phase, all normal modes decay exponentially in space as $e^{-l/\xi}$, with the localisation length $\xi = 1/\ln(\lambda/2)$ being independent of the eigenenergy. The eigenenergy spectrum $\sigma_\lambda(\alpha, \beta)$

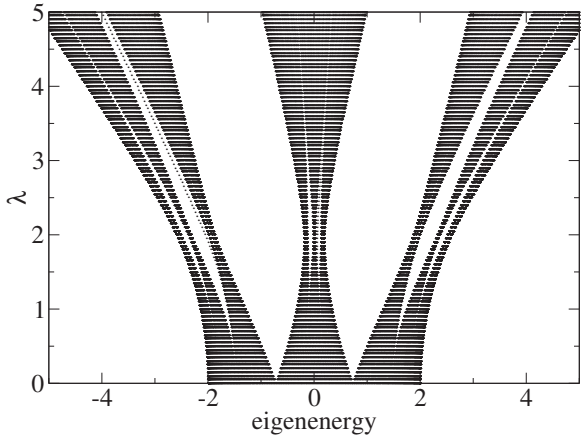

Figure 3.1: Spectrum σ_λ of the Aubry-André model when $\alpha = (\sqrt{5} - 1)/2$.

of the Aubry-André model has a Cantor set structure for all $\lambda \neq 0$ [105]. When the incommensurate parameter is chosen as the golden mean $\alpha = (\sqrt{5} - 1)/2$, the spectrum exhibits a self-similiar structure which consists of three bands which again each consists of three sub-bands and so forth (Fig. 3.1). The self-similiar structure does not depend on β. The Lebesgue measure [106] can be found analytically by the formula

$$\mu(\sigma_\lambda) = 2|2 - |\lambda|| \ .$$

while the spectral decomposition has been discussed in [112–114]. The spectrum's fractal dimension has been object of several studies, in particular at the critical value. This dimension is an index for characterizing fractal sets, by relating their distribution in space to

the change in scale. There exist several definition of fractal dimension, and in the following we will refer to the so-called *box-counting* dimension (detail can be found in [99, 129]). For $\lambda \neq 2$ in 1986 Tang *et al.* [107] showed that the fractal measure is 1. Instead, at the critical value $\lambda = 2$, former studies [107–109] show that the fractal dimension is 0.5. Note that our working golden mean value for α is covered by the above statements. Latter works [110,111] show that 0.5 is in fact an upper bound, and find classes of irrational numbers α for which the correspondent spectrum's fractal dimension is lower than 0.5. Remarkably, there are much more exact results for the spectral properties of the Aubry-André model as compared to the dynamical properties of wave packet spreading

$$i\dot{\psi}_l = (H\psi)_l \tag{3.6}$$

where the numerical results known are [111, 127, 128]. Let's consider a single site excitation for a normalized wave function $\sum_l |\psi_l|^2 = 1$. Its evolution in time leads to a time dependent distribution $n_l(t) = |\psi_l(t)|^2$. The dynamics can be characterized by the second moment $m_2 = \sum_l (l - \sum_k k n_k)^2 n_l$, which in a delocalized regime is expected to grow algebraically in time $m_2 \sim t^\gamma$ with real exponent γ. For the case of the golden mean we can distinguish three different notable spreading regimes [127, 128]:

$$m_2(t) \sim \begin{cases} v_g^2\, t^2 & \text{Ballistic Spreading} \\ Dt & \text{Diffusive Spreading} \\ \xi^2 & \text{Localisation} \end{cases} ,$$

where the coefficients are: the group velocity v_g, the diffusion coefficient D and the localisation length ξ. In particular, spreading is expected to be ballistic in the metallic regime $\lambda < 2$ and diffusive at the critical point $\lambda = 2$ [127, 128]. Other studies [111] showed cases where at the critical value the spreading is slightly sub-diffusive (with $\gamma \lesssim 1$). Further interesting issues concern the connection between the spectral measure, the fractal dimension, temporal correlations, and the diffusive growth [130]. We plot our calculations of the time evolution of the second moment for the different regimes in Fig.3.2.

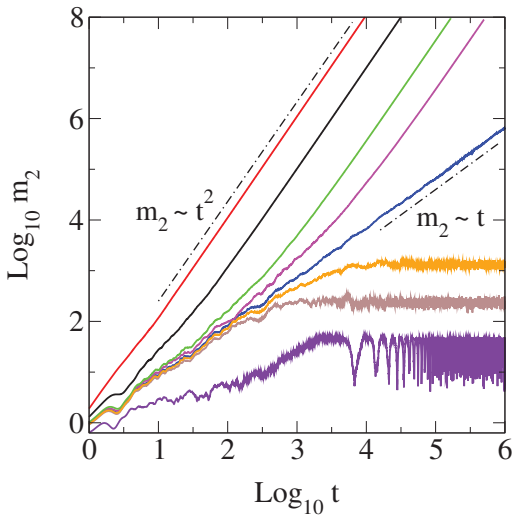

Figure 3.2: The second moment m_2 for a single site excitation as a function of time in a log-log plot. From top to bottom: $\lambda = 0.5$ (red), $\lambda = 1.5$ (black), $\lambda = 1.9$ (green), $\lambda = 1.97$ (orange), $\lambda = 2$ (blue), $\lambda = 2.05$ (brown) and $\lambda = 2.5$ (violet). The dashed-dotted lines indicate power laws $m_2 \sim t$ (diffusive) and $m_s \sim t^2$ (ballistic). Here $\alpha = (\sqrt{5} - 1)/2$ and $\beta = 0$.

We see that for $\lambda = 2$ spreading appears to be diffusive in agreement with [127, 128]. However we can not exclude a slightly subdiffusive spreading with $\gamma \approx 0.95$ as reported in Ref. [111]. We also confirm the predicted ballistic asymptotics in the metallic regime and localisation in the insulating regime. However, we also observe a diffusive transient in these regimes, which becomes longer the closer one gets to the critical point. We compute the

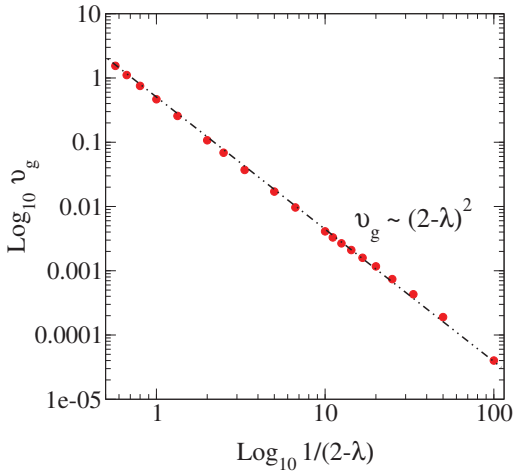

Figure 3.3: The dependence of the group velocity v_g on $1/(2-\lambda)$ in the metallic phase in a log-log plot. The symbols are the actual computed values, the dashed line corresponds to the law $v_g \sim (2-\lambda)^2$.

group velocity v_g which is given by the square root of m_2 up to a constant prefactor, and plot it in Fig.3.3. We find that it vanishes at the critical point as $v_g \sim (2-\lambda)^2$.

It remains an intriguing task to explain these spreading regimes in their relation to the Cantor spectrum of the model. This concerns in particular the crossover time τ_λ, the critical exponent for v_g, and the question why spreading into a large but finite localization volume in the insulating regime happens to be diffusive and not ballistic, as for one-dimensional uncorrelated disorder (e.g. [131]). These observations may be rather special features of the highly symmetric Aubry-André model which enjoys duality.

3.3 Approximating Metal-Insulator Transition - A Cantor-like Construction of a Class of Quasiperiodic Potentials

We now construct quasiperiodic potentials in a systematic way approximating them by periodic potentials at each iteration step. The standard construction of a 1/3 Cantor set (cut out the middle third of an interval, then repeat with the reamining subintervals ad infinitum) gives a set of measure zero and nonzero Hausdorff dimension $\frac{\log 2}{\log 3}$. Here we modify this procedure for the eigenenergy spectrum effectively by stretching and changing the cutting ratio. This is all achieved by defining sequences of periodic potentials with increasing spatial period. For simplicity we shall start with an example which has a three-band structure (where each band again subdivides into three sub-bands etc) similar to the golden mean case of the Aubry-André spectrum before we generalize.

3.3.1 The Scheme

Consider a sequence of discrete periodic functions $E_k(l)$ with $k = 1, 2, 3, ...$ Each function is periodic with spatial period $L_k = 3^k$: $E_k(l + L_k) = E_k(l)$. The function E_1 has period

$L_1 = 3$ and it is defined for $l \in \mathbb{Z}$ and for the real positive value a_1

$$E_1(l) := \begin{cases} -a_1 & l = 3m \\ 0 & l = 3m+1 \\ +a_1 & l = 3m+2 \end{cases} \quad , \quad m \in \mathbb{Z}$$

and it has the schematic form represented in Fig. 3.4

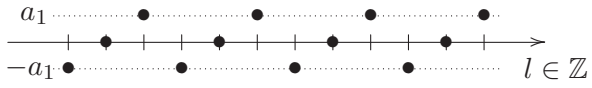

Figure 3.4: Schematic picture of the potential E_1, for a real positive value a_1

The second function E_2 has period $L_2 = 9$ and it is defined for $l \in \mathbb{Z}$ and for the real positive value a_2

$$E_2(l) := \begin{cases} -a_2 & l = 9m + \{0,1,2\} \\ 0 & l = 9m + \{3,4,5\} \\ +a_2 & l = 9m + \{6,7,8\} \end{cases} \quad , \quad m \in \mathbb{Z}$$

and it has the schematic form represented in Fig. 3.5

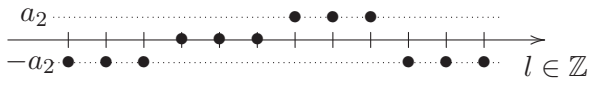

Figure 3.5: Schematic picture of the potential E_2, for a real positive value a_2

Higher order functions $E_k(l)$ are defined along the lattice $l \in \mathbb{Z}$ in a similar way and are characterized by the corresponding real positive amplitude a_k:

$$E_k(l) := \begin{cases} -a_k & \text{if } l = 3^k m + q \\ 0 & \text{if } l = 3^{k-1}(3m+1) + q \\ +a_k & \text{if } l = 3^{k-1}(3m+2) + q \end{cases} \quad , \quad m \in \mathbb{Z}$$

with $0 \le q \le 3^{k-1} - 1$, and their schematic form is represented in Fig. 3.6. Now we consider

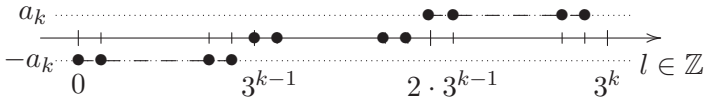

Figure 3.6: Schematic picture of the potential E_k for a real positive value a_k

the superposition of all $E_k(l)$ for all $1 \le k \le K$:

$$\epsilon_{l,K} := \lambda \sum_{k=1}^{K} E_k(l) \ , \quad \forall l \in \mathbb{Z} \ , \tag{3.7}$$

where $\lambda > 0$ is again the potential strength parameter. The potential $\epsilon_{l,K}$ is periodic with period L_K. For example, for $K = 2$ we obtain a potential of period $L_2 = 9$: $\epsilon_{l,2} = E_1(l) + E_2(l)$ with the spatial profile represented in Fig. 3.7

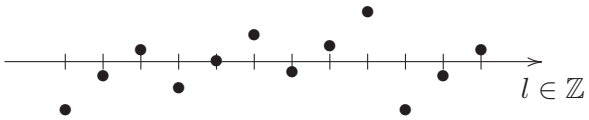

Figure 3.7: Schematic picture of the potential $E_1 + E_2$ for the real positive values a_1 and a_2

The same construction could be done for sequences of periodic functions $E_{k,s}(l)$ with $k = 1, 2, 3, ...$ of spatial period $L_{k,s} = s^k$ with $s \in \mathbb{N}$: $E_{k,s}(l + L_{k,s}) = E_{k,s}(l)$. We can simplify notations by using the definition $[l]_m \equiv l \; mod \; m$ to arrive at

$$E_{k,s}(l) = \left(\left\lfloor \frac{[l]_{s^k}}{s^{k-1}} \right\rfloor - \left\lfloor \frac{s}{2} \right\rfloor \right) a_k =: \phi_{k,s}(l) a_k \; , \quad \forall l \in \mathbb{Z} \; . \tag{3.8}$$

where $\lfloor . \rfloor$ denotes taking the integer part of a real number. The final expression for the potential $\epsilon_{l,K}$ is

$$\epsilon_{l,K} := \lambda \sum_{k=1}^{K} \phi_{k,s}(l) a_k \; , \quad \forall l \in \mathbb{Z} \; , \tag{3.9}$$

where $\{a_k\}_{k=1}^K$ is the generating sequence of the potential and $\{\phi_{k,s}(l)\}_{k=1}^K$ the partitioning sequence.

In the absence of any potential ϵ_l the spectrum of the operator in Eq.(3.1) is given by one band $\sigma = 2 \cos p$ where p is a Bloch wave number. For $K = 1$ and in the case $s = 3$, the spectrum splits into three bands which are separated by two gaps. The first step in the above construction therefore cuts two segments out of the one band spectrum. At the next step of the approximation $K = 2$, the spatial period $L_2 = 9$, and the spectrum consists now of 9 bands and 8 gaps. Therefore each of the three bands of the $K = 1$ spectrum is split into three narrower ones, with the new subgaps removing parts of the $K = 1$ bands. At the same time the bands edges may also shift, thus we obtain a Cantor-like iterative construction.

3.3.2 The Quasiperiodic Limit

We now push the iterative construction to its limit by extending (3.9) to an infinite sum

$$\epsilon_l := \lambda \sum_{k=1}^{+\infty} \phi_{k,s}(l) a_k \; , \quad l \in \mathbb{Z} \; . \tag{3.10}$$

The boundedness of this sum depends on the convergence properties of the generating sequence. We make the following definition: a sequence $\{\epsilon_l\}_{l \in \mathbb{Z}}$ is *quasiperiodic* if for every $\delta > 0$, there is $T = T(\delta) > 0$ such that for all $l \in \mathbb{Z}$ we have $|\epsilon_{l+T} - \epsilon_l| < \delta$. We have the following:

Lemma. Let's consider a family $\{\{\epsilon_l^k\}_{l \in \mathbb{Z}}\}_{k=0}^{+\infty}$ of potentials, and suppose that for each k the sequence $\{\epsilon_l^k\}_{l \in \mathbb{Z}}$ is periodic with period L_k and the tails satisfy

$$\lim_{N \to \infty} \sup_{l \in \mathbb{Z}} \sum_{k=N}^{\infty} \epsilon_l^k = 0 \; .$$

Then the sequence $\{\tilde{\epsilon}_l\}_{l \in \mathbb{Z}}$ defined by the sum

$$\tilde{\epsilon}_l = \sum_{k=0}^{\infty} \epsilon_l^k \tag{3.11}$$

is quasiperiodic.

The proof is simply to observe that any partial sum $\sum_{k=0}^{N} \epsilon_l^k$ is periodic with period $T_N := lcm(L_1, L_2, \ldots, L_N)$ (here lcm means least common multiple) and that the tail sums $\sum_{k=N}^{\infty} \epsilon_l^k$ are uniformly small, independent of l. So, for a given $\delta > 0$, we choose $N = N(\delta)$ such that

$$\sup_{l\in\mathbb{Z}} \sum_{k=N+1}^{\infty} \epsilon_l^k < \frac{\delta}{2} \ .$$

It follows that $\forall l \in \mathbb{Z}$ we have

$$\begin{aligned} |\tilde{\epsilon}_{l+T_N} - \tilde{\epsilon}_l| = \Big| &\sum_{k=0}^{N} \epsilon_{l+T_N}^k + \sum_{k=N+1}^{+\infty} \epsilon_{l+T_N}^k \\ &- \sum_{k=0}^{N} \epsilon_l^k - \sum_{k=N+1}^{+\infty} \epsilon_l^k \Big| < 2 \cdot \frac{\delta}{2} = \delta \ . \end{aligned}$$

The property of quasiperiodicity stated above holds for the potential $\tilde{\epsilon}_l$ stated in (3.11). This ends the proof of the lemma.

As a direct corollary we see that the potential defined by (3.10) is quasiperiodic. Thus the above class of potentials, which is defined by its generating sequence $\{a_k\}_{k=1}^{+\infty}$ and the choice of the integer s of the partitioning sequence $\{\phi_{k,s}(l)\}_{k=1}^{+\infty}$, is quasiperiodic.

3.3.3 Numerical Results

In this section, we analyze a particular case of the potentials Eq.(3.9), defined by the geometric sequence $a_k = \mu^k$ for a real value $\mu \in]0, 1[$ and $s = 3$

$$\epsilon_{l,K} := \lambda \sum_{k=1}^{K} \phi_{k,3}(l)\mu^k \ , \quad \forall l \in \mathbb{Z} \ . \tag{3.12}$$

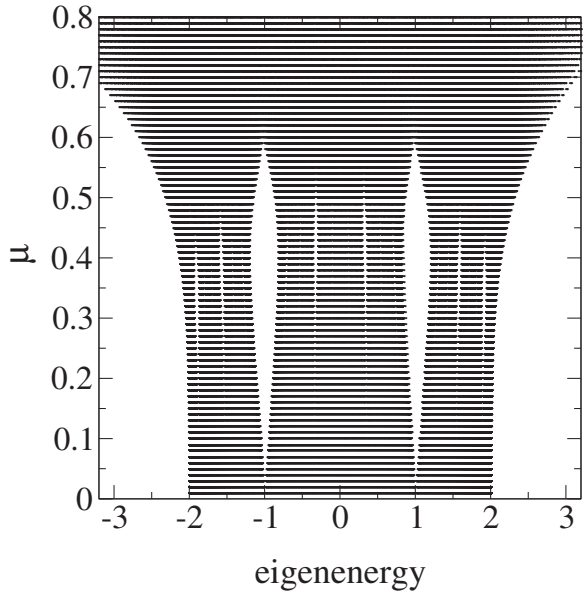

Figure 3.8: The eigenenergy spectrum versus μ. Here $s = 3$, $\lambda = 1$ and $K = 9$.

In Fig. 3.8 we show how the spectrum changes for different potential strength parameter $\mu \in]0,1[$ obtained for $\lambda = 1$. For μ from 0 to 0.5 the width of the spectrum and its sub-band shrinks and then, for $\mu \geq 0.5$ it starts to stretch. A similar effect is seen in the Aubry-André model spectrum around the transition value $\lambda = 2$. To characterize localization of the corresponding eigenstates, we compute the Participation Number $P = 1/\sum_l |\psi_l|^4$ of each eigenmode $(\psi_l)_{l\in\mathbb{Z}}$ and consider the maximum P_{max} for a given μ. We find that P_{max}^{-1}

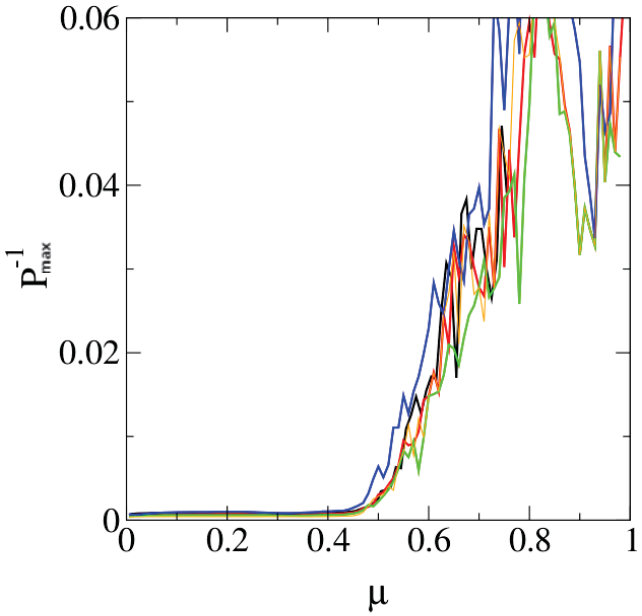

Figure 3.9: Inverse of the largest participation number P_{max} versus μ for $N = 1000, 2000, 3000, 4000, 5000$. Here $s = 3$, $\lambda = 1$ and $K = 9$.

drops down to zero around $\mu = 0.5$ irrespective of the used system size (Fig.3.9). These graphs suggest that at $\mu \leq 1/2$ some eigenstates become extended, and so the insulating regime is lost. Calculations for other $\lambda > 0$ show how this threshold value of the loss of the insulating regime evolves continuously along the set of parameters $(\mu, \lambda) \in]0,1[\times]0,+\infty[$. The outcome is shown in Fig.3.10, where the MIT curve limits the red shaded area in which metallic delocalized states appear.

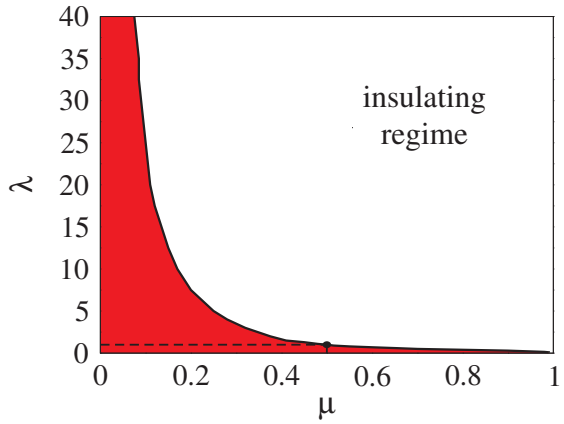

Figure 3.10: Phase diagram of the quasiperiodic chain defined with potential (3.12). The red shaded area corresponds to where extended eigenstates exist. Here $s = 3$ and $K = 9$.

We have observed (not showed here) similar MIT with potential (3.10) defined with different generating sequence a_k (for example, and algebraic sequence $a_k = 1/k^\nu$, for a real value $\nu \in]1, +\infty[$) We compute again for $\lambda = 1$ the Participation Number P of eigenstates for different values $\mu \in]0.25, 0.6[$. Now we consider energy intervals which correspond to various sub-bands of the spectrum (see caption in Fig.3.11). In each of these intervals we choose the largest value of P_{max} and plot its inverse as a function of μ in Fig.3.11. We

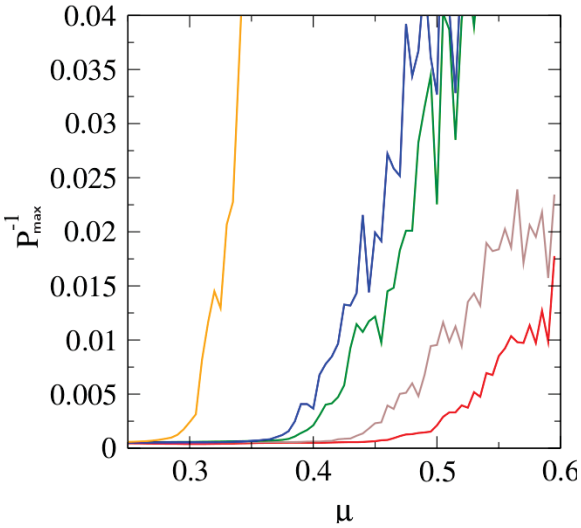

Figure 3.11: Curves of Inverse of the largest Participation Number P_{max} vs $\mu \in]0.25, 0.6[$ for $N = 5000$ for five evergy sub-intervals. From bottom to top: $0 < E < 0.31$ (red), $0.31 < E < 1$ (brown), $1 < E < 1.58$ (green), $1.58 < E < 1.92$ (blue), $1.92 < E < 2.5$ (yellow). Here $s = 3$, $\lambda = 1$ and $K = 9$.

find that the MIT transition values of μ and the sharpness of the transition depend on the chosen energy sub-band. Therefore we observe energy dependent MIT values of μ, i.e. an energy dependent mobility edge Fig.3.12.

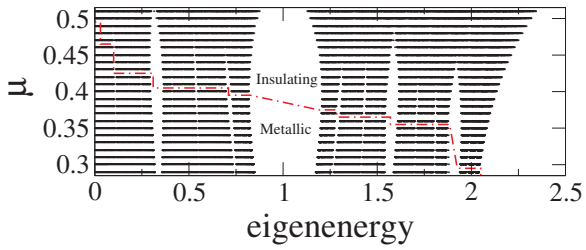

Figure 3.12: Zoom of the eigenenergy spectrum versus μ from Fig. (3.8). The mobility edge is indicated by the thick dashed red line. Here $s = 3$, $\lambda = 1$ and $K = 9$.

Next we study the dynamics of this quasiperiodic chain similarly to the Aubry-André case. We compute the time evolution of the second moment m_2 for a single site excitation for different values μ of the generating sequence in the interval $]0, 1[$ (Fig. 3.13). We find that the basic properties of the Aubry-André model are qualitatively recovered. For small values $\mu \sim 0.05 - 0.1$ the spreading is close to ballistic. An increase of μ changes the dynamics: an increasingly long transient region of slower spreading is emerging. At $\mu \approx 0.5$, the dynamics is close to diffusive up to the largest times of computation. A more in-depth analysis of these dynamical processes can be rather interesting and complicated especially in the parameter region of the mobility edge $0.3 \leq \mu \leq 0.5$ where extended states coexist with localised states with arbitrary large localisation length. For μ closer to 1, the wave

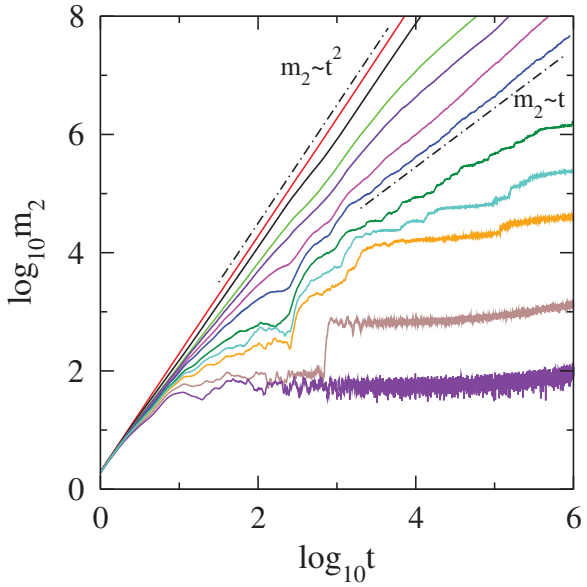

Figure 3.13: The second moment m_2 for a single site excitation as a function of time in a log-log plot. From top to bottom: $\mu = 0.05$ (red), $\mu = 0.29$ (black), $\mu = 0.4$ (green), $\mu = 0.43$ (indaco), $\mu = 0.47$ (magenta), $\mu = 0.5$ (blue), $\mu = 0.55$ (dark green), $\mu = 0.575$ (celeste), $\mu = 0.6$ (orange), $\mu = 0.65$ (brown) and $\mu = 0.7$ (purple). The dashed-dotted lines indicate power laws $m_2 \sim t$ (diffusive) and $m_2 \sim t^2$ (ballistic). Here $s = 3$, $\lambda = 1$ and $K = 9$.

dynamics shows spreading into a finite volume, which imply localisation.

3.4 Summary and Discussions

We obtained an iterative construction of quasiperiodic potentials from sequences of potentials with increasing spatial period. At each finite iteration step the eigenstates reflect the properties of the limiting quasiperiodic potential properties up to a controlled maximum system size. We observe approximate metal-insulator transitions (MIT) at finite iteration steps. We observe mobility edges, at variance to the celebrated Aubry-Andre model. The dynamics near the MIT shows a critical slowing down of the ballistic group velocity in the metallic phase. An important open question concerns the existence of suitable choices of the generating sequence (and even different periodic modulations) so that the model has a duality principle. In particular it would be interesting to find such a special choice which will reobtain the Aubry-Andre case. Further, as observed in [132, 133], the spectral properties of a few-body Hamiltonians may follow from the spectral properties of the Hamiltonian of the one-body case. The presented potential construction algorithm may be of use for future studies concerning the property of self-similarity of the energy spectrum between one and few-body quantum systems.

CHAPTER 4

Quasiperiodicity and Mobility Edges in Flat-Band Topologies

Flat-band topologies are lattices that in the crystalline case, due to local symmetries and macroscopic degeneracies, exhibit one or more dispersionless energy bands. The eigenstates associated with these flat energy bands are compact and localized in space. In this chapter, we discuss the effects of quasiperiodic modulations in certain flat-band lattices. We will first review general features of these networks, and a technique that rotates flat-band lattices into lattices of Fano defects. We will then introduce an Aubry-André-type of spatial modulation. The Aubry-André duality principle jointly with the rotation technique allow to a precise engineering and fine tuning of mobility edges. We obtain analytic expressions for singular mobility edges for two flat-band lattice examples. In particular, we engineer cases with arbitrarily small energy separations of mobility edge, zeroes, and divergencies.

This chapter is based on the following publication:

- **C. Danieli**, J. D. Bodyfelt and S. Flach, "*Flatband engineering of mobility edges*", Phys. Rev. B **91**, 235134 (2015);
- J. D. Bodyfelt, D. Leykam, **C. Danieli**, X. Yu and S.Flach, "*Flat bands under correlated perturbations*", Phys. Rev. Lett. **113**, 236403 (2014).

4.1 Introduction

As discussed in Sec.2.2 of the introduction, the crystalline case of a lattice is solved in a Bloch wave basis, which yields a decomposition of the linear spectrum into spectral bands. The number and the nature of the bands, their multiplicities, and the characteristics of the associated eigenmodes depend on the model's spatial topology. In this chapter we will discuss a particular topology class, where the band decomposition is characterized by the existence of one or more horizontal (and thus, "*flat*") bands.

Flat-bands are macroscopically degenerate spectral bands that occur in crystalline lattices. The origin of these bands is local symmetry and the consequent destructive interference that suppresses transport of the Bloch waves along the lattice. The modes of the flat (or dispersionless) bands are usually compact localized states (CLS), *i.e.* modes with nonzero amplitude only at a finite number of lattice sites. There exist flexible approaches to design flat-band lattices in a variety of dimensions [134–137], which can support new topological phases [138], and even model the fractional quantum Hall effect resulting from flat-band degeneracies of electronic Landau levels interacting within a magnetic field [139]. Moreover, in recent studies the presence of a disordered potential [140, 141], nonlinearity [142], and magnetic field [143, 144] have been considered.

Well-known within condensed matter, flat-band lattices have gained great interest in the scientific community, due to theoretical advancements, applications for modeling of natural systems, and experimental realizations. The *cross-stitch* lattice (see Sec.4.3.3) has been used as a model for DNA transport [145–148]. Experimentally, flat-band topologies have been realized in optical lattices [149–151], ultra cold atomic gases [152, 153], trapped ions, [154], Josephson junctions [155–157], plasmons [158], lasers [159], and waveguides arrays [160,161].

An innovative procedure to detangle flat-band states from dispersive ones has been recently developed for a certain subclass of lattice models [162]. The detanglement yields dispersive states on a lattice of tight-binding form, while the flat-band states rest on Fano defects (see Sec.4.3.1). In this chapter, we will study specific onsite potential correlations that allow the finding of metal-insulator transition occurring in flat-band lattices under quasiperiodic Aubry-André perturbations.

The chapter is structured as follows: in Sec.4.2 we introduce examples flat-band topologies, discussing their fundamental aspects and features. In Sec.4.3 we discuss the detangling procedure of flat-band lattices, focusing on two particular models (cross-stitch and diamond lattices). We will define the quasiperiodic Aubry-André onsite perturbation, and will highlight the distinct chain correlations. In Sec.4.4, our findings for these two topologies are presented. Where applicable, the exact mathematical expression obtained for the mobility edge is jointly shown with numerically obtained transitions for these particular onsite correlations. Finally, in Sec.4.5 we conclude and summarize.

4.2 Flat-Band Topologies

Let's consider the time-independent quasi one-dimensional Schrödinger equation with nearest-neighbor hopping

$$E\psi_l = \epsilon_l\psi_l - \hat{V}\psi_l - \hat{T}\psi_{l-1} - \hat{T}^\dagger\psi_{l+1} \ . \tag{4.1}$$

For all $l \in \mathbb{Z}$, each component of the vector $\psi_l = (\psi_l^1, \ldots, \psi_l^\ell)^T$ represents a site of a periodic lattice, while the set of sites represented by ψ_l is the l-th unit cell. E is the eigenenergy of the problem. The real $\ell \times \ell$ matrix $\hat{V}$ defines the geometry of the unit cell, while the real $\ell \times \ell$ matrix $\hat{T}$ describes hopping to neighboring cells (as will be clarified below for each model). The $\hat{T}^\dagger$ represents the Hermitian conjugate of the matrix $\hat{T}$. At each of the lattice's i-th leg $\{\psi_l^i\}_l$, an onsite perturbation $\{\epsilon_l^i\}_l$ is defined. The unit cell perturbation ϵ_l of Eq.(4.1) is thus given by the diagonal square matrix $\epsilon_l = \text{diag}\left(\epsilon_l^a, \epsilon_l^b, \ldots, \epsilon_l^\ell\right)$.

The model geometry is contained in the matrices $\hat{T}$ and $\hat{V}$. The dispersion spectrum can be derived in the unperturbed crystalline $\epsilon_l = 0$ via the Bloch solution $\psi_l = \phi_{\mathbf{k}} e^{i\mathbf{k}l}$ for the wave vector $\mathbf{k}$. Eq.(4.1) yields the dispersion relation

$$\begin{aligned} E\phi_{\mathbf{k}} &= (\hat{V} + e^{-i\mathbf{k}}\hat{T} + e^{i\mathbf{k}}\hat{T}^\dagger)\phi_{\mathbf{k}} = B(\mathbf{k})\phi_{\mathbf{k}} \\ \Rightarrow \quad & p(E;\mathbf{k}) \equiv \det[E\ \mathbb{I}_\ell - B(\mathbf{k})] \end{aligned} \tag{4.2}$$

The solution of this linear system yields a **k**-dependent polynomial p of order ℓ in E (ℓ is the number of lattice sites of the unit-cell). Each root of p defines a spectral band, and their union gives the band decomposition of the spectrum. In general, the bands depend on the wave vector **k**. These bands are called *dispersion* bands. If one band is independent of the wave vector **k**, in the Brillouin zone it assumes a constant value. This band is called *dispersionless*, or *flat*. The corresponding eigenmodes to this flat-band energy are usually compact localized states (CLS), *i.e.* modes whose amplitude is nonzero only across a finite number of sites [162]. These compact modes are due to the local symmetries of the lattice topologies and consequent macroscopic degeneracies. We call *Flat-band topology* a lattice model in which in the crystalline case $\epsilon_l = 0$ exhibits *at least* one flat-band in the spectrum. In Fig.4.1, we show some examples of quasi one-dimensional flat band topologies. For each topology, the correspondent band structure is shown.

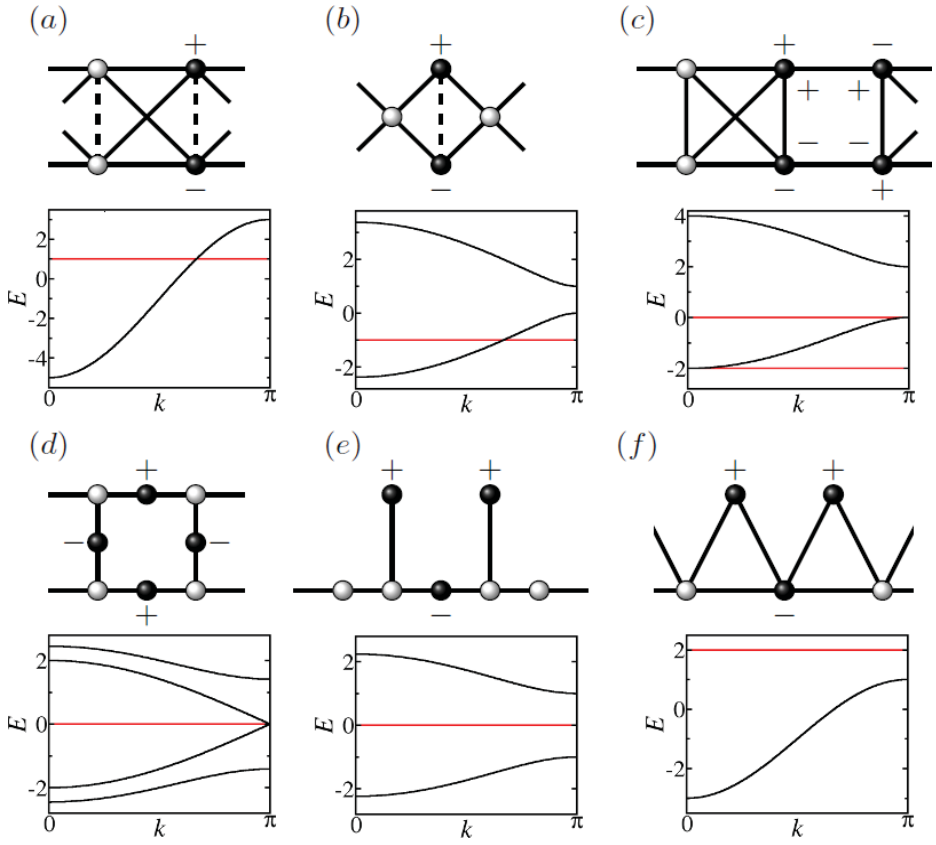

Figure 4.1: Quasi one-dimensional flat-band topologies. Circles denote the lattice sites, solid lines the hopping terms with value one and dashed lines are hopping elements with tunable value t. The black circles indicated the sites of the compact localized state with identical amplitude. The signs refer to the amplitudes. All the other sites have zero amplitudes in these flat band states. The band structure is shown below each lattice. Dispersive bands are denoted in black, flat-bands in red. Onsite energies are all zero, except in (f) where it is set all constant to one. (a) cross-stitch, $t = 1$; (b) diamond, $t = 1$; (c) one-dimensional pyrochlore; (d) one-dimensional Lieb; (e) stub; (f) saw-tooth. Figure taken from Ref. [162].

One possible generalized version of the time-independent Eq.(4.1) in the crystalline case $\epsilon_l = 0$ is a lattice topology with long range hopping

$$E\psi_l = \sum_k \hat{H}_{l-k}\psi_{l-k} \ , \tag{4.3}$$

where $\psi_l = (\psi_l^1, \ldots, \psi_l^\ell)^T$ and the $\ell \times \ell$ matrices satisfy the condition $\hat{H}_{l-k} = \hat{H}_{l+k}^\dagger$. This model equation Eq.(4.3) can either be a flat-band model with finite size interaction (*i.e.* there exists an $1 \geq m < +\infty$ such that $\hat{H}_k = 0$ for $|k| > m$) and with non-local hopping. Multi-dimensional flat-band topologies follow $E\psi_\mathbf{l} = H\psi_\mathbf{l}$ for a vector $\psi_\mathbf{l} = (\psi_\mathbf{l}^1, \ldots, \psi_\mathbf{l}^\ell)^T$. The index $\mathbf{l}$ is a multi-index $\mathbf{l} = (l_1, \ldots, l_D)$ and D is the spatial dimension of the topology. The Bloch representation $\psi_\mathbf{l} = \phi_\mathbf{k} e^{i\mathbf{k}\cdot\mathbf{l}}$ holds for the wave vector $\mathbf{k} = (k_1, \cdots, k_D)$. This expansion yields the band decomposition of the spectrum, which rests in D-dimensional manifolds. An example is the two-dimensional Lieb lattice. In this case, $\mathbf{l} = (l, m)$ and the unit cell is made by three lattice sites $\psi_\mathbf{l} = (a_{l,m}, b_{l,m}, c_{l,m})^T$, as shown in Fig.4.2. The wave component $\mathbf{k} = (k_x, k_y)$ of the Bloch wave gives $\psi_l = \phi_\mathbf{k} e^{i\mathbf{k}\cdot\mathbf{l}} = \phi_\mathbf{k} e^{i(k_x \cdot l + k_y \cdot m)}$ which make the spectral bands to be composed of three surfaces (Fig.4.2 - right). This particular model has two dispersive bands and one flat-band

$$E_\pm(k_x, k_y) = \pm 2\sqrt{\cos^2\frac{k_x}{2} + \cos^2\frac{k_y}{2}}\ , \quad E_{FB} = 0\ . \tag{4.4}$$

The two dispersive bands $E_\pm$ touch each other at $\mathbf{k} = (k_x, k_y) = (0, 0)$. At this point, the two dispersive bands intersect at a singular point, whose neighborhood is called the *Dirac cone*.

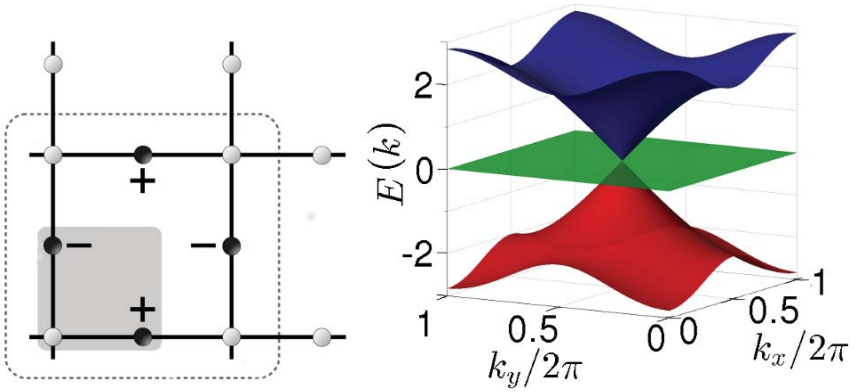

Figure 4.2: Left: The two dimensional Lieb lattice – the grey shaded region indicates the unit cell. The black circles indicated the sites of the compact localized state with identical amplitude. The signs refer to the amplitudes. Right: The band structure. The blue (top) and red (bottom) are dispersive bands, while the central one (green) is flat.

The geometry of the topologies and their local symmetries give rise to the shape and the properties of the compact localized states correspondent to the flat-band(s). In Sec.4.2.1, we will review the most important concepts regarding the compact states of the flat-band lattices. In Sec.4.2.2 we will briefly discuss the effect of the presence of disorder, nonlinearity, and a magnetic field on the diamond chain. In Sec.4.3 we will introduce a coordinate rotation that arises from the presence and the nature of the compact states. We will use this technique in Sec.4.4 to study the effect of a certain type of quasiperiodic perturbation on flat-band topologies.

4.2.1 Flat-Band States, Topology, Class and Open Issues

Compact localized states corresponding to a flat-band energy are states that span over a finite amount of lattice sites of the topology. As seen in Fig.4.1 and Fig.4.2, the shape and the distribution of the compact states vary amongst for different topologies. The relation

between the lattice portion occupied by the compact states, and the minimal unit cell of the topology is one way to classify the flat-band lattices. From [162], we state the following:

Definition. *For a flat-band topology, the class U of one flat-band is the minimum number of unit cells the compact localized states occupies.*

For the one-dimensional topologies shown in Fig.4.1, this definition yields: (a) cross-stitch $U = 1$; (b) diamond $U = 1$; (c) one-dimensional pyrochlore $U = 1$; (d) one-dimensional Lieb $U = 2$; (e) stub $U = 2$; (f) saw-tooth $U = 2$. All these lattices have a single flat-band,while the one-dimensional pyrochlore (c) has two different bands. In this case, both bands have the same U, which defines the model's class. In general for multiple flat-band lattices, each flat-band class needs to be separately specified. This definition can also be used for higher dimensional topologies. For the two-dimensional Lieb lattice in Fig.4.2, according to the definition given above, the class is $U = 3$. However, the definition of flat-band class can be extended to D-dimensional lattices in the following way

Definition. *For a D-dimensional flat-band lattice, the class $\mathbf{U} = (U_1, \ldots, U_D)$ is the minimal number of unit cells occupied by a compact localized state along each of the lattice dimensions.*

According to this definition, the class of the Lieb lattice shown in Fig.4.2 is $\mathbf{U} = (2, 2)$. In general for higher-dimensional case, this definition allows better representation of the extension of the compact states along each of lattice dimensions. Moreover, this class definition is able to represent those topologies with states unbounded in one or more direction, but bounded in the others (*i.e.* there exists $1 \leq i \leq D$ where $U_i = \infty$, while $U_j < \infty$ for $j \neq i$).

Even if the topic of flat-band lattice is not new, it has recently gained attention due to several analytical advancements in certain sub-classes of flat-band models. Particular attention has been given to the nature of the compact localized states and their relation with the spectral properties of the flat-band lattice. Recently, these issues have been approached analyzing the topological invariants of the models's spectrum: Chern number, Berry curvature and Berry phase. These quantities have been regularly used during this last decade to study periodic physical systems [163–167]. An intriguing issue consists in finding examples or families of topologically non-trivial flat-band lattices (non-triviality defined as flat-band with a nonzero Chern number). Haldane in 1988 [168] and later Chen *et. al.* [169] showed that a two dimensional topologically non-trivial flat-band cannot exist with local hopping (finite hopping in Eq.(4.3)). Several works aimed to design long-range hopping lattices with exactly specified compact modes corresponding to nonzero Chern number bands [170, 171]. Recently however, Scaffidi and Simon proposed a topology with an exact topologically non-trivial flat-band with finite range hopping occuring in a finite lattice [172].

Flat-band lattices is an open research area, where several intriguing issues are still unsolved, for the interest of mathematicians, theoreticians and experimentalists - as said, topologically non-trivial flat-band lattices could potentially be new setting for exploring novel states of lights and matter. While these exciting aspects are not the central objects of this chapter, they are worth mentioning, as they are closely related to current hot research topics in condensed matter. We then move back towards fundamental examples of flat-band lattices. However, before to proceed discussing the detangling procedure of the compact localized states and the introduction of quasiperiodic modulations in flat-band lattices, we review some recent results obtained for one of the most important flat-band lattice: the *diamond chain*.

4.2.2 Diamond Chain - Disorder, Nonlinearity and a Magnetic Field

In the last decade, several studies were dedicated to the class of flat-band topologies. However, most of them have been focused on either examples in the presence of external agents, or crafting particular topologies endowed with specific features. Among the different cases, the diamond chain (Fig.4.1 (b) - formal definition in Sec.4.3.3) is one of the most studied flat-band lattice. Despite its class $U = 1$ and its topological triviality, it has heavily used model for testing theories, analyzing perturbations, and performing experiments. This subsection reviews recent studies regarding the diamond chain.

In [142], Leykam *et.al.* discussed the presence of an onsite disorder in the diamond chain. They considered an uncorrelated uniformly distributed random variable $\epsilon_n^i \in [-W/2, W/2]$ with disorder strength $W < +\infty$, which in a one-dimensional tight-binding model yields Anderson localization [2]. Numerical calculations show that the localization length ξ, obtained using an iterative scheme (see Appendix A), exhibits different exponents of the scaling law $\xi(W) \sim W^\gamma$ on/off the flat-band energy $E = E_{FB}$. These scaling exponents are yet unexplained, and remain objects for further investigations.

In the same work, Leykam *et.al.* also discussed the presence of a cubic nonlinearity (as in Eq.(2.3)) in the diamond chain and its interplay with disorder. In the disorder-free pure flat-band energy excitation case, it was shown that the presence of the nonlinearity does not provoke any spreading. For a disordered nonlinear diamond chain (as for the a one-dimensional chain), the nonlinearity introduces hybridization between the localized modes of the linear case, causing different spreading regimes. These different regimes (weak, intermediate and strong) correspond to different strengths of the nonlinear term, and respectively yields complete localization, spreading and self-trapping.

The effects of a uniform magnetic field in the diamond chain were analyzed by Vidal *et.al.* in [143]. The magnetic field is introduced by multiplying the hopping by a phase factor $e^{i\gamma_{i,j}}$ [173] which, for convenience, it can be put in only one hopping per unit cell $e^{i\gamma}$ - Fig.4.3 (a). This yields to the presence of a magnetic flux $\phi = \gamma/2\pi$ in the chain [173].

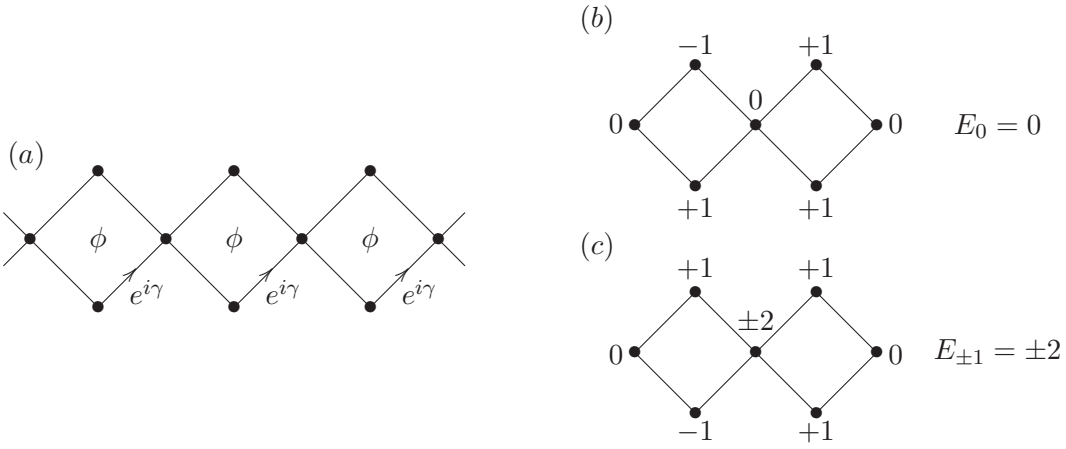

Figure 4.3: (a) Diamond chain under uniform magnetic field. (b) and (c) Compact localized states correspondent to the flat-band energies $E_0 = 0$ and $E_{\pm1} = \pm2$. Figures taken from [143].

The three spectral bands have equations

$$E_n(\mathbf{k}) = 2n\sqrt{1 + \cos(\gamma/2)\cos(\mathbf{k})}\ , \quad n = 0, \pm1\ . \tag{4.5}$$

The flat-band $E_0 = 0$ exists for any value of the flux ϕ. For $\gamma = \pi$, both dispersive bands $E_{\pm 1}$ are independent from the wave vector $\mathbf{k}$. The correspondent states of each band are compact localized states. In the case of the already existent flat-band $E_0 = 0$, the states turns from class $U = 1$ for zero flux $\phi = 0$ to class $U = 2$ - Fig.4.3 (b). The states of the flat-bands $E_{\pm 1} = \pm 2$ are also of class $U = 2$ - Fig.4.3 (c).

We notice how many different features arise from the same flat-band topology. Among the discussed results, several questions remain open from either the spectral or the dynamical point of view. Many questions and issues appear about this class of lattice. One of them (quasiperiodic modulation) will be discussed in the following section. To perform our study, we use an innovative technique to analyze flat-band topologies, which has been introduced by Flach *et.al.* in 2014 [162].

4.3 Rotation of Flat-Band lattices into Lattices of Fano Defects

In this section, we discuss the rotation of a flat-band lattice into a Fano defect lattice. We will discuss existence and properties of the coordinate rotations in relation to the nature of the flat-band states, and we will describe in detail the rotation for the class $U = 1$ lattices in presence of spatial perturbation. Before to proceed, let's motivate the choice of the name *lattices of Fano defects*.

4.3.1 Fano-Anderson Model

The name lattices of Fano defects has been introduced in [162] to call the rotated version of certain flat-band lattices, due to their analogy with the Fano-Anderson model [174]. The Fano-Anderson model consists in the combination of two systems: the first is a one-dimensional linear chain, like Eq.(2.4); the second consists of one or many non-interacting states (called *Fano states*, or also *Fano defects*) coupled to the chain. In Eq.(4.6) we introduce one example of Fano-Anderson model with a single Fano state of energy E_F, represented by the complex field ϕ, hopping to the chain with the coupling constant V

$$\begin{aligned} i\frac{\partial}{\partial t}\psi_l &= \epsilon_l\psi_l + C\left(\psi_{l-1} + \psi_{l+1}\right) + \delta_{n,0}V\phi \\ i\frac{\partial}{\partial t}\phi &= E_F\phi + V\psi_0 \ . \end{aligned} \tag{4.6}$$

A representation of this example of Fano-Anderson model is showed below

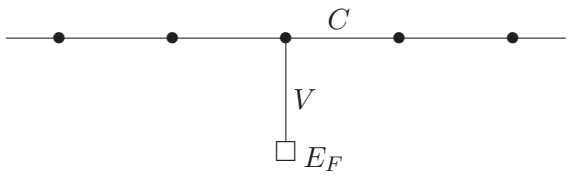

Figure 4.4: One-dimensional Fano-Anderson model with a single Fano defect. C is the hopping of the dispersive chain, E_F is the Fano state energy, and V is the hopping between the Fano state and the dispersive chain.

The coordinate rotation proposed in [162] transforms one-dimensional class $U = 1$ flat-band lattices into one-dimensional tight-binding models, where the compact localized states act like Fano defects. In the crystalline case ($\epsilon_l = 0$ in Eq.(4.1)), the rotated compact

localized states are decoupled from the dispersive chain, and they have Fano energy equal to the flat-band energy. Onsite perturbations of the flat-band lattice ($\epsilon_l \neq 0$ in Eq.(4.1)) couple the Fano defects to the dispersive states.

4.3.2 Detangling Compact Localized States

The basic idea of the detanglement procedure is to map the unit cell(s), expressed in the canonical basis ε, into a basis v made of the model's compact localized states and their orthonormal vectors. This new basis should isolate the compact states from the orthonormal ones, which represent the dispersive states of the crystalline model. From Sec.4.2.1, we learned that a compact state's *class* is the minimum number of unit cells the state occupies. In one-dimensional lattices, the compact localized states are usually (all the known cases) linearly independent for any class $U \geq 1$. For higher dimensional flat-band topologies with $U > 1$, the states can be linearly dependent (for example the $2D$ Lieb lattice - Fig.4.2).

For class $U = 1$, the compact states lie within a single unit cell. Different states then do not overlap (no shared lattice site), therefore they are orthogonal according to the standard scalar product. It follows that the compact states form a complete orthonormal basis for the flat-band. From Eq.(4.1), the flat-band states belong to a ℓ-dimensional vector space $V \simeq \mathbb{R}^\ell$ (ℓ is the number of sites per unit cell). The new basis v of V then spans vectors orthogonal to the flat-band ones. Mapping the topology from the canonical basis ε into the basis v detangled the compact states from the orthogonal (*dispersive*) ones. This forms a *dispersive chain*, *i.e.* it isolates the flat-band states from each other (zero hopping), and they are only connected to dispersive states of their same lattice index. A class $U = 1$ topology allows detangling all compact localized states simultaneously. For class $U > 1$, in general the flat-band states spatially overlap, which lifts their orthogonality. To perform a similar detangling done for the $U = 1$ case, the minimal unit-cell needs to be extended to a super unit-cell made by a group of U unit-cells. In this representation, the lattice become of class $U = 1$ for certain compact states (one every U). Therefore, those flat-band states within the enlarged unit-cells belong to a $U \cdot \ell$-dimensional vector space $\tilde{V} \simeq \mathbb{R}^{U\cdot\ell}$, and the rotation can be constructed as with the basic case $U = 1$. This procedure detangles one compact states every U.

Both the compact states and the orthonormal counterparts for either class $U = 1$ and class $U \geq 1$ topologies will define a rotation matrix $\hat{U}$. This rotation $\varphi_l = \hat{U}\psi_l$ is then used to map the lattice equation Eq.(4.1) into

$$E\varphi_l = \hat{U}\epsilon_l\hat{U}^{-1}\varphi_l - \hat{U}\hat{V}\hat{U}^{-1}\varphi_l - \hat{U}\hat{T}\hat{U}^{-1}\varphi_{l-1} - \hat{U}\hat{T}^\dagger\hat{U}^{-1}\varphi_{l+1} \ . \tag{4.7}$$

where some coordinates of the rotated vector $\varphi_l = (\varphi_l^1, \ldots, \varphi_l^{U\cdot\ell})$ correspond to the compact states, which will be isolated and act as Fano coordinates. Let us indicated these coordinates by f_l^i. The complementary set of coordinates representing the dispersive bands will be indicated by p_l^i. It is interesting to note that the rotating scheme proposed for the crystalline case also provides a rotation method that remains valid also with the presence of onsite perturbation ϵ_l, of any nature. This method is then very effective for understand the effects of onsite perturbation on flat-band topology, and it also remain valid for lattices of class $U > 1$.

4.3.3 Cross Stitch and Diamond chains

In this subsection we consider two lattice topologies – the cross-stitch and chains. Both are examples of "frustrated two-leg ladders", which garnered the interest of the quantum spin community [175–178]. The cross-stitch model, shown on the left of Fig.4.5, is defined for

a unit cell $\psi_l = (a_l, b_l)^T$ with a 2×2 perturbation matrix ϵ_l. This yields for Eq.(4.1) the following matrices

$$\hat{V}_{CS} = \begin{pmatrix} 0 & t \\ t & 0 \end{pmatrix}, \quad \hat{T}_{CS} = \begin{pmatrix} 1 & 1 \\ 1 & 1 \end{pmatrix}. \tag{4.8}$$

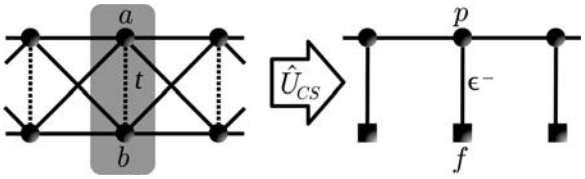

Figure 4.5: Left: The cross-stitch lattice – the grey shaded region indicates the unit cell. Right: The transformed Fano defect lattice of Eq.(4.16).

Likewise for the diamond lattice, as shown on the left of Fig.4.6, the unit cell is $\psi_l = (a_l, b_l, c_l)^T$ with a 3×3 perturbation matrix ϵ_l. In this case, the matrices in Eq.(4.1) are

$$\hat{V}_{DC} = \begin{pmatrix} 0 & t & 1 \\ t & 0 & 1 \\ 1 & 1 & 0 \end{pmatrix}, \quad \hat{T}_{DC} = \begin{pmatrix} 0 & 0 & 0 \\ 0 & 0 & 0 \\ 1 & 1 & 0 \end{pmatrix}. \tag{4.9}$$

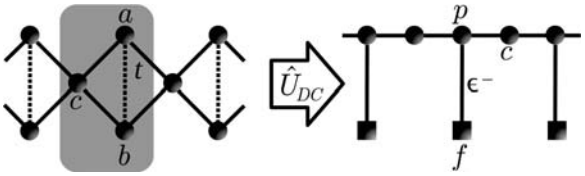

Figure 4.6: Left: The diamond lattice – the grey shaded region indicates the unit cell. Right: The transformed Fano defect lattice of Eq.(4.27).

In the unperturbed crystal $\epsilon_l = 0$, the dispersive bands are

$$E(k) = \begin{cases} -t - 4\cos k, & \text{Cross-Stitch,} \\ -\frac{1}{2}\left(t \pm \sqrt{t^2 + 16\cos k + 16}\right), & \text{Diamond.} \end{cases} \tag{4.10}$$

Additionally, both models contain a flat-band at $E(k) = t$.

Associated with the flat-band energy, a resulting compact localized states (CLS) is constructed: $\psi_l = (1, -1)^T \delta_{l,l_0}/\sqrt{2}$ (cross-stitch) and $\psi_l = (1, -1, 0)^T \delta_{l,l_0}/\sqrt{2}$ (diamond). Note that both are contained within a single unit cell. Therefore, according to the definition previously stated, both lattices are of flat-band model class $U = 1$. Coordinate transformations local to the unit cells rotate these lattices into a Fano defect form [162]. For the cross-stitch, the rotation is defined by the real matrix $\hat{U}_{CS}$

$$\begin{pmatrix} p_l \\ f_l \end{pmatrix} = \hat{U}_{CS}\, \psi_l, \quad \hat{U}_{CS} = \frac{1}{\sqrt{2}} \begin{pmatrix} 1 & 1 \\ 1 & -1 \end{pmatrix}. \tag{4.11}$$

Similarly for the diamond lattice the transformation is defined by the real matrix U_{DC}

$$\begin{pmatrix} p_l \\ f_l \\ c_l \end{pmatrix} = \hat{U}_{DC}\, \psi_l, \quad \hat{U}_{DC} = \frac{1}{\sqrt{2}} \begin{pmatrix} 1 & 1 & 0 \\ 1 & -1 & 0 \\ 0 & 0 & \sqrt{2} \end{pmatrix}. \tag{4.12}$$

Lastly, this local coordinate transformation must also rotate the onsite perturbation. For both lattices, this gives

$$\epsilon_l^{\pm} = (\epsilon_l^a \pm \epsilon_l^b)/2. \tag{4.13}$$

From Eq.(4.13), notable correlations between the a-leg and b-leg perturbations appear and will be object of our studies for both models; namely

$$\begin{aligned} \text{Symmetric:} \quad \epsilon_l^- = 0 \Leftrightarrow \quad \epsilon_l^a = \epsilon_l^b \,, \\ \text{Antisymmetric:} \quad \epsilon_l^+ = 0 \Leftrightarrow \quad \epsilon_l^a = -\epsilon_l^b \,. \end{aligned} \tag{4.14}$$

4.4 Flat-Band Engineering of a Mobility Edge

The effect of quasiperiodic Aubry-André perturbations on the cross-stitch and diamond topologies is the focus of this subsection. For both lattices, the onsite perturbations $\{\epsilon_n^i\}$ are defined as *independent* Aubry-André potentials

$$\epsilon_l^i = \lambda_i \cos\left[2\pi\left(\alpha l + \theta_i\right)\right] \,, \tag{4.15}$$

for the $i = a, b$ (cross-stitch) and $i = a, b, c$ (diamond) legs. The parameters λ_i are positive real values controlling the perturbative strength, θ_i is the phase-shift, and α is an irrational number (here set to the golden ratio) called the *incommensurate parameter*. Without loss of generality, the a-leg phase can be zeroed ($\theta_a = 0$). We also set the leg potential strengths equal to each other, $\lambda_i = \lambda$. Since the a-leg phase has been zeroed, from Eq.(4.15) these two correlations - Eq.(4.14) - are obtained solely from the b-leg phase, e.g. $\theta_b = 0.5$ ($\theta_b = 0$) for the antisymmetric (symmetric) case.
Note that in the crystalline case $\epsilon_l = 0$, the number of bands in the dispersion relation equals the number of sites in the unit cell for each of the above models, Eq.(4.10). Breaking the translation invariance of the lattices with the introduction of a non-periodic onsite perturbation [e.g. Eq.(4.15)] will generally lead to a loss of the spectral band structure due to hybridization, resulting in one single energy spectrum for the model. However as seen here, the symmetric case of Eq.(4.14) renormalizes the flat-band states, yet keeps their compact localized form due to the absence of any hybridization with the rest of the dispersive states. Note that the resulting eigenstate separation into two groups (compact localized states and dispersive) is unrelated to the abovementioned band structure of the crystalline case, since the spectra of both groups will overlap in general. We start the analysis of these models with the cross-stitch in Sec.4.4.1, and then with the diamond lattice in Sec.4.4.2.

4.4.1 Cross-Stitch Lattice

By Eqs.(4.11,4.13), the cross-stitch lattice transforms into

$$\begin{aligned} (E+t)\, p_l &= \epsilon_l^+ \, p_l + \epsilon_l^- \, f_l - 2\left(p_{l-1} + p_{l+1}\right), \\ (E-t)\, f_l &= \epsilon_l^+ \, f_l + \epsilon_l^- \, p_l \,. \end{aligned} \tag{4.16}$$

This results in a Fano chain, as shown in the right of Fig.4.5. The local rotation yields a dispersive coordinate p_l and a compact Fano coordinate f_l. The sequence ϵ_l^+ describes onsite perturbations of both p_l and f_l, while the sequence ϵ_l^- couples the dispersive to the Fano coordinate within the rotated unit cell [162]. Solving for the Fano coordinates f_l in the second equation above, we obtain a new equation for the dispersive portion

$$(E+t)\, p_l = \left[\epsilon_l^+ + \frac{(\epsilon_l^-)^2}{(E-t) - \epsilon_l^+}\right] p_l - 2\left(p_{l-1} + p_{l+1}\right). \tag{4.17}$$

The reduced topology assumes a tight-binding form. If eigenmodes are exponentially localized, their asymptotic decay is $\psi_l^\nu \sim e^{-\frac{l}{\xi}}$. The rate $\xi^{-1}(E)$ is the inverse localization length of a localized state at eigenenergy $E \in \mathbb{R}$, found by applying the recursive iteration

$$\xi^{-1}(E,\lambda) = \lim_{M\to+\infty} \frac{1}{M} \sum_{l=1}^{M} \ln\left|\frac{p_{l+1}}{p_l}\right|. \tag{4.18}$$

for any given potential strength λ. We will use this method in all the numerical computations of the two models' localization lengths, for $M = 10^6$. The energy E in Eq.(4.17) will be numerically found from an exact diagonalization of a finite lattice of $N = 512$ unit cells. In all the figures showed in the rest of this chapter, if the recursive iteration converges to a finite value (chosen [179] here as $\xi \leq N/10$), the datapoint (E,λ) is declared a localized state and plotted in blue. Otherwise if the iteration diverges, the datapoint is declared an extended state and plotted in red.

4.4.1.1 Symmetric Case: Metal-Insulator Transition

We analyze first the symmetric case $\epsilon_l^- = 0$, obtained for $\theta_b = 0.0$. Eq.(4.16) reads

$$\begin{aligned} (E+t)\, p_l &= \epsilon_l^+\, p_l - 2\,(p_{l-1} + p_{l+1})\,, \\ (E-t)\, f_l &= \epsilon_l^+\, f_l \end{aligned} \tag{4.19}$$

with $\epsilon_l^+ = \epsilon_l^a = \epsilon_l^b$. The two sets of states p_l and f_l decouple and generate two independent spectra, respectively labeled σ_p and σ_f. The parameter t then simply operates as a shift parameter, translating σ_p and σ_f relative to each other by $2t$.

The dispersive states p_l are described by an Aubry-André chain, displaying a MIT at $\lambda_c = 4$. The σ_f states keep their compact feature, but the degeneracy of their eigenenergies is now removed - these eigenenergies are given by $E = \epsilon_l^+ + t$. In Fig.4.7, we plot the dispersive spectrum from Eq.(4.19), as a function of λ. In this symmetric case, the spectra σ_p and σ_f are independent, since the p_l and the f_l coordinates decouple. For every potential strength $\lambda > 0$, the Fano states spectrum $\sigma_f = \{\epsilon_l^+\}_l$ is equidistributed within the interval $[t-\lambda, t+\lambda]$. In Fig.4.7 we indicate its boundaries by dashed lines. For the dispersive spectrum σ_p, the localization length is numerically found with the recursive iteration (4.18), and the localized phase (red) is demarcated from the extended one (blue). At the critical value $\lambda_c = 4$, all dispersive states switch from extended to localized. In this case, there is no mobility edge.

4.4.1.2 Asymmetric Case $\epsilon_l^- \neq 0$: Numerical Evidence for a Mobility Edge

Breaking the symmetry $\epsilon_l^- \neq 0$ ($\theta_b \neq 0$) of the Fano chain, Eq.(4.16) effectively couples the dispersive states p_l to their compact Fano counterparts f_l. Therefore, the self-duality is lost, and the two independent spectra ($\sigma_{p,f}$) are now joint. Nevertheless, we expect a transition between localized and extended states via an energy-dependent mobility edge. In Fig.4.8 we plot the spectrum of the lattice in the asymmetric case for $\theta_b = 0.25$ and $t = 0$. A mobility edge is clearly observed separating the localized regime (red) from that which is extended (blue).

4.4.1.3 Antisymmetric Case ($\epsilon_l^+ = 0$): Analytic Mobility Edge

Among all the non-symmetric cases obtained for $\theta_b \neq 0$, antisymmetry ($\theta_b = 0.5$) deserves special attention. It was already introduced in [180], providing a starting point in which to

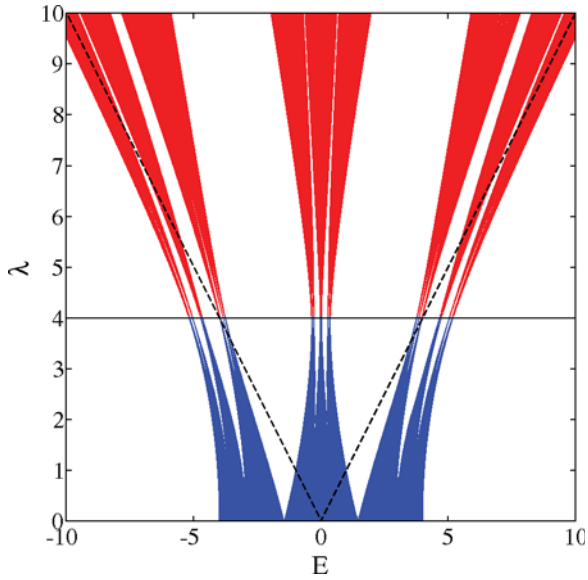

Figure 4.7: Symmetric Case: The dispersive spectrum (σ_p) of the cross-stitch lattice, for $\epsilon_l^- = 0$ and $t = 0$. The Fano state spectrum σ_f is omitted, but its boundaries indicated by black dashed lines. The black line represents the MIT at $\lambda = 4$, which clearly separates extended states (blue) from those localized (red).

clarify technical details and to obtain a closed form for mobility edge curves; this will be made use of later on for discussion of the diamond chain.

In this situation $\epsilon_l^+ = 0$ and Eq.(4.16) transforms into

$$\begin{aligned} (E+t)\, p_l &= \epsilon_l^- f_l - 2(p_{l-1} + p_{l+1}), \\ (E-t)\, f_l &= \epsilon_l^- p_l. \end{aligned} \tag{4.20}$$

Since $\epsilon_l^- \neq 0$, from the second equation of (4.20) it follows that at the flat-band energy

$$\epsilon_l^- \, p_l = 0 \quad \Rightarrow \quad p_l = 0 \ , \tag{4.21}$$

Then, from the first equation of (4.20) we conclude

$$\epsilon_l^- \, f_l = 0 \quad \Rightarrow \quad f_l = 0. \tag{4.22}$$

Therefore, only $(p_l, f_l) = (0, 0)$ satisfies Eq.(4.20) exactly at the flat-band energy $E = t$. It follows that all compact localized states are expelled from the unperturbed flat-band energy $E = t$, since their energies are shifted away from this energy due to hybridization with the dispersive states. The resulting states are then localized modes, located in the localized portion of the energy spectrum.

For this case we identify the analytical form of the mobility edge. Indeed the dispersive part, Eq.(4.17), reads

$$(E+t)\, p_l = \frac{(\epsilon_l^-)^2}{E-t}\, p_l - 2(p_{l-1} + p_{l+1}) \ . \tag{4.23}$$

By trigonometric bisection

$$(\epsilon_l^-)^2 = \lambda^2 \cos^2(2\pi\alpha l) = \frac{\lambda^2}{2}\left[1 + \cos(4\pi\alpha l)\right]. \tag{4.24}$$

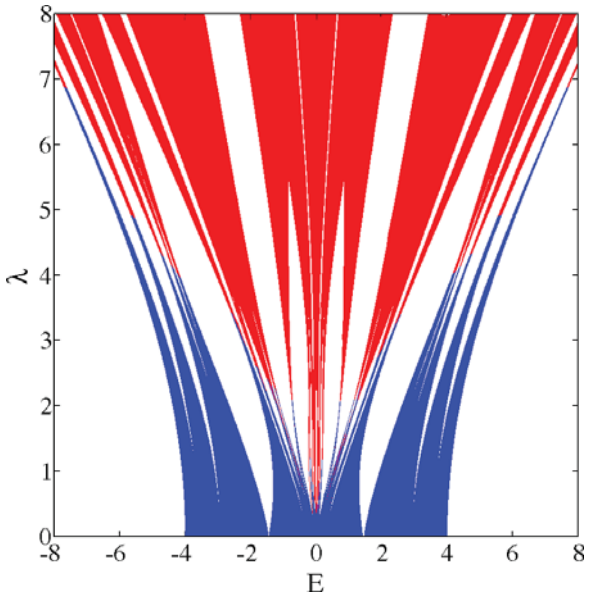

Figure 4.8: Asymmetric Case: Spectrum of the cross-stitch lattice, for $\theta = 0.25$ and $t = 0$. The extended (localized) portion of the spectrum is shown in blue (red), while the color boundary is a mobility edge approximation of the spectrum.

Substituting Eq.(4.24) back into the previous equation, we obtain

$$\begin{aligned} \tilde{E} p_l &= \frac{\lambda^2}{4(E-t)} \cos(4\pi\alpha l) - (p_{l-1} + p_{l+1}), \\ \text{where } \tilde{E} &:= \frac{E+t}{2} - \frac{\lambda^2}{4(E-t)}. \end{aligned} \tag{4.25}$$

Therefore, the model becomes an Aubry-André chain eigenvalue equation, but with an onsite perturbation strength depending on both λ and E. From [86], the MIT occurs when the potential strength is twice larger than the hopping strength. Imposing this condition, an analytic expression is found for the mobility edge, $\lambda_c(E_c)$:

$$\left| \frac{\lambda_c^2}{4(E_c - t)} \right| = 2 \quad \Rightarrow \quad \lambda_c(E_c) = 2\sqrt{2|E_c - t|}\,. \tag{4.26}$$

Note that for $E_c = t$, the critical potential strength λ_c vanishes in a square root manner, where the previously discussed lack of states at the unperturbed flat-band energy $E = t$ occurs. The analytic curve of the mobility edge plot in Fig.4.9 displays excellent agreement with the numerical result.

4.4.2 Diamond Lattice

Under the transformation in Eqs.(4.12, 4.13), the diamond lattice's Eq.(4.1) become

$$\begin{aligned} (E+t)\, p_l &= \epsilon_l^+ p_l + \epsilon_l^- f_l - \sqrt{2}(c_l + c_{l+1}), \\ (E-t)\, f_l &= \epsilon_l^+ f_l + \epsilon_l^- p_l, \\ (E - \epsilon_l^c)\, c_l &= -\sqrt{2}(p_{l-1} + p_l), \end{aligned} \tag{4.27}$$

as illustrated graphically in the right plot of Fig.4.6. Expressing the f_l and c_l variables through the p_l ones, we reduce these equations to a tight-binding form which contains the

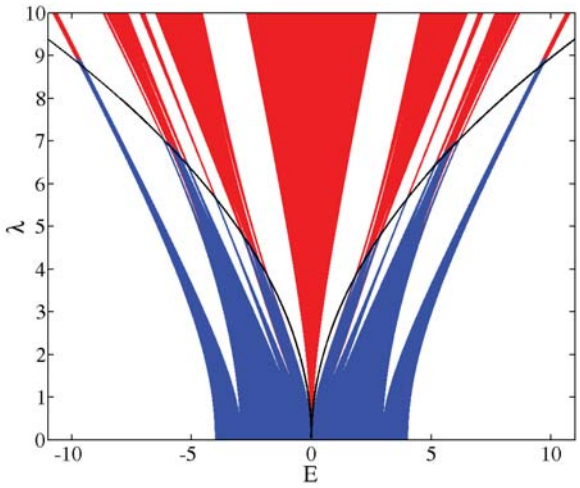

Figure 4.9: Anti-symmetric Case: Spectrum of the cross-stitch lattice, for $\theta = 0.5$ and $t = 0$. The analytically predicted mobility edge Eq. (4.26) (black line) separates extended (blue) and localized (red; $\xi < 51$) modes.

p_l coordinates only:

$$\begin{aligned}(E+t)\,p_l &= \left[\epsilon_l^+ + \frac{(\epsilon_l^-)^2}{(E-t)-\epsilon_l^+} + \frac{2}{E-\epsilon_l^c} + \frac{2}{E-\epsilon_{l+1}^c}\right] p_l \\ &\quad + \frac{2}{E-\epsilon_l^c} p_{n-1} + \frac{2}{E-\epsilon_{l+1}^c} p_{l+1}, \\ &\equiv \tilde{\epsilon}_l\, p_l + \gamma_{l-1}\, p_{l-1} + \gamma_{l+1}\, p_{l+1}\,. \end{aligned} \tag{4.28}$$

The effective onsite potential $\tilde{\epsilon}_l$ is a function of the three onsite energies of the diamond lattice $\epsilon_l^{a,b,c}$ in Eq.(4.15). However, the effective hopping terms $\gamma_{l\pm1}$ depend on the onsite energy ϵ_l^c of the c-chain. Since the model has both quasiperiodic onsite energies and hopping coefficients, one may expect that the Aubry-André duality does not generally hold.

Also note that the functional dependence of several terms in Eq.(4.28) is of the form

$$\frac{2}{E-\epsilon_l^c} = \frac{2}{E-\lambda\cos\left[2\pi\left(\alpha l+\theta_c\right)\right]}\,, \tag{4.29}$$

which was used in Ref. [181] for a model with constant hopping coefficients, arriving to analytically expressable mobility edges. Therefore, one can expect that mobility edges will be present in our model as well. As an example, in Fig.4.10 the spectrum of the diamond lattice Eq.(4.28) is plotted, for $\theta_b = 0.5$, $\theta_c = 0.05$ and $t = 0$ – a mobility edge is clearly observed.

To obtain closed forms of the mobility edge, the hopping terms are set constant: $\gamma_{l\pm1} = \Gamma$. From Eq.(4.29), this choice corresponds to

$$\frac{2}{E-\epsilon_l^c} = \Gamma \quad \Leftrightarrow \quad \epsilon_l^c = K \tag{4.30}$$

for a real constant value K. Eq.(4.28) becomes

$$\begin{aligned}(E+t)\,p_l = &\left[\epsilon_l^+ + \frac{(\epsilon_l^-)^2}{(E-t)-\epsilon_l^+} + \frac{4}{E-K}\right] p_l \\ &+ \frac{2}{E-K}\left(p_{l-1}+p_{l+1}\right)\,. \end{aligned} \tag{4.31}$$

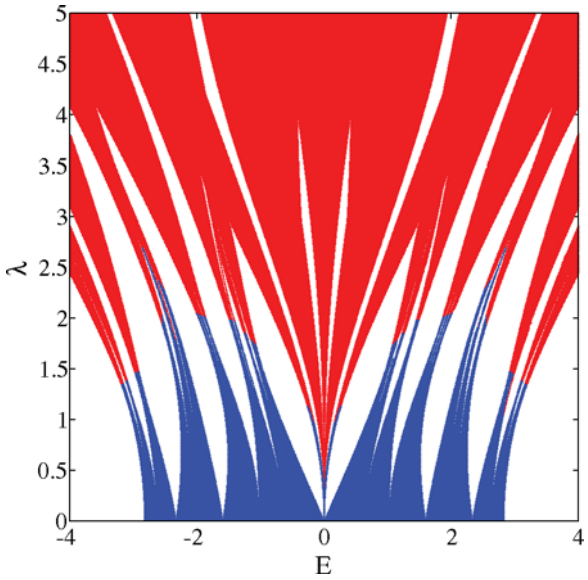

Figure 4.10: Spectrum of the diamond lattice, for $\theta_b = 0.5$, $\theta_c = 0.05$ and $t = 0$. The extended (localized) spectral portion is shown in blue (red), while the color boundary is again a spectral mobility edge approximation.

As a consequence of this choice, an extended state $\mathcal{D}$ exists at energy $E = K$, regardless of any other control parameters of Eq.(4.27):

$$E = K \ , \ c_l = (-1)^n \ , \ f_l = p_l = 0 \ . \tag{4.32}$$

The state's amplitudes reside only on the c sites (see Fig.4.11). The existence of this

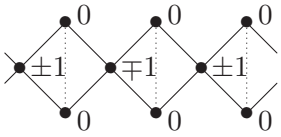

Figure 4.11: Extended state $\mathcal{D}$ at energy $E = K$ on the diamond lattice in case of constant onsite potential $\epsilon_l^c = K$ on the c-chain (up to normalization).

extended state is not affected by the perturbation strength λ, the flat-band energy $E = t$, nor any specific correlation of the onsite potential. Therefore, if the model admits a mobility edge curve $\lambda_c(E_c)$, it follows that it will diverge $\lambda_c(E_c = K) = \infty$, yielding a singularity.

4.4.2.1 Symmetric Case: Analytic Mobility Edge

We consider first the symmetric case $\epsilon_l^- = 0$, obtained for $\theta_b = 0.0$. In this situation, Eq.(4.27) reads

$$\begin{aligned} (E+t)\, p_l &= \epsilon_l^+ \, p_l + -\sqrt{2}(c_l + c_{l+1}) \ , \\ (E-t)\, f_l &= \epsilon_l^+ \, f_l \ , \\ (E-K)\, c_l &= -\sqrt{2}(p_{l-1} + p_l) \ . \end{aligned} \tag{4.33}$$

The f_l states decouple from both p_l and c_l states, generating two independent spectra σ_f and $\sigma_{p,c}$. The flat-band energy t shifts the two energy spectra of $2t$ relative to each other.

The rotated Eq.(4.31) now turns into

$$\begin{aligned} \tilde{E}\, p_l &= \frac{(E-K)\lambda}{2}\cos(2\pi\alpha l)\, p_l + p_{l-1} + p_{l+1}, \\ \text{where} \quad \tilde{E} &:= \frac{(E+t)(E-K)}{2} - 2. \end{aligned} \tag{4.34}$$

Note the onsite potential strength is now dependent on λ and E. Imposing the equality between the potential strength and the Aubry-André critical value, we arrive at the mobility edge

$$\left|\frac{(E_c-K)}{2}\lambda_c\right| = 2 \quad \Rightarrow \quad \lambda_c(E_c) = \left|\frac{4}{E_c-K}\right| . \tag{4.35}$$

The mobility edge curve diverges at $E = K$ due to the existence of the delocalized state $\mathcal{D}$. We plot this mobility edge curve in Fig.4.12 and observe very good agreement with the numerical results.

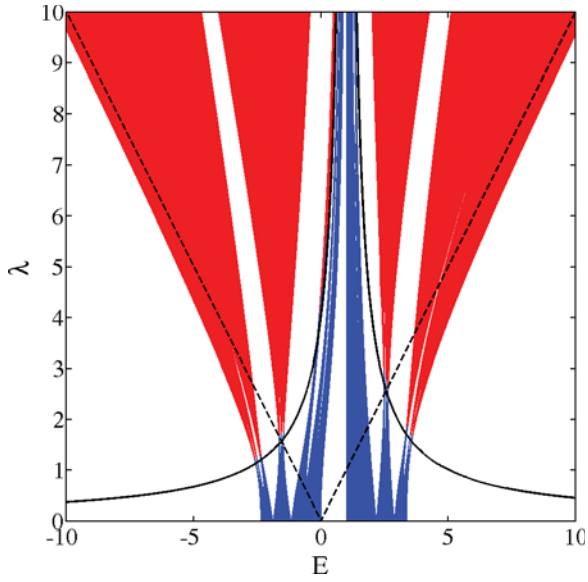

Figure 4.12: Symmetric Case: Dispersive spectrum ($\sigma_{p,c}$) of the diamond lattice, for $\epsilon_l^- = 0$, $K = 1$, $t = 0$. The Fano state spectrum (σ_f) is omitted, but its boundaries are indicated by black dashed lines. The extended (localized) states of the dispersive spectrum are shown in blue (red) – the boundary between these is a mobility edge approximation, in good agreement with its analytical form of Eq.(4.35), shown as a solid black line. Note that at $E = K$, the mobility edge diverges to infinity.

4.4.2.2 Antisymmetric Case: Analytic Mobility Edge

We consider the antisymmetric case $\epsilon_l^+ = 0$ obtained with $\theta_b = 0.5$, and with $\epsilon_l^c = K$. Eq.(4.27) reads

$$\begin{aligned} (E+t)\, p_l &= \epsilon_l^-\, f_l - \sqrt{2}(c_l + c_{l+1}) , \\ (E-t)\, f_l &= \epsilon_l^-\, p_l , \\ (E-K)\, c_l &= -\sqrt{2}(p_{l-1} + p_l) . \end{aligned} \tag{4.36}$$

For $t \neq K$, all eigenenergies are expelled from the flat-band energy $E = t$.

In Fig.4.13 we plot the spectrum for this antisymmetric case for $t = -1$ and $K = 1$. We derive an analytical expression of the mobility edge by reducing Eq.(4.36) to an Aubry-André form for the p_l coordinates:

$$\begin{aligned} \tilde{E}\, p_l &= \frac{E-K}{2}\frac{\lambda^2}{2(E-t)}\cos(4\pi\alpha l)\, p_l + p_{l-1} + p_{l+1}, \\ \text{where} \quad \tilde{E} &:= \frac{E-K}{2}\left[(E+t) - \frac{\lambda^2}{2(E-t)}\right] - 2. \end{aligned} \tag{4.37}$$

The condition for the MIT yields

$$\left|\frac{E-K}{2}\frac{\lambda_c^2}{2(E-t)}\right| = 2 \;\Rightarrow\; \lambda_c(E) = 2\sqrt{2\left|\frac{E-t}{E-K}\right|} \tag{4.38}$$

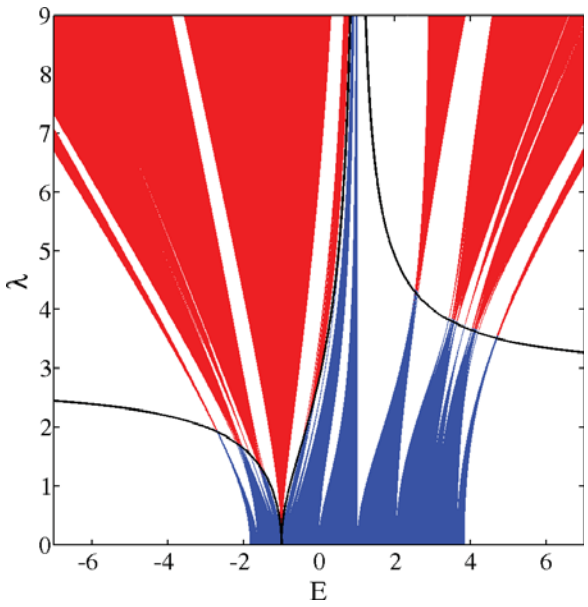

Figure 4.13: Antisymmetric Case: Spectrum of the diamond lattice, for $\epsilon_l^+ = 0$, $K = 1$, $t = -1$. The extended (localized) spectral portion is shown in blue (red). The boundary between is an approximation of the spectrum's mobility edge – in good agreement with the analytical form of Eq.(4.38), plotted as a black line. Not the mobility edge curve zeroes at $E = t$, as well as diverges at $E = K$.

In Eq.(4.38), the mobility edge curve $\lambda_c(E_c)$ diverges to infinity at $E = K$, in correspondence to the delocalized state $\mathcal{D}$. The curve also displays a zero at $E = t$, which corresponds to the lack of any states at the flat-band energy [182]. The mobility edge curve of Eq.(4.38) is plotted in Fig.4.13 and shows excellent agreement with the numerical data.

4.5 Summary and Discussions

In this chapter we have discussed two examples of class $U = 1$ flat-band lattices. General perturbations of these topologies lead to a removal of the degeneracy. This has especially dramatic consequencies for quasiperiodic Aubry-André form perturbations. The flat-band energy now hosts a zero of a mobility edge curve $\lambda_c(E_c)$. When approaching this zero the density of states grows, and the spatial extent of the eigenstates drops, making them more

localized. For specific symmetries of the applied quasiperiodic potential, the dependence $\lambda_c(E_c)$ is obtained analytically, confirming the predicted zero, and further proving the strict nonexistence of any state at the former flat-band energy. Some flat-band topologies allow the existence of completely delocalized eigenstates at certain energies $E = K$. This leads to even more complex mobility edge curves which allow for a coexistence of zeroes and divergencies of $\lambda_c(E_c)$. Possible future topics of study include extension to $U > 1$ topological classes and higher dimensional flat-band models. It is our hope that the use of flat-band topologies contributes interest to tunable mobility edges, e.g. by those realized in graphene [183], monolayered dichalcogenides [184], or vandium dioxide films [185, 186].

CHAPTER 5

Driven Lattices with Quasiperiodic and Random Potentials

In this chapter, we study the effects of time-dependent perturbations on one-dimensional lattices in the presence of localizing potentials. In the following sections, we discuss two particular types of driven systems, one with quasiperiodicity in space, and one with quasiperiodicity in time. Specifically, in the first we consider a quasiperiodic one-dimensional Aubry-André model chosen to be well in the localized regime and add a weak time-space dependent periodic perturbation. In the second, we instead consider a disordered one-dimensional Anderson chain in the presence of a quasiperiodic multi-frequency driving. Remarkably, the drivings generate two distinct outcomes. In the former, for particular frequency values the perturbation resonantly couples groups of localized eigenstates of the undriven model and turns them into extended ones. In the latter, for regimes of slow driving the multi-frequency perturbation substantially increases the localization length of the localized modes. However, the localization length stays finite for any finite number of frequency components.

This chapter is based on the following publication:

- H. Hatami, **C. Danieli**, J. D. Bodyfelt and S. Flach, "*Quasiperiodic driving of Anderson localized waves in one dimension*", Phys. Rev. E **93**, 062205 (2016);
- L. Morales-Molina, E. Doerner, **C. Danieli** and S. Flach, "*Resonant metallic states in driven quasiperiodic lattices: Aubry-Andre localization by design*", Phys. Rev. A **90**, 043630 (2014).

5.1 Introduction

During the last few decades, a very intense theoretical and experimental research activity has been dedicated to the understanding of novel features of quantum and classical systems in presence of either strong or weak time-dependent external field [187]. In particular, driving

in time finds interest not only because it can modify the system's asymptotic dynamics, but also because it might profoundly change its spectral properties, and even generate novel states of matter and light.

The realization of new states of light and matter is a hot topic within the scientific community. Among the different routes investigated to achieve this goal, driving the system using external fields in order to obtain synthetic gauge structures is an highly-considered one [188–191]. For example, a number of works have recently proposed different methods to design spin-orbit coupling or mimicking a magnetic field in driven cold atoms by using shaken optical lattices [192–196]. Another case is in superfluids, where the *Floquet Majorana fermions* have been created by proper external drivings of superconducting systems [197–200].

An important aspect associated with the introduction of an external driving in a system is the possible loss of the phase coherence. This effect usually involves the presence of random fluctuations in time. Such dephasing might potentially yield a complete change of the physical phenomena observed in the undriven system. In one-dimensional disordered lattices, for example, Anderson localization is lost by introducing a random dephasing of the onsite energy [131] (see Sec.5.3 for details). Both models considered in this chapter are spatially non-periodic one dimensional lattices in the presence of coherent driving. We will approach the issue of the phase decoherence in Sec.5.3, where we will discuss the case of a one-dimensional disordered lattice in presence of a quasiperiodic driving. Such driving is characterized by the presence of $D \geq 2$ incommensurate frequencies (colors). With any finite number of colors the driving is effectively coherent, however the randomness of the driving (and the consequent decoherence) is then achieved in the limit of $D \longmapsto +\infty$ (see Sec.5.3 and Appendix B.1 for details).

Interest of spatially non-periodic systems exists in the scientific community, ever since Anderson's prediction of wave localization in a one-dimensional lattice under an uncorrelated random disorder [2] (Sec.2.3 of the introduction). The question whether certain driving terms would effect the localization of this chains naturally follows. This might depend on the spectral properties of the undriven model, as well as on the nature of the the driving terms themselves. Often these systems allow one to construct solid analytical frameworks based on Floquet and/or harmonic analysis, in order to support numerical evidences of alteration in the time behaviour of the model.

The chapter is structured as follows: in Sec.5.2 we discuss the case of a one-dimensional Aubry-André lattice in the presence of time-periodic and spatially quasiperiodic weak drive. In Sec.5.3, we discuss a one-dimensional random chain in presence of a multi-frequency quasiperiodic drive of the onsite energy. Finally in Sec.5.4 we conclude and summarize the results. We refer to Appendix B.1 for all the technical details omitted in the main text.

5.2 Resonant Metallic States in Driven Quasiperiodic Lattices

As introduced in Sec.2.4 and Sec.3.2, one-dimensional quasiperiodic lattices usually allow for the existence of localized and extended states. In the Aubry-André case, the metal-insulator transition (MIT) separates extended states (metallic regime) from localized states (insulating regime) and is controlled by the depth of the quasiperiodic potential. Notably, the MIT for the Aubry-André model is energy-independent, due to a duality symmetry [86]. Extensions can include driven-AC forces to allow additional control over the MIT [201]. Here, we address the question whether a weak (but resonant) space-quasiperiodic and time-periodic perturbation can destroy the Aubry-André localization. Early studies of Anderson localization with uncorrelated random potentials show that the absence of

correlations allows for a finite increase of the localization length in the presence of time-periodic AC perturbations, but keeps to a finite upper bound [202–204]. Despite a number of further publications on driven Harper models [205,206] and versions of driven Aubry-André models [207], the results are basically soft modifications of the properties of the unperturbed eigenstates in the presence of driving. We consider a time-periodic moving lattice which mimics the effect of a driving force. The amplitude of the moving lattice is taken to be small, but its oscillation frequency is chosen such that it resonantly couples localized states from distinct bands of the undriven Aubry-André system. At the same time the additional spatial quasiperiodic perturbation effectively increases the reciprocal space dimensionality from $D = 1$ to $D = 2$. At a spatial resonance, this is reduced to an effective one-dimensional ladder topology. As a result of this resonant coupling, delocalization takes place. We use a Floquet representation to extract the eigenstates of the driven system. We find that at certain resonant values of the driving frequency, groups of eigenstates completely delocalize. We study the properties of these resonant extended eigenstates, and perform wave packet evolution tests to show that off-resonance AA localization holds, but on-resonance ballistic transport is obtained.

5.2.1 The Model

Ultra-cold atoms in optical lattices offer an ideal benchmark for the study of Anderson localization, since disordered lattices are experimentally feasible to build. For instance, a quasiperiodic lattice potential can be created by a bichromatic lattice [208,209] of the form

$$U(x) = U_1 \cos(k_1 x) + U_2 \cos(k_2 x + \phi), \tag{5.1}$$

where ϕ is a constant phase introduced to shift the two lattices relative to each other. Here k_1 and k_2 are the wavevectors and U_1 and U_2 are the amplitudes of the two lattice potentials (see [210] for generalizations).

Within the tight-binding approximation obtained in the limit $U_1 \gg U_2$ [209], the quantum dynamics for a particle moving in a quasiperiodic potential Eq.(5.1) can be described by the Aubry-André (AA) [86] or the Harper model [85]. Details of the derivation of the AA model can be found, for instance, in [211]. The experimental verification of the MIT of the AA model, and therefore the realizability of the tight-binding approximation, was demonstrated in Ref. [20] for ultracold atoms. Here we consider the driven Aubry-André model

$$\begin{aligned} i\frac{\partial}{\partial t}\psi_l = {} & \psi_{l+1} + \psi_{l-1} + V_1 \cos(2\pi\alpha l + \delta)\psi_l \\ & + V_2 \cos(2\pi\beta l + \Omega t)\psi_l \ . \end{aligned} \tag{5.2}$$

The first line in Eq.(5.2) corresponds to the undriven AA model in dimensionless units. Here ψ_l is the complex wave function amplitude at lattice site l, V_1 is the strength of the quasiperiodic potential, α is an irrational number setting the spatial period $1/\alpha$ which is incommensurate with the lattice spacing $\Delta l \equiv 1$ (here α will be chosen as $\alpha = \sqrt{3} - 1 \approx 0.732$), and δ is a relative phase. Note that V_1 is a certain function of $U_{1,2}$ from Eq.(5.1) [209]. The second line in Eq.(5.2) represents a time-space-periodic perturbation potential with amplitude V_2, spatial period $1/\beta$, and the AC driving frequency Ω. It can be realized by ultracold atomic gases adding a term $U_3 \cos(k_3 x)$, $U_3 \ll U_1$, to the trichromatic lattice laser potential, together with a time-dependent variation [208] (see also [187], page 95). Note that the Eq.(5.2) are invariant under shifts of α or β by any integer, therefore their irreducible space is confined to the unit interval. Despite the time-dependent perturbation, the above equations maintain a generalized symmetry $\beta \to -\beta$, $t \to -t$ and $\psi \to \psi^*$. For all practical computational purposes, we use a finite system size N with fixed boundary conditions $\psi_0 = \psi_{N+1} = 0$.

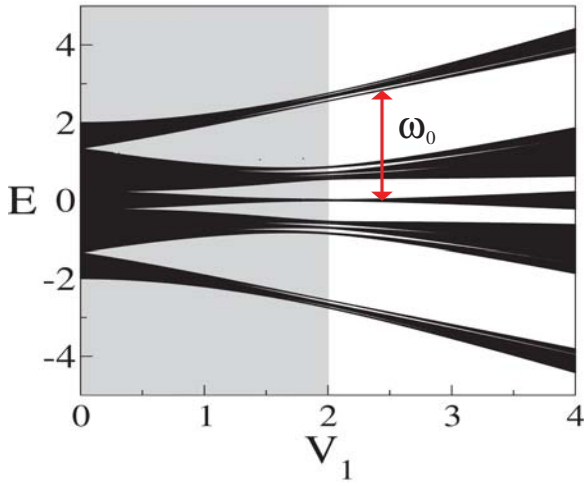

Figure 5.1: Energy spectrum E vs. V_1 of the undriven Aubry-Andre model ($V_2 = 0$) with $\alpha = \sqrt{3} - 1$. The shadowed region indicates the metallic regime for $V_1 < 2$. The arrow indicates the separation between edge and center bands for $V_1 = 2.5$ within the insulating regime. Length of the separation is denoted with ω_0.

In the absence of ac driving, $V_2 = 0$, the system (5.2) is self-dual, and is known to possess a MIT at the critical depth of the potential $V_1 = 2$ [86]. This is usually shown through a duality transformation. We generalize this transformation to our driven model. In analogy to the procedure in [86] we define

$$\psi_l \equiv \mathrm{e}^{i2\pi Kl} \sum_{n,m} f_{n,m} \mathrm{e}^{i[(2\pi\alpha l+\delta)n+(2\pi\beta l+\delta)m]} \ . \tag{5.3}$$

Here $f_{n,m}$ are the complex wave function amplitudes in reciprocal (spatial Fourier) space with the Bloch wave number $K \in \mathbb{R}$. The indices n, m can take all integer values. They correspond to the two lattice frequencies $2\pi\alpha$ and $2\pi\beta$ of the model. So far we consider the case when the ratio α/β is irrational as well. Then the equations (5.2) turn into a two-dimensional lattice problem in reciprocal space:

$$\begin{aligned} i\frac{\partial}{\partial t} f_{n,m} &= 2\cos\left[2\pi(\alpha n + \beta m + K)\right] f_{n,m} \\ &+ \frac{V_1}{2}(f_{n+1,m} + f_{n-1,m}) \\ &+ \frac{V_2}{2}\left(\mathrm{e}^{i2\pi g(t)} f_{n,m-1} + \mathrm{e}^{-i2\pi g(t)} f_{n,m+1}\right) \end{aligned} \tag{5.4}$$

where the function

$$g(t) = \Omega t - \delta \tag{5.5}$$

takes care of the time-dependent relative phase shifts of the two potentials. The complex term $\mathrm{e}^{\pm i2\pi g(t)}$ introduced in the hopping along the momentum direction of Eq.(5.4) by the time-dependent relative phase shifts $g(t)$ suggests that the second perturbation potential acts as a magnetic field. However, the total flux ϕ per plaquette in the two-dimensional reciprocal lattice Eq.(5.4) is zero, since in each plaquette, $\phi = (2\pi g(t) - 2\pi g(t))/2\pi = 0$. [173].

Let us discuss these results for $\Omega = 0$. Eq.(5.2) is a one-dimensional Schrödinger equation (on a lattice). We could always transform it into a Bloch basis of extended plane waves. However the consequence of that will be, in general, some nonlocal coupling between the

Bloch states for irrational α and β. Instead, the transformation Eq.(5.3) uses a basis which transforms Eq.(5.2) by keeping a nearest neighbour interaction network as observed in Eq.(5.4). In particular, for $V_2 = 0$ the resulting network interaction is an infinite set of noninteracting one-dimensional networks, while for $V_2 \neq 0$ it becomes two-dimensional. Conceptually, this is close to recent advances in emulating three-dimensional Anderson MIT using quantum kicked rotors with several additional temporal frequencies [212].

For $V_2 = 0$, the two-dimensional lattice Eq.(5.4) decouples into independent and equivalent one-dimensional ones. These chains are identical to the unperturbed Aubry-Andre case in real space Eq.(5.2) and exhibit a MIT at the critical value $V_1 = 2$. With the ansatz $\psi_l(t) = \mathrm{e}^{-iEt}\phi_l$ we solve the corresponding eigenvalue problem for the eigenenergies E. Fig.5.1 shows the spectrum of energy E as function of V_1. A well defined hierarchy of gaps and subgaps appears in the spectrum between different eigenenergies, due to its topological structure (for all $V_1 \neq 0$, the spectrum is a Cantor set [105, 213]). However, the nature of the corresponding eigenmodes depends on V_1, since for $V_1 > 2$ all the eigenstates are localized, whereas for $V_1 < 2$ they are extended. This means that any initially localized wavepacket for $V_1 > 2$ will remain localized at all times.

5.2.2 Driven Lattice Resonances

Spatial resonances happen for $V_2 \neq 0$ but with a commensurate ratio of the two spatial frequencies $\alpha/\beta = p/q$ with $\{p, q\}$ integers. Then the transformation (5.3) extends only over a q independent integers $m = 0, 1, 2, ..., q-1$, turning the two-dimensional lattice (5.4) into a one-dimensional ladder with q legs. The boundary conditions between the 1st and the qth leg are defined by the second integer p.

Let us add a weak perturbation potential $V_2 = 0.25$ for the case $V_1 = 2.5$, where the eigenstates of the undriven system are localized. We hunt for a resonant coupling of the eigenstates of the undriven case through the AC driving. Therefore the driving frequency Ω should take values of the order of the gaps of the spectrum of the undriven case in Fig.5.1.

Due to the time-periodic forcing, it is convenient to use the Floquet formalism. The wavefunction is expanded in terms of Floquet states $u_l(t) = e^{-i\epsilon t}\phi_l(t)$, with $\phi(t+T)_l = \phi_l(t)$, where $T = 2\pi/\Omega$ (see also [214] for details). To determine the degree of (de)localization of Floquet states, we compute the participation number [83, 215]

$$P = \frac{\sum_l |u_l|^2}{\sum_l |u_l|^4}. \tag{5.6}$$

with the lower bound $P = 1$ which accounts for maximal localization, and the upper bound $P = N$ corresponding to an extended state with constant amplitude (here N is the number of lattice sites). Any localized eigenstate will produce a finite P which does not scale with the system size $N \gg P$. Extended eigenstates have fluctuating amplitudes, and their P is always less than N, strictly speaking with no lower bound on the ratio P/N. However, their distinct feature is that P scales linearly with N. For each parameter set $\{\beta, \Omega\}$ we find all Floquet eigenstates, compute P for each of them, and identify the highest value. Fig.5.2 shows the intensity plot of the highest participaton number as a function of β and Ω. While even the states with largest spatial extend stay very localized for almost all parameter values, we find a strong resonant spot at $\beta \approx 0.37$ and $\Omega \approx 2.9$, and its symmetry related partner point at $\beta \approx 0.63$. Weaker spots are observed at $\Omega \approx 2.4, 4, 5.8$.

At the main resonance, β corresponds approximately to $\alpha/2$. Therefore the two-dimensional lattice in reciprocal space Eq.(5.4) is reduced to a two-leg ladder. The resonance frequency $\Omega = 2.9$ fits very well the distance between the edge and center bands ω_0 in Fig.5.1. To make sure that the observed resonance is indeed due to extended states, we plot in Fig.5.3

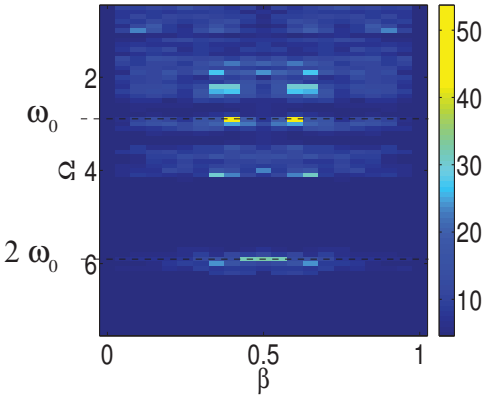

Figure 5.2: Left plot: Density plot of highest participation number vs Ω and β. Dashed lines indicates the resonances $\Omega = \omega_0 = 2.9$ and $\Omega = 2\omega_0 = 5.8$. Here $V_1 = 2.5$, $V_2 = 0.25$, $\alpha = \sqrt{3} - 1$, Here $N = 200$.

the participation numbers P for all Floquet eigenstates of a system with size $N = 200$ sorted according to their increasing value. In addition we also plot their second moments

$$m_2 = \sum_l (l - \langle l_0 \rangle)^2 |u_l|^2, \tag{5.7}$$

where $\langle l_0 \rangle = \sum_l l|u_l|^2$ is the first moment of the wavepacket. Note that we do not reorder

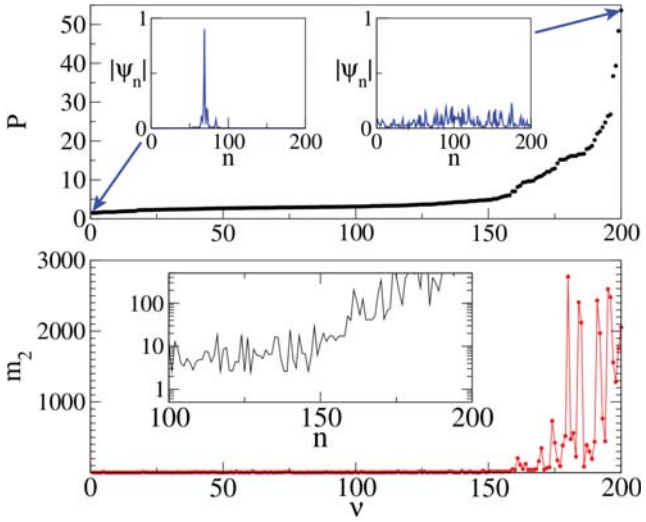

Figure 5.3: Upper panel: Ordered values of P of the Floquet states vs Floquet state number ν. The insets show the absolute value of the wave function versus lattice site n for the state with smallest and largest P. Lower panel: Same for the second moment m_2, with the sorting index from the upper panel. Inset shows enlargement of the region around the number 150 for a logarithmic scale. Here $V_2 = V_1/10 = 0.25$, $\alpha = \sqrt{3} - 1$, $\beta = 0.37$, $\Omega = 2.9$. $N = 200$.

the second moments, but plot them using the same sorting as for the participation numbers. We find that states with increasing size are detected using both measures. In the inset of the upper panel in Fig.5.3, we show the wave function of the state with the smallest P and the highest one. While the former one is strongly localized, the state with the highest participation number is clearly delocalized over the whole system.

If the observed resonance is leading to complete delocalization in an infinite system, the highest participation number should scale linearly with the system size N of a finite lattice. We test this prediction and show in Fig.5.4 that it is indeed correct. Therefore the observed resonance at $\Omega = 2.9$ and $\beta = 0.37$ generates extended eigenstates.

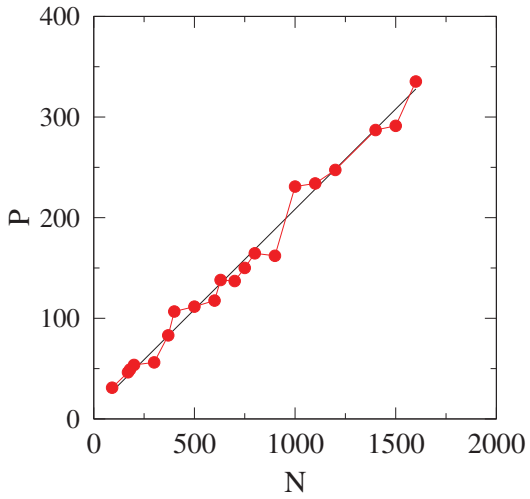

Figure 5.4: Highest participation number as a function of the system size N at resonance $\beta = 0.37$, $\Omega = 2.9$. Other parameters $V_1 = 2.5$, $V_2 = 0.25$, $\alpha = \sqrt{3} - 1$.

In the presence of stronger driving the observed resonances are expected to broaden. We test this prediction repeating the calculation in Fig.5.2 while doubling the strength of the driving potential $V_2 = 0.5$. The outcome is shown in Fig.5.5 and confirms our expectations.

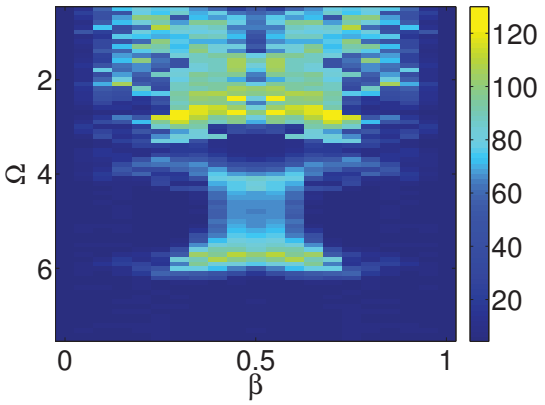

Figure 5.5: Density plot of the highest participation number vs Ω and β. Here $V_1 = 2.5$, $V_2 = 0.5$, $\alpha = \sqrt{3} - 1$. Here $N = 200$.

5.2.3 Wave Packet Spreading

Another consequence of the generation of delocalized extended eigenstates is that an initially localized wave packet will spread, if at least a part of it has nonzero overlap with extended eigenstates. We perform an integration of the time-dependent Eq.(5.2) using a modified $SBAB_2$ symplectic integrator [216–220] with initial condition $\psi_{N/2}(t = 0) = 1$ and $\psi_{l \neq N/2}(t = 0) = 0$. For the Floquet eigenvalue problem on an infinite lattice, the eigen-

values and eigenvectors are insensitive to the value of the relative phase δ (see Eq.(5.2)), which essentially shifts the potential, relative to the lattice. The overlap of a given initial state with Floquet eigenstates however does depend in general on the location of the initial state, or equivalently on the value of δ. We perform short runs for the resonance case $\beta = 0.37, \Omega = 2.9$ up to $t = 10^3$ with system size $N = 2^8$, and measure the second moment m_2 as a function of δ (Fig.5.6). Note that in all cases the system size was large enough so that the wave packet did not reach the system boundaries. As expected we find strong

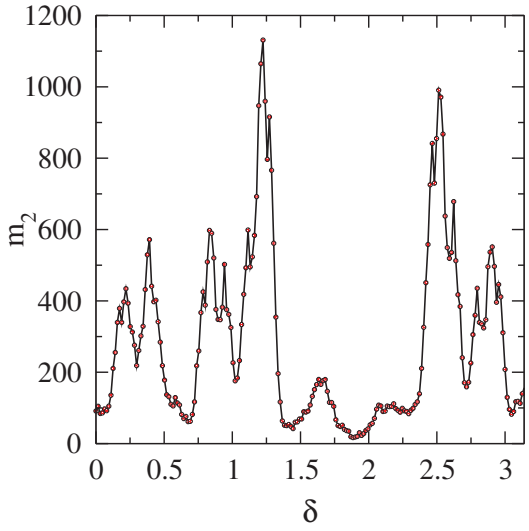

Figure 5.6: Second moment m_2 of $|\psi_l(t = 10^3)|^2$ as a function of δ for a single site excitation at resonance $\beta = 0.37$, $\Omega = 2.9$. Other parameters $V_1 = 2.5$, $V_2 = 0.25$, $\alpha = \sqrt{3} - 1$, $N = 2^8$.

fluctuations due to varying overlap. We choose $\delta \approx 1.225$ and perform long-time runs up to $t = 10^5$ with system size up to $N = 2^{15}$ for several values of $V_2 = 0.25, 0.275, 0.325, 0.5$. We plot the time dependence of $\log_{10} m_2(t)$ versus $\log_{10} t$ in Fig.5.7. For $V_2 = 0.5$ (blue top line) we observe ballistic spreading $m_2 \sim t^2$ over three decades in time. When lowering V_2, the onset of ballistic spreading is postponed and preceeded by an intermediate spreading regime which resembles normal diffusion $m_2 \sim t$. This is a typical feature of approaching a MIT, since at the critical point (here $V_2 \to 0$) the system transits into a localized insulating regime. The inset in Fig.5.7 shows that the density distribution for $t = 10^5$ and $V_2 = 0.25$ has a clearly visible extended part (originating from the overlap with extended eigenstates). A test run off-resonance with $\Omega = 2.6$ shows no signature of spreading, a small second moment which is constant on average, and a highly localized wave function density at the final integration time in Fig.5.7.

5.3 Quasiperiodic Driving of Anderson Localized Waves in One Dimension

In this section, we consider a quantum particle in a one-dimensional disordered lattice under multi-frequency perturbation of the onsite energies. The randomly chosen onsite energies are coherently driven in time by an finite sum of $D < +\infty$ time-periodic drives (*cosine* wave) with incommensurate frequencies (*quasiperiodic* driving). In the following section, we will use the term *colors* to indicate the driving terms.

A series of computational studies was devoted to this very issue [202–204]. While the first conclusion was that Anderson localization can be destroyed for $D \geq 2$, a more accurate

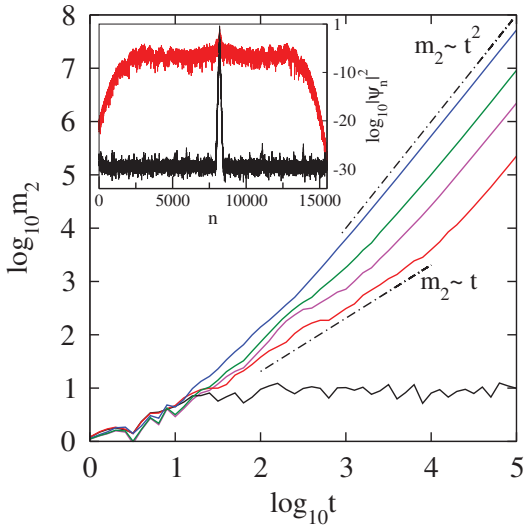

Figure 5.7: $\log_{10} m_2$ versus $\log_{10} t$. From top to bottom: $\Omega = 2.9$ and $V_2 = 0.5$ (blue), $V_2 = 0.325$ (green), $V_2 = 0.275$ (magenta), $V_2 = 0.25$ (red), and $\Omega = 2.6$ and $V_2 = 0.25$ (black, off resonance). The dashed-dotted lines indicate normal diffusion $m_2 \sim t$ and ballistic spreading $m_2 \sim t^2$. In all cases $\beta = 0.37$, $V_1 = 2.5$, $\alpha = \sqrt{3} - 1$, $\delta \approx 1.225$, $N = 2^{15}$. Inset: density distribution of the wavefunction at the final time of integration for $V_2 = 0.25$. Red extended curve:$\Omega = 2.9$ (on resonance), black localized curve: $\Omega = 2.6$ (off resonance). Other parameters as in the main figure.

recomputation showed that the localization length might well increase, yet stay finite. Other studies considered the case of single color $D = 1$ homogenous external AC fields [221–223]. In particular, Martinez *et. al.* [221] reported on numerical evidence of the localization length increase with decreasing driving frequency, while Refs. [222, 223] focused on the properties of conductance statistics in finite samples.

Wave localization inherently relies on the phase coherence within the wave state. If the disordered potential is allowed to temporarily fluctuate in a random way, phase coherence is lost, and the previously localized wave starts to diffuse without limits [131, 224]. Assuming that the temporal fluctuations are represented as a quasiperiodic function of time with D incommensurate fundamental frequencies, the random noise can be effectively reached in the limit of $D \to \infty$. Here we address the case of a finite number of frequencies (colors) D. Will the localization length ζ stay finite for any finite D? If yes, what is its dependence on D? At fixed D how does ζ depend on the remaining control parameters, such as frequency, fluctuation amplitude and disorder strength?

In the following, we try to answer these questions. We first consider a single frequency color (that is, a time-periodic drive). We use the Floquet representation to arrive at a time-independent eigenvalue problem on a two-dimensional lattice, with one direction corresponding to the original spatial extension, and the second one to the Floquet (driving) one. We transform into a Wannier-Stark basis which is diagonal along the Floquet direction, and analyze the resulting eigenvalue problem. For large driving frequencies, the equations reduce to uncoupled single channel ones, which are essentially equivalent to the undriven case. For small driving frequencies, we obtain a multi-channel regime with a substantial increase of the localization length, and its divergence in the limit of vanishing frequency. This multi-channel regime divides into two further regimes of weak and strong driving amplitudes, which yield different scaling laws. We then generalize to the case of many incommensurate frequencies, and compare our findings to numerical results.

The section is organized as following. In Sec. 5.3.1 we introduce the model and its general features. In Sec. 5.3.2, we derive the results for one frequency (color) drive. We generalize to many colors in Sec. 5.3.3, and discuss numerical results in Sec. 5.3.4. We conclude with discussions, a summary, and an outlook.

5.3.1 The Model

We consider a disordered one-dimensional tight-binding chain in the presence of a coherent time-dependent driving of the onsite energies. The equations of motion read

$$i\frac{\partial}{\partial t}\psi_l = \epsilon_l\left[1+\sum_{i=1}^{D}\mu_i\cos(\omega_i t+\phi_l^i)\right]\psi_l - \lambda(\psi_{l+1}+\psi_{l-1})\ , \tag{5.8}$$

The onsite energies of each lattice site ϵ_l are random uncorrelated numbers with a probability density function (PDF) of value $1/W$ inside the interval $\epsilon_l \in [-W/2,+W/2]$ and zero outside. The parameter W parametrizes the strength of the disorder. The coefficient λ is the strength of the hopping between nearest neighbor lattice sites, while μ_i and ω_i respectively are the amplitude and frequency of the i-th driving. D is the total number of frequencies (colors) in the driving. The frequencies $\Omega = (\omega_1,\ldots,\omega_D)$ are chosen incommensurate with each other

$$\mathbf{k}\cdot\Omega = k_1\omega_1+\cdots+k_D\omega_D \neq 0\ , \quad \forall\ \mathbf{k}\in\mathbb{Z}^D\setminus\{0\}\ . \tag{5.9}$$

The random phases ϕ_l are uncorrelated and have a PDF of value $1/(2\pi)$ inside the irreducible interval $\phi_l \in [-\pi,\pi]$. Their presence ensures broken time reversal symmetry of Eq.(5.8). For $\mu_i = 0$, Eq.(5.8) reduces to the well-known Anderson model with all eigenstates being localized with a finite upper bound on the localization length [2, 83].

The above model can be realized experimentally in atomic Bose-Einstein condensates when laser beams with different frequencies perturb the atomic system and also the optical lattice itself. Similar models have also been considered for the conductivity of electrons in two-dimensional confinements where local scatterers (defects, phonons) act as time-dependent sources of dephasing [224]. Other approaches consider noise in external AC fields, which should not change the physics outcome dramatically [221–223].

5.3.2 One Color

We first consider a driving with only one frequency $D = 1$. In this case, Eq.(5.8) reads

$$i\frac{\partial}{\partial t}\psi_l = \epsilon_l\left(1+\mu\cos(\omega t+\phi_l)\right)\psi_l - \lambda(\psi_{l+1}+\psi_{l-1})\ . \tag{5.10}$$

Since the perturbation is time periodic with period $T = \frac{2\pi}{\omega}$, we first perform a Floquet expansion which will yield an effective two-dimensional lattice problem. The details calculations of the expansion is performed in Appendix B.2.1.

5.3.2.1 From Floquet to Wannier-Stark

According to the Floquet theorem [225, 226], a solution of (5.10) is given by

$$\psi_l(t) = u_l(t)e^{-iEt}\ , \tag{5.11}$$

where E is the quasienergy and the Floquet functions $u_l(t) = u_l(t+T)$. They can be represented in a Fourier series

$$u_l(t) = \sum_k A_{l,k}e^{ik(\omega t+\phi_l)}\ . \tag{5.12}$$

The Floquet expansion of the wave function $\psi_l(t)$ is then given by

$$\psi_l(t) = \sum_k A_{l,k} e^{-i[(E-k\omega)t - k\phi_l]} \ . \tag{5.13}$$

This transformation maps Eq.(5.10) into a time independent eigenvalue problem on a two-dimensional lattice

$$\begin{aligned} EA_{l,k} = (\epsilon_l + k\omega)A_{l,k} + \frac{\mu\epsilon_l}{2}(A_{l,k-1} + A_{l,k+1}) \\ - \lambda(\xi^-_{l,k}A_{l-1,k} + \xi^+_{l,k}A_{l+1,k}) \end{aligned} \tag{5.14}$$

with the coefficients

$$\xi^\pm_{l,k} = e^{-ik(\phi_l - \phi_{l\pm1})} = e^{-ik\theta^\pm_l} \tag{5.15}$$

dependent on the random phase differences $\theta^\pm_l = \phi_l - \phi_{l\pm1}$, which introduce a synthetic gauge field in the two dimensional lattice of Eq.(5.14)

Consider first $\lambda = 0$. We can solve the remaining eigenvalue problem for each lattice site l independently, as this case corresponds to the well-known Wannier-Stark ladder [227] under an effective DC electric field ω and l-dependent hopping coefficient $\mu\epsilon_l/2$. The eigenfunctions $B^{(\nu)}_{l,k} = J_{k-\nu}(\mu\epsilon_l/\omega)$ are obtained using the Bessel function of the first kind $J_k(x)$ with fixed argument x, and their eigenvalues form equidistant spectra $E_{\nu,l} = \epsilon_l + \omega\nu$ [228, 229]. These eigenfunctions are localized (along the Fourier direction k), with tails decaying super-exponentially. The localization volume (size) $\mathcal{L}$ of an eigenstate is estimated as $\mathcal{L} \sim 2\left|\frac{\mu\epsilon_l}{\omega}\right|$ for $\frac{\omega}{\mu\epsilon_l} \leq 10$, and reaches its asymptotic value $\mathcal{L} = 1$ for $\frac{\omega}{\mu\epsilon_l} \geq 10$ [230].

We use these Wannier-Stark eigenstates as a new basis for each lattice site l of Eq.(5.14) :

$$A_{l,k} = \sum_\nu c_{l,\nu} B^{(\nu)}_{l,k} \ . \tag{5.16}$$

The transformed eigenvalue problem for $\lambda \neq 0$ reads as

$$\begin{aligned} Ec_{l,\nu} = (\epsilon_l + \omega\nu)c_{l,\nu} \\ -\lambda \sum_s \left[\mathrm{e}^{is\varphi^-_l} J_s(\Delta^-_l) c_{l-1,\nu-s} + \mathrm{e}^{is\varphi^+_l} J_s(\Delta^+_l) c_{l+1,\nu-s} \right] \end{aligned} \tag{5.17}$$

where

$$\begin{aligned} \tan\varphi^\pm_l &= -\frac{\epsilon_{l\pm1}\sin\theta^\pm_l}{\epsilon_l - \epsilon_{l\pm1}\cos\theta^\pm_l} \ , \\ \Delta^\pm_l &= \frac{\mu}{\omega}\sqrt{\epsilon_l^2 + \epsilon_{l\pm1}^2 - 2\epsilon_l\epsilon_{l\pm1}\cos\theta^\pm_l} \ . \end{aligned} \tag{5.18}$$

This eigenvalue problem has zero hopping along the Fourier direction ν. Instead, each lattice site $c_{l,\nu}$ is connected to a number of nearest neighbor sites $c_{l\pm1,\nu-s}$ given by the complex hopping coefficients $\mathrm{e}^{is\phi^\pm_l} J_s(\Delta^\pm_l)$ (see Fig. 5.8). The number of strong links (connectivity) with a given site at l, ν depends on the ratio of the difference in the new onsite energies $|\epsilon_l - \epsilon_{l\pm1} + s\omega|$ and the hopping strength $|J_s(\Delta^\pm_l)|$. Strong links are thus characterized by $|(\epsilon_l - \epsilon_{l\pm1} + s\omega)/J_s(\Delta^\pm_l)| \ \leq \ 1$.

5.3.2.2 Single channel vs. multi-channel regimes

In the case of zero driving strength $\mu = 0$, it follows $\Delta^\pm_l = 0$ for all l, and $J_s(0) = \delta_{s,0}$. The two dimensional lattice Eq.(5.17) turns into an infinite set of independent one-dimensional Anderson chains. For nonzero driving strength ($\mu \neq 0$), all the Floquet channels

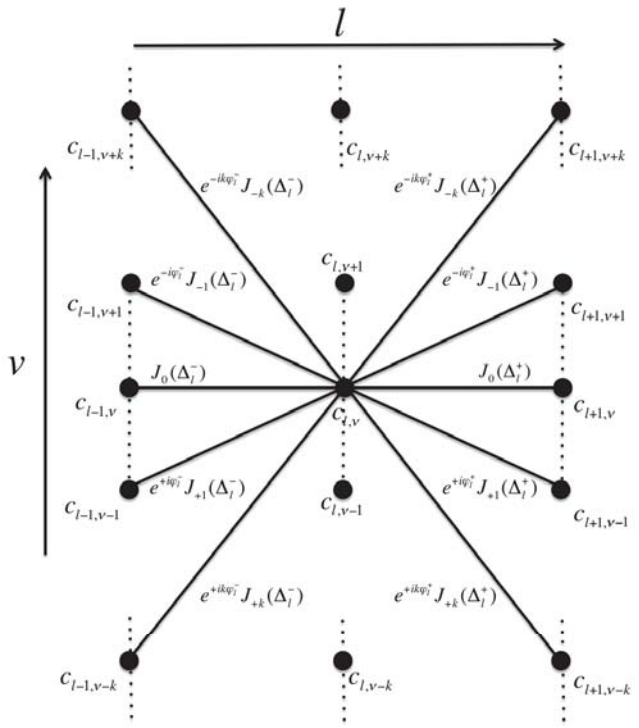

Figure 5.8: Two-dimensional eigenvalue problem Eq. (5.17). Each given site (l, ν) is connected to a set of sites $(l \pm 1, \nu - s)$ through the hopping $e^{is\phi_l^\pm} J_s(\Delta_l^\pm)$.

are connected. Since [228, 229]

$$J_s(\Delta_l^\pm) \longmapsto \frac{(\Delta_l^\pm)^s}{2^s s!} \ , \quad \text{for} \ \ s \longmapsto +\infty \tag{5.19}$$

only a finite number of channels will have a non-exponentially weak hopping strength, and that number depends on the value of the argument of the Bessel functions $\Delta_l^\pm$. If for every l the argument is close to zero $|\Delta_l^\pm| \leq \delta \ll 1$, it follows that $J_0(\Delta_l^\pm) \approx 1$, and for $s \neq 0$ the Bessel functions $J_s(\Delta_l^\pm)$ decay as Eq.(5.19). As a consequence Eq.(5.17) becomes an infinite set of uncoupled equivalent Anderson chains, and the model resembles the unperturbed case. We call this the *single channel regime*. This result is true irrespective of the ratio of ω/W which controls the energy differences between connected sites. While this is evident for large frequencies $\omega \gg W$ (where the energy difference is of order W), it is also true in the opposite limit $\omega \ll W$ where the energy difference can be of order ω for a suitably large value of $s \sim W/\omega$, since the hoppings decay superexponentially fast with large s (5.19).

In contrast, when $\Delta_l^\pm \geq 1$, a finite number $\mathcal{L}_l^\pm$ of the Bessel functions $J_s(\Delta_l^\pm)$ for $s \neq 0$ are not negligible. Their typical values can be approximated as [228, 229]:

$$J_s(\Delta_l^\pm) \approx \sqrt{\frac{2}{\pi \Delta_l^\pm}} \cos\left(\Delta_l^\pm - \frac{s\pi}{2} - \frac{\pi}{4}\right) \ , \quad |s| \leq \frac{\mathcal{L}_l^\pm}{2} \tag{5.20}$$

In Eq.(5.18), the square root of $\Delta_l^\pm$ is on the order of the disorder strength W. We define the parameter Δ as

$$\Delta_l^\pm \quad \longmapsto \quad \Delta = \frac{\mu W}{\omega} \ , \tag{5.21}$$

It follows that, if $\Delta \geq 1$, the averaged number of connected channels $\mathcal{L}$ is given by

$$\mathcal{L}_l^\pm = 2\Delta_l^\pm \quad \longmapsto \quad \mathcal{L} = 2\Delta = \frac{2\mu W}{\omega} \ , \tag{5.22}$$

while in Eq.(5.20), neglecting the cosine term that represents the Bessel function oscillation, the general value of the hopping can be approximated as

$$J_s \approx \sqrt{\frac{2}{\pi\Delta}} = \sqrt{\frac{2\omega}{\pi\mu W}} \ , \quad |s| \leq \frac{\mathcal{L}}{2} \tag{5.23}$$

We call this regime the *multi-channel regime*. Therefore, for any given disorder and driving strengths W and μ, this regime will be realized in the limit of small frequencies ω. This latter regime will be the focus of our investigation, since in the single channel regime the model acts similar to the undriven case. Our results confirm earlier intuitive interpretations, that the increase in the channel number can be responsible for a substantial increase in the localization length in the presence of adiabatic single color external AC driving [221, 222].

5.3.2.3 The multi-channel regime

5.3.2.3.1 Weak driving Let us first consider the case $\mu \ll 1$. For a given site (l, ν), there are $\mathcal{L}$ matrix elements connecting this site to a set of sites $(l+1, \nu')$. The onsite energies of these connected sites vary in an interval $[\epsilon_{l+1} - \mu W, \epsilon_{l+1} + \mu W]$. For $\mu \ll 1$ this interval is narrow compared to W which characterizes the spread of ϵ_l. Therefore the difference in the onsite energies between two connected sites is still of the order W.

In general, for ladders with a finite number N of equivalent Anderson chains, Dorokhov, Mello, Pereyra and Kumar [231, 232] estimate the localization length ζ of a N-leg ladder as a product of the localization length $\zeta_{\mathcal{A}}$ of each leg and the number of legs N:

$$\zeta \sim N \cdot \zeta_{\mathcal{A}} \ . \tag{5.24}$$

The number of legs N corresponds to $\mathcal{L}$. The single channel localization length can be estimated using the ratio W_{eff} between the energy mismatch (disorder strength) W and the matrix element λJ_s from Eq.(5.23):

$$W_{\text{eff}} = \frac{W^{\frac{3}{2}}}{\lambda}\sqrt{\frac{\mu\pi}{2\omega}} \ . \tag{5.25}$$

We then obtain [83]

$$\zeta_{\mathcal{A}}(\omega) \sim \begin{cases} \frac{100}{W_{\text{eff}}^2} & \text{if} \quad W_{\text{eff}} \leq 10, \\ \frac{1}{|\ln(1/W_{\text{eff}})|} & \text{if} \quad W_{\text{eff}} > 10. \end{cases} \tag{5.26}$$

It follows that in the case of weak effective disorder $W_{\text{eff}} \leq 10$, the localization length ζ of our driven model is given by

$$\zeta(\omega) \sim \frac{400\lambda^2}{\pi W^2} \ , \ \omega \geq \frac{\mu\pi W^3}{200\lambda^2} \ . \tag{5.27}$$

The localization length ζ does not depend on the frequency ω and the driving strength μ, since the increase of the number of connections $\mathcal{L}$ and the decrease of the localization length $\zeta_{\mathcal{A}}$ along each Anderson chain balance each other. Upon further decrease of the frequency ω, this balancing effect is destroyed since Δ grows, the matrix element λJ_s decays, and the effective disorder $W_{\text{eff}} > 10$. With Eq.(5.26) it follows

$$\zeta(\omega) = \frac{2\mu W}{\omega} \cdot \left| \ln\left(\frac{\lambda}{W^{\frac{3}{2}}}\sqrt{\frac{2}{\pi\mu}\omega}\right)\right|^{-1} \ , \ \omega \leq \frac{\mu\pi W^3}{200\lambda^2} \ . \tag{5.28}$$

The localization length then diverges for $\omega \to 0$.

To summarize: in the weakly driven multichannel regime we expect a plateau in the dependence $\zeta(\omega)$ for $\omega \geq \frac{\mu\pi W^3}{200\lambda^2}$, which is replaced by a divergence for $\omega \leq \frac{\mu\pi W^3}{200\lambda^2}$.

5.3.2.3.2 Strong driving Let us consider the case $\mu \geq 1$, and constant phases $\phi_l = \text{const}$. For a given site (l, ν), there are $\mathcal{L}$ matrix elements connecting this site to a set of sites $(l+1, \nu')$. The onsite energies of these connected sites vary in an interval $[\epsilon_{l+1} - \mu W, \epsilon_{l+1} + \mu W]$. For $\mu \geq 1$ this interval is larger than W, which characterizes the spread of ϵ_l. Therefore there will be typically one onsite energy amongst the connected set which is detuned by a mismatch of order ω from the one on site (l, ν). It follows that for $\mu \geq 1$ and $\omega \ll W$, we can trace a path in Eq.(5.17) where the onsite mismatch is of the order of the frequency $|\epsilon_l - \epsilon_{l\pm1} + s\omega| \sim \omega$ and the hopping scales with the square root of the frequency $J_s \sim \sqrt{\omega}$ for every l. We call this the *optimal path*. The optimal path is a one dimensional random walk within the two dimensional network. Along that optimal path, the localization length $\zeta_{\mathcal{OP}}$ follows from the effective disorder W_{eff} between the energy mismatch (disorder strength) ω and the matrix element λJ_s from (5.23)

$$\zeta_{\mathcal{OP}}(\omega) = \frac{100 J_{\hat{s}}^2}{\omega^2} = \frac{100}{\omega^2} \cdot \left(\sqrt{\frac{2\omega}{\pi \mu W}} \right)^2 = \frac{200}{\pi \mu W} \frac{1}{\omega} \ . \tag{5.29}$$

For small frequencies this optimal path consists of strong links. Furthermore, paths neighboring the optimal one, are also strong links, as long as the energy detuning is not exceeding the matrix element. Since the matrix element scales with $\sqrt{\omega}$, the number of strong links diverges as $N \sim 1/\sqrt{\omega}$. Using the Dorokhov estimates, we conclude that the localization length on the network is scaling as

$$\zeta \sim \frac{200}{\pi \mu W} \frac{1}{\omega^{3/2}} \ . \tag{5.30}$$

Therefore the localization length diverges for vanishing frequency faster than in the weak driving case.

5.3.2.3.3 Local suppression of strong driving The presence of random phases will suppress the optimal path through an increase of the minimal value of the driving strength:

$$\mu \sqrt{1 + \frac{2\epsilon_l \epsilon_{l\pm1}}{(\epsilon_l - \epsilon_{l\pm1})^2} (1 - \cos \theta_l^{\pm})} \geq 1 \tag{5.31}$$

where $\theta_l^{\pm} = \phi_l - \phi_{l\pm1}$. In particular if $\theta_l^{\pm} = \pi$, the square root term of Eq.(5.31) is equal to zero if

$$-2\epsilon_l \epsilon_{l\pm1} = \epsilon_l^2 + \epsilon_{l\pm1}^2 \quad \Leftrightarrow \quad \epsilon_l = -\epsilon_{l\pm1} \tag{5.32}$$

In this case, Eq.(5.31) does not hold for any finite value of μ, and locally between site l and site $l \pm 1$ the optimal path is not accessible.

Therefore, for uncorrelated phases ϕ_l, the square root term of Eq.(5.31) can be arbitrarily close to zero if $\theta_l^{\pm} \approx \pi$ and $\epsilon_l \approx -\epsilon_{l\pm1}$. As a consequence, μ must diverge to infinity in order to satisfy Eq.(5.31) at every step l and so, for given finite values of the driving strength, the optimal path is interrupted. This will lead to a slower divergence of the localization length, which is still expected to be faster than in the weak driving regime, since there will be finite volume parts in which the optimal path will survive.

5.3.2.3.4 Local suppression of the multi-channel regime Since ϵ_l and ϕ_l are random phases, the square root term of Eq.(5.18) can be arbitrarily close to zero. Therefore, even deep in the multi-channel regime $\Delta \gg 1$, there might exist one or more lattice sites l such that the Bessel function argument $\Delta_l^{\pm} \ll 1$. In that case, the hopping $J_s(\Delta_l^{\pm}) \approx \delta_{s,0}$, as in

the single channel regime. As a result, the multi-channel regime between site l and $l \pm 1$ becomes locally suppressed.

In the case of constant phases ($\phi_l = \text{const}$), this local suppression appears if $|\epsilon_l - \epsilon_{l\pm1}| \ll \omega/\mu$. The single channel then still shows an energy difference of the order of ω or less, similar to the optimal path. For uncorrelated phases ϕ_l, the probability of a local suppression of the multi-channel regime is reduced. Indeed, in order to violate the multi-channel condition $\Delta_l^{\pm} \gg 1$, we now need satisfy either $|\epsilon_l - \epsilon_{l+1}| \ll \omega^2/\mu^2$ and $|\theta_l^{\pm}| \ll 1$, or $|\epsilon_l + \epsilon_{l+1}| \ll \omega^2/\mu^2$ and $||\theta_l^{\pm}| - \pi| \ll 1$. The previously obtained estimates on the localization length ζ in either weak and strong driving regimes are then the upper bounds.

5.3.3 Many Colors

For the general case of Eq.(5.8), the Floquet expansion in the momentum space and the rotation of the eigenvalue problem in a basis of Bessel functions for each frequency is a natural generalization of what we have previously described in Sec.5.3.2 for one color $D = 1$ (details in Appendix B.2.2). Since the frequency components of Ω are chosen to be incommensurate Eq.(5.9), the general form of the Floquet expansion (5.13) runs over the vector index $\mathbf{k} = (k_1, \ldots, k_D) \in \mathbb{Z}^D$ [233] (See also appendix B.1), and yields a $D+1$ dimensional time independent eigenvalue problem:

$$\begin{aligned} E c_{l,\mathbf{v}} &= (\epsilon_l + \Omega \cdot \mathbf{v}) c_{l,\mathbf{v}} \\ -\lambda \sum_{\mathbf{s}} \left[\mathrm{e}^{i\mathbf{s}\cdot\Phi_l^-} \mathcal{J}_{\mathbf{s}}^- c_{l-1,\mathbf{v}-\mathbf{s}} + \mathrm{e}^{i\mathbf{s}\cdot\Phi_l^+} \mathcal{J}_{\mathbf{s}}^+ c_{l+1,\mathbf{v}-\mathbf{s}} \right] , \end{aligned} \tag{5.33}$$

where $\mathbf{s}, \mathbf{v} \in \mathbb{Z}^D$ and $\Phi_l^{\pm} = (\varphi_{l,i}^{\pm})_{i=1}^D$. The coefficients are defined as

$$\begin{aligned} \tan \varphi_{l,i}^{\pm} &= -\frac{\epsilon_{l\pm1} \sin \theta_{l,i}^{\pm}}{\epsilon_l - \epsilon_{l\pm1} \cos \theta_{l,i}^{\pm}} , \\ \mathcal{J}_{\mathbf{s}}^{\pm} &= \prod_{i=1}^{D} J_{s_i}(\Delta_{l,i}^{\pm}) , \\ \Delta_{l,i}^{\pm} &= \frac{\mu_i}{\omega_i} \sqrt{\epsilon_l^2 + \epsilon_{l\pm1}^2 - 2\epsilon_l \epsilon_{l\pm1} \cos \theta_{l,i}^{\pm}} , \end{aligned} \tag{5.34}$$

which depend on the random phase difference $\theta_{l,i}^{\pm} = \phi_l^i - \phi_{l\pm1}^i$ for $i = 1, \ldots, D$. The resulting eigenvalue problem Eq.(5.33) has D frequency (color) directions (with zero hopping along them) and each site $c_{l,\mathbf{v}}$ is connected to the nearest neighbor ones $c_{l\pm1,\mathbf{v}-\mathbf{s}}$ through the complex matrix elements $\mathrm{e}^{i\mathbf{s}\cdot\Phi_l^{\pm}} \mathcal{J}_{\mathbf{s}}^{\pm}$. Each frequency color will add to the total number of channels.

Let us assume that all frequency components satisfy the same condition for single or multi-channel (either strong or weak driving) regimes. Then we conclude that the single channel regime will be applicable to multi-color driving as well, i.e. in the limit of large frequencies localization length corresponds to its value from the undriven case. In the multi-channel regime, the localization length ζ_D will be of the order of $\zeta_D \sim D\zeta$ with ζ being the corresponding single color localization length discussed in the previous section. Therefore the localization length will stay finite for any finite number of colors. The divergence of ζ_D in the limit of $D \to \infty$ is in agreement with the result that a random noise driving leads to dephasing and complete delocalization [131, 224].

5.3.4 Numerical Results

We first analyze the single color driving and then discuss the two color case. We decide not to diagonalize the eigenvalue problem Eq.(5.14), since this will limit the required system size

N and the number of colors D. Instead, we compute the spreading of the wave packet over time for a single site excitation $\psi_l(t=0) = \delta_{l,N/2}$ as an initial condition using a numerical symplectic integration scheme SBAB_2 [216–220] This method keeps the norm fluctuations bounded, and allows one to easily incorporate any number of colors, without significant additional computational expense. However, the number of colors increases the expected localization length, and therefore there will be an overall restriction on the number of colors which can be implemented in a computational run, under a CPU time of the order of one week.

To measure the evolution of the wave packet, we calculate the second moment m_2, which for localized modes estimates the squared distance between the eigenmode tails. It is related to the localization length ζ of one mode as $m_2 \sim \zeta^2$, and is defined as

$$m_2(t) = \sum_l \left(l - \sum_{l'} l' |\psi_{l'}(t)|^2 \right)^2 |\psi_l(t)|^2 \,. \tag{5.35}$$

Hereafter, unless indicated differently, in Eq.(5.8) we choose the hopping amplitude $\lambda = 1$ and the disorder strength $W = 4$. Furthermore, for the numerical computations we choose a system size $N = 1024$ and we average $\log_{10} m_2(t)$ over 512 disorder realizations, unless stated otherwise.

5.3.4.1 One color

Let us analyze the frequency dependence of the time evolution. For the *weak driving* case, we choose the driving strength $\mu = 0.1$. The multi-channel regime ($\Delta \geq 1$) is then obtained for frequencies $\omega \leq 0.4$. The time evolution of the second moment m_2 is shown in the left plot of Fig.5.9.

We observe that the second moment first increases with time, but saturates at later times; indicating a halt of spreading, and a localization of the wave packet. Therefore we conclude that there is a finite upper bound on the localization length ζ of the corresponding eigenvalue problem. The onset of spreading beyond the undriven reference curve (black plot in left of Fig.5.9) scales inversely with the driving frequency as expected.

We use the saturated value of the second moment at time $t = 10^6$ as a measure of the squared localization length and plot it as a function of frequency ω in the right plot of Fig.5.9. Increasing ω in the single channel regime ($\omega > 0.4$) leads to a quick decay of the saturated second moment, reaching the undriven case reference value already at $\omega \approx 4$. In the multichannel regime, we observe two features: a plateau at an intermediate frequency interval, and a subsequent increase of the saturated second moment by further lowering the frequency. This is in agreement with our analytics in Sec. 5.3.2.3.1.

For the *strong driving* regime, we consider a driving strength $\mu = 1$. In the left plot of Fig.5.10, we show the time evolution of the second moment m_2 for different frequencies in the multi-channel regime $\omega \leq 5$. The second moment m_2 increases as the frequency ω decreases, in agreement with Eq.(5.30). Moreover, we observe the appearance of transient regions of normal diffusion that extend their length as the frequency ω decreases. Again $m_2(t)$ saturates at larger time, indicating a halt of spreading, and a localization of the wave packet. The frequency dependence of the saturated values of the second moment m_2 is shown in Fig. 5.10, where we plot the second moment of the wave packet at time $t = 10^5$ as function of the frequency ω. For comparison we also replot the weak driving curve from Fig.5.9; right plot. Similar to the weak driving (blue curve), the second moment for the strong driving (red curve) tends to the undriven case (black horizontal line) for large frequencies and diverges for small ones. In agreement with Eq.(5.30), the plateau (which was observed for weak driving) is suppressed, although a reminding shoulder exists at $\omega \approx 2.5$.

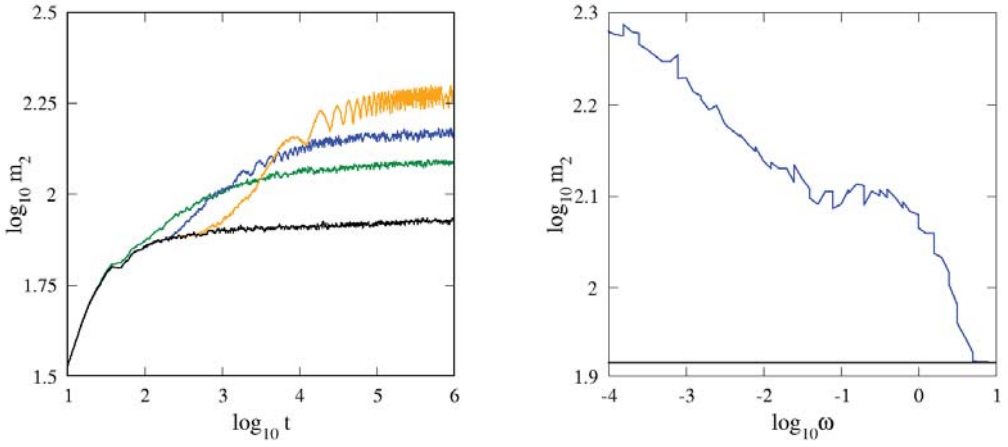

Figure 5.9: Left plot: Time evolution of the second moment m_2 with driving strength $\mu = 0.1$. Frequency values (from top to bottom at the right edge of the plot): $\omega = 5 \cdot 10^{-4}$ (orange), $\omega = 5 \cdot 10^{-3}$ (blue), $\omega = 10^{-1}$ (green), undriven (black). Right plot: Saturated second moment m_2 at $t = 10^6$ as a function of frequency ω of a one-color perturbation with $\mu = 0.1$. The black horizontal line indicates the value for the undriven case.

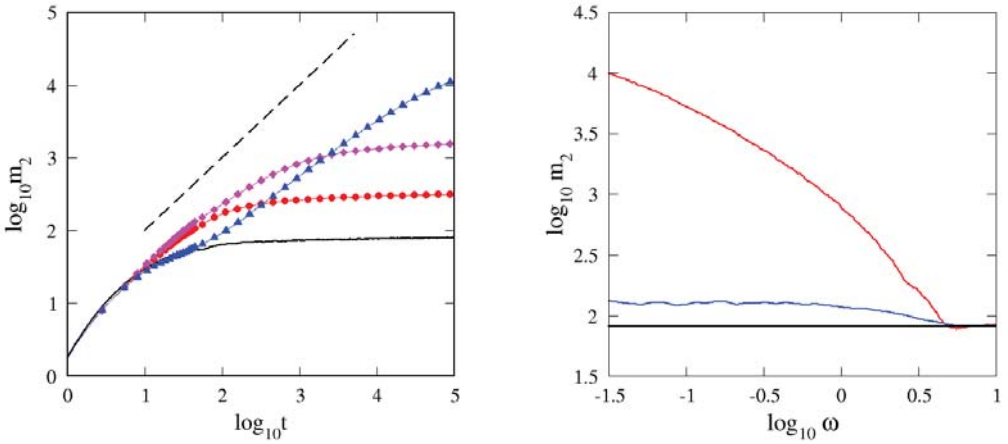

Figure 5.10: Left plot: Time evolution of the second moment m_2 with driving strength $\mu = 1$. The dashed line indicates normal diffusion $m_2 \sim t$. Frequency values: $\omega = 5$ (black), $\omega = 2$ (red/circles), $\omega = 0.5$ (magenta-diamonds), $\omega = 0.02$ (blue-triangles). Right plot: Saturated second moment m_2 at $t = 10^5$ as a function of frequency ω of a one-color perturbation with $\mu = 0.1$ (blue, bottom) and $\mu = 1$ (red, top). The black horizontal line indicates the value of the undriven case.

The strong driving yields much larger values of the saturated second moment as compared to the weak driving case, in accord with our predictions. The frequency dependence is weaker than the predicted law in Eq.(5.30), most likely due to local suppression of strong driving and multi-channel regimes, as previously discussed.

In Fig.5.11 we plot the time evolution of the second moment m_2 for different values of the driving strength μ in the strong driving regime. The inset of Fig. 5.11 shows the dependence of the almost saturated second moment m_2 at $t = 10^7$ on μ. We observe that

the saturated moment increases up to $\mu \approx 1$ and starts to decrease for larger values of μ. This subsequent decrease is qualitatively in agreement with the prediction $\zeta \sim \frac{1}{\mu}$ following from Eq.(5.17). We also note that the data for large values of μ did not completely saturate, due to limitations in the computational power.

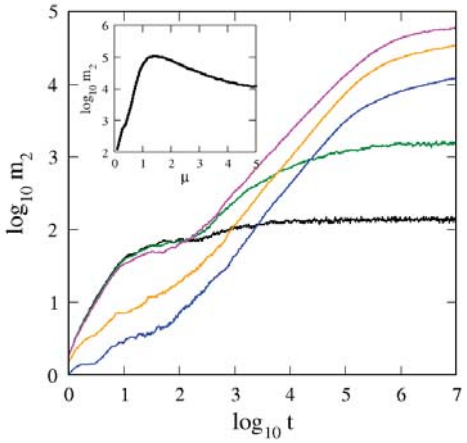

Figure 5.11: Time evolution of the second moment m_2 with frequency $\omega = 5 \cdot 10^{-3}$. Driving strength values (from top to bottom at the right edge of the plot): $\mu = 1.0$ (magenta), $\mu = 3.0$ (orange), $\mu = 5.0$ (blue), $\mu = 0.5$ (green), $\mu = 0.1$ (black). The inset plot shows the dependency of the almost saturated second moment m_2 at $t = 10^7$ on the drive strength. System size $N = 2048$, and $\log_{10}$ m$_2$ is averaged over 32 disorder realizations.

We note that Nakanishi *et. al.* [224] have studied the dynamics of a quantum particle (electron) in a two-dimensional setting with a single color strong driving in the adiabatic regime of small frequencies. There an unbounded normal diffusion was reported, which is probably due to the higher dimensionality of the underlying lattice. We further mention the numerical study of the increase of the localization length with decreasing frequency of an external AC field [221], which is similar to our analytical and numerical results for single color fluctuating potentials.

5.3.4.2 Two colors

We assume the driving strengths to be equal $\mu_1 = \mu_2$ and we fix the frequency relation $\omega_2 = \sqrt{2}\omega_1$. We first consider the *weak driving* case. In the left of Fig. 5.12, we compare one and two color cases for same driving strength $\mu_1 = \mu_2 = 0.1$ and frequency $\omega_1 = \omega 2 = 3 \cdot 10^{-2}$. The presence of a second incommensurate driving term enhances the spreading of the wave packet. However, the integration time $t = 10^5$ is not enough to see the saturation of the second moment. To obtain saturation at time $t = 10^5$, we reduce the driving strength to $\mu_1 = \mu_2 = 0.05$. In the right of Fig.5.12, we show the saturated value of the second moment m_2 at time $t = 10^5$, as a function of the frequency ω_1, and compare it to the weak driving single color result ($\mu = 0.1$) from Fig.5.9's right plot. The values approach the undriven case (black horizontal line) for approximately $\omega_1 \geq 4$, in good agreement with the single channel regime $\omega_1, \omega_2 \geq 2$. Similar to the one color case, the saturated second moment exhibits a plateau in the multi-channel regime. Notably, the height of the plateau is practically equal to the single color one reported in Fig.5.9. This is in full accord with our estimate of the localization length in Eq.(5.27), which is independent of the driving strength μ, and more in general, independent of the number of participating channels. Therefore the presence of a

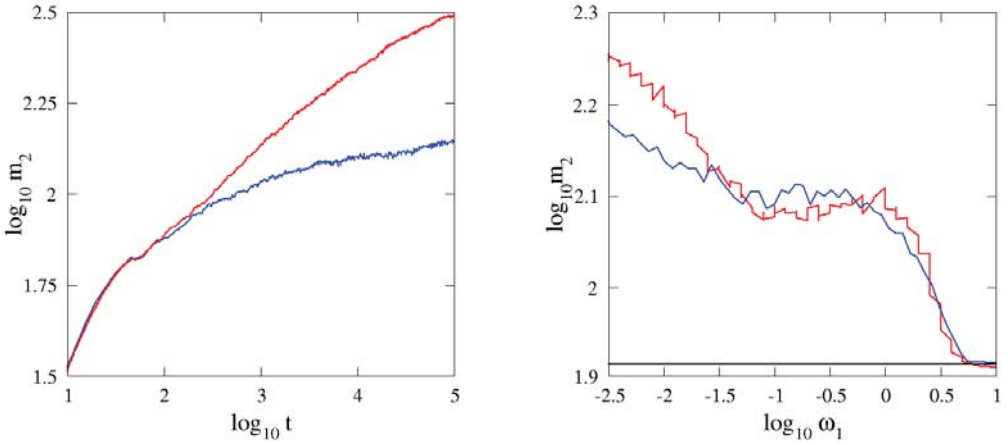

Figure 5.12: Left plot: Time evolution of the second moment m_2 for one-color (blue, bottom) and two-color (red, top) cases with driving strength $\mu = \mu_1 = 0.1$ and frequency $\omega = \omega_1 = 3 \cdot 10^{-2}$. We recall $\omega_2 = \sqrt{2}\omega_1$ for the two color case. Right plot: Saturated second moment m_2 at $t = 10^5$ as a function of driving frequency ω_1 with driving strengths $\mu_1 = \mu_2 = 0.05$ (red curve, top at left corner). The blue curve corrsponds to the single color one from Fig.5.9. We recall $\omega_2 = \sqrt{2}\omega_1$. The black horizontal line indicates the value of the undriven case.

second frequency (which increases the number of channels), should not change the plateau value, as observed.

For the *strong driving* case, we consider $\mu_1 = \mu_2 = 1$. In Fig. 5.13, we show the time evolution of the second moment m_2 for frequencies $\omega_{1,2}$ chosen in the multi-channel regime. We observe long lasting transient regions of diffusive spreading, with a clear tendency to-

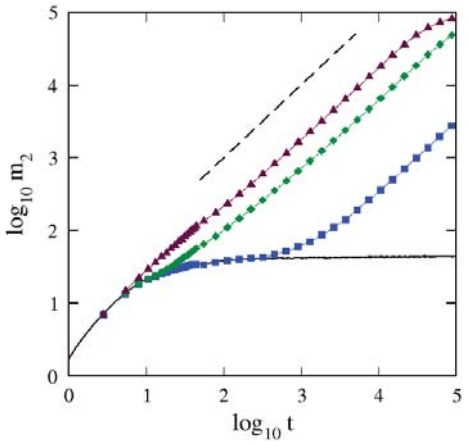

Figure 5.13: Time evolution of the second moment m_2 with driving strength $\mu_1 = \mu_2 = 1$. We recall $\omega_2 = \sqrt{2}\omega_1$. The dashed line indicates normal diffusion $m_2 \sim t$. Frequency values: $\omega_1 = 5 \cdot 10^{-1}$ (maroon/triangles), $\omega_1 = 5 \cdot 10^{-2}$ (green/diamonds), $\omega_1 = 5 \cdot 10^{-4}$ (blue/squares), undriven (black).

wards a subsequent halt and localization. Again the onset of spreading beyond the undriven reference curve (black one in Fig.5.13) is scaling inversely with the driving frequency as expected, similar to the $D = 1$ case. We also observe a significant increase in the localization

length as compared to the single color case, in agreement with our predictions.

5.4 Summary and Discussions

In this chapter we have studied two examples of spatially non-periodic one-dimensional lattices that exhibit exponential localization of their eigenmodes, in the presence of two different kinds of coherent driving. Both drivings, in certain situations, lead to a profound change of the localization features of the models.

In Sec.5.2 we have studied the Aubry-Andre system in the presence of a weak driving force. The driving force is introduced by superimposing a moving time-periodic lattice over a stationary quasiperiodic potential. The undriven Aubry-André model is chosen to be well in the insulating regime. For a spatial resonance which reduces the reciprocal space dynamics to an effective one-dimensional two-leg ladder case, the AC perturbation resonantly couples groups of localized eigenstates of the undriven Aubry-André model and turns them into extended ones. Slight detuning of the spatial and temporal frequencies off resonance returns these states into the family of localized ones. Initial wave packets overlap with resonant extended eigenstates and lead to ballistic spreading. Therefore the proposed AC perturbation can be used as a simple and elegant method to control the degree of localization of wave packets in quasiperiodic lattices.

In Sec.5.3 we have studied the spreading of a wave packet for a one-dimensional disordered chain in the presence of a multi-frequency quasi-periodic drive. For each term (color) of the driving, the Floquet representation is used to arrive at a time-independent eigenvalue problem on a two-dimensional lattice, with one direction corresponding to the original spatial extension, and the second one to the Floquet (driving) one. We transform into a Wannier-Stark basis which is diagonal along the Floquet direction, and analyze the resulting eigenvalue problem. For large driving frequencies the equations reduce to uncoupled single channel ones, which are essentially equivalent to the undriven case. For small driving frequencies we obtain a multi-channel regime with a substantial increase of the localization length, and its divergence in the limit of vanishing frequency. This multi-channel regime divides into two further regimes of weak and strong driving amplitudes, which yield different scaling laws.

In the many-color case, we have shown that each incommensurate color is independent from the others and can be treated separately. The localization length of the model will then be proportional to the single color localization length, and scales with the number of colors set in the multi-channel regime. Therefore, it will remain finite for any finite number of colors.

Numerically we have observed that in the strong driving, the model exhibits transient regions of diffusive dynamics before the onset of localization. The localization volume increases as the number of colors increases, when satisfying the multi-channel regime condition. It follows that for $D \to \infty$, the localization length will diverge to infinity and the region of diffusive dynamics will extend to infinity, until a complete delocalization is observed. The divergence of the number of colors D corresponds to the loss of quasiperiodicity of the driving term, and consequently to an effective random driving which leads to a loss of Anderson localization in that limit [131, 224].

Mathematical studies of the single color $D = 1$ case [234] and multicolor case $D > 1$ [235] predict stability of Anderson localization in the regime of strong disorder. These results are in line with our findings, since the limit of strong disorder is corresponding to the single channel regime; which is essentially independent on the number of colors, with a localization length close to the one of the undriven case.

CHAPTER 6

The Two Interacting Particles Problem in Quasiperiodic Chains

In this chapter we study the problem of two interacting particles in a one-dimensional Aubry-André chain, under a coherent driving in the interaction. We first introduce the two interacting particle problem as a fundamental case of the field of the many-body problem. Then, we will present the two interacting particles problem in a one-dimensional Aubry-André chain, highlighting the appearance of correlated metallic states within the insulating regime of the single particle. Next, we introduce a coherent drive in the interaction term of the model. Aim of the driven interaction is to generate these families of states by design, inducing delocalization in regions of the parameter space where it does not occur. On the other hand, we observe strong evidences that within regions where correlated metallic states exist, the driving suppress the delocalization of the two interacting particles.

6.1 Introduction

Within condensed matter physics, one of the most active research topic during the last decades has been the *Many-Body Localization* (MBL). The MBL belongs to the class of Many-Body Problems, and it aims to understand the transport properties (or the absence of transport) of systems with an arbitrary number of interacting particles, where each one in the non-interacting case exhibit spatial localization. Within the MBL, the interplay between Anderson localization and many-body interaction has been one of the first considered and still one of the most important cases [236–240]. Several fundamental concepts have been introduced in 2006 in a seminal work of *Basko, Aleiner and Altshuler* [8], where they studied the transport of many electrons in disordered chains in regimes of small temperatures. Since then, theoretical and experimental results followed with an impressive rate.

One of the fundamental cases of the many-body problem is the *two interacting particles problem* (TIP), since the comprehension of the basic particle-particle interaction is essential to study systems with an arbitrary number of particles. This case has been discussed

and analyzed extensively during these past years, in one-dimensional chains with different localizing potentials, as well as lattices of higher dimensions. Particular interests received the case of TIP in Anderson chains, where several works focused on the possible relation between the localization length ξ_1 of a single particle to the localization length ξ_2 of the two interacting ones [10, 241–247] and subdiffusion of the TIP in case of large values of the single particle localization length [248].

In this chapter we will focus of the TIP in presence of quasiperiodic Aubry-André potentials. The quasiperiodic TIP has been analyzed for decades [255–260], reporting strong evidences of spreading in the single particle insulating regime. Recently, delocalization for the TIP has been observed in two dimensional lattices [261] and for weakly interacting bosons in one dimension [262]. In the following we will discuss the TIP in a one-dimensional Aubry-André chain and the spreading effect due to the existence of correlated metallic states within the single particle insulating regime [123].

In the first section Sec.6.2, we review one of the main framework used to analyze systems of interacting particles, the *Bose-Hubbard* model. We will discuss this hamiltonian system and introduce the formalism of the Fock states. Then, in the case of two interacting particles, we will first overview the mapping of the one dimensional quantum model to a two dimensional lattice. Then, in Sec.6.3 we enter the case of two interacting particles in a quasiperiodic Aubry-André chain. We first discuss the appearance of correlated metallic states within the single particle insulating regime for certain values of the interactions strength [123]. We consider the interaction term of the system coherently driven in time in order to generate correlated metallic states in regimes of smaller interaction strengths. The driven problem is studied analytically and numerically, expanding the model equation using the Floquet analysis and computing numerically the time evolution of the wave packet. The original purpose though has not been achieved with this class of driving.

6.2 The Two Particles Problem

As a special, yet fundamental, case of the many-body problems, in this section we introduce the two interacting particles (TIP) on a one dimensional lattice, in presence of a local interaction term. This model, in presence of an Aubry-André potential, will be the main focus of the following section and of the whole chapter. The Hamiltonian of the system reads

$$\mathcal{H} = \sum_l \epsilon_l \hat{b}_l^+ \hat{b}_l + \hat{b}_{l+1}^+ \hat{b}_l + \hat{b}_{l+1} \hat{b}_l^+ + \frac{U}{2} \hat{b}_l^+ \hat{b}_l^+ \hat{b}_l \hat{b}_l \ , \tag{6.1}$$

where $\hat{b}_l^+$ and $\hat{b}_l$ are the creation and the annihilation operators. The scalar U controls the interaction strength between the two particles. This model ultimately leads to the hamiltonian equation of the model $i|\dot{\psi}\rangle = \mathcal{H}|\psi\rangle$, where the dot indicates the time derivative of the state $|\psi\rangle$. In the single particle case, the interactions term does not contribute. The Bose-Hubbard model can be generalized to higher dimensional lattice, longer range and anisotropic hopping, non local interactions and presence of frustration [249–251]. It moreover can be reformulated for describe ring-shaped optical lattice [252] or for topologically nontrivial flat-band lattices [253]. In the following subsection we discuss the one dimensional case Eq.(6.1), introducing the Fock states and the equivalent model associated that arises from the expansion in this alternative basis (details in Appendix C.1).

6.2.1 Expansion in Fock states

In quantum mechanics, the *Fock states* are elements of an Hilbert space (the *Fock space*), and they describe the displacements of distinguishable or undistinguishable particles on a

lattice. These states are characterized by the numbers $\{l_k\}$, each one describing the k-th particle on the site l_k

$$|l_1, l_2, \dots, l_k, \dots\rangle \tag{6.2}$$

The presence of absence of the particles are described by the *creation* and the *annihilation* operators $\hat{b}_l^+$ and $\hat{b}_l$, operators that put or remove a particle on the site l. In the case of fixed number of particles N, these states can be rewritten where the number $\{l_k\}_{k=1}^N$ define the lattice site each particle is occupying. For the single particle case $N = 1$, the Fock states are defined as $|l\rangle := \hat{b}_l^+|0\rangle$, where l is the lattice site. The set $|l\rangle$ form a basis with which a state $|\psi\rangle$ can then be expanded as $|\psi\rangle = \sum \varphi_l \hat{b}_l^+|0\rangle$. This expansion reduces the hamilton equation $i|\dot{\psi}\rangle = \mathcal{H}|\psi\rangle$ for the hamiltonian $\mathcal{H}$ in Eq.(6.1) to a one-dimensional tight-binding model Eq.(2.4) on the expansion coefficient φ_l,

$$i\frac{\partial}{\partial t}\varphi_l = \epsilon_l\varphi_l + \varphi_{l+1} + \varphi_{l-1} \ . \tag{6.3}$$

For the two indistinguishable particles case $N = 2$ we will use the basis $|l, m\rangle$, for l and m lattice sites, defined as

$$|l, m\rangle := \frac{\hat{b}_l^+\hat{b}_m^+|0\rangle}{\sqrt{1+\delta_{l,m}}} \ , \qquad l \leq m \ . \tag{6.4}$$

The condition $l \leq m$ holds since the two particles are considered indistinguishable. The expansion of a state $|\psi\rangle$ in this basis follows

$$|\psi\rangle = \sum_l \sum_{m\geq l} \varphi_{l,m}|l, m\rangle \ , \tag{6.5}$$

This basis yields the Hamiltonian quantum model into a two-dimensional problem on the expansion coefficient $\varphi_{l,m}$ [254], that exists on half of the two-dimensional lattice $\Gamma \equiv \{(l, m)|l \leq m\}$.

$$\begin{cases} i\frac{\partial}{\partial t}\psi_{l,m} & = (\epsilon_l + \epsilon_m)\psi_{l,m} + \psi_{l-1,m} + \psi_{l+1,m} + \psi_{l,m-1} + \psi_{l,m+1} \ , & l < m-1 \\ i\frac{\partial}{\partial t}\psi_{l,l+1} & = (\epsilon_l + \epsilon_{l+1})\psi_{l,l+1} + \psi_{l,l+2} + \psi_{l-1,l+1} + \sqrt{2}\psi_{l,l} + \sqrt{2}\psi_{l+1,l+1} \ , & l = m-1 \\ i\frac{\partial}{\partial t}\psi_{l,l} & = (2\epsilon_l + U)\psi_{l,l} + \sqrt{2}\psi_{l+1,l} + \sqrt{2}\psi_{l-1,l} \ , & l = m \end{cases} \tag{6.6}$$

A representation of the lattice Γ is shown in Fig.6.1. This lattice problem Eq.(6.6) can be unfolded to a two dimensional lattice via the transformation

$$\begin{cases} \varphi_{l,l} = \sqrt{2}\psi_{l,l} \ , & l = m \ ; \\ \varphi_{l,m} = \psi_{l,m} \ , & l \neq m \ . \end{cases} \tag{6.7}$$

The unfolded two dimensional lattice equation than holds

$$i\frac{\partial}{\partial t}\varphi_{l,m} = \epsilon_{l,m}\varphi_{l,m} + \varphi_{l+1,m} + \varphi_{l-1,m} + \varphi_{l,m+1} + \varphi_{l,m-1} \ ; \tag{6.8}$$

where the onsite energy terms $\epsilon_{l,m}$ are

$$\epsilon_{l,m} = \epsilon_l + \epsilon_m + U\delta_{l,m} \ . \tag{6.9}$$

Let's notice that the two dimensional lattice has the interaction term U present only in the diagonal term, as the interaction between particles is local and occurs only when the particles are located in the same site. We refer the details to the Appendix C.1.

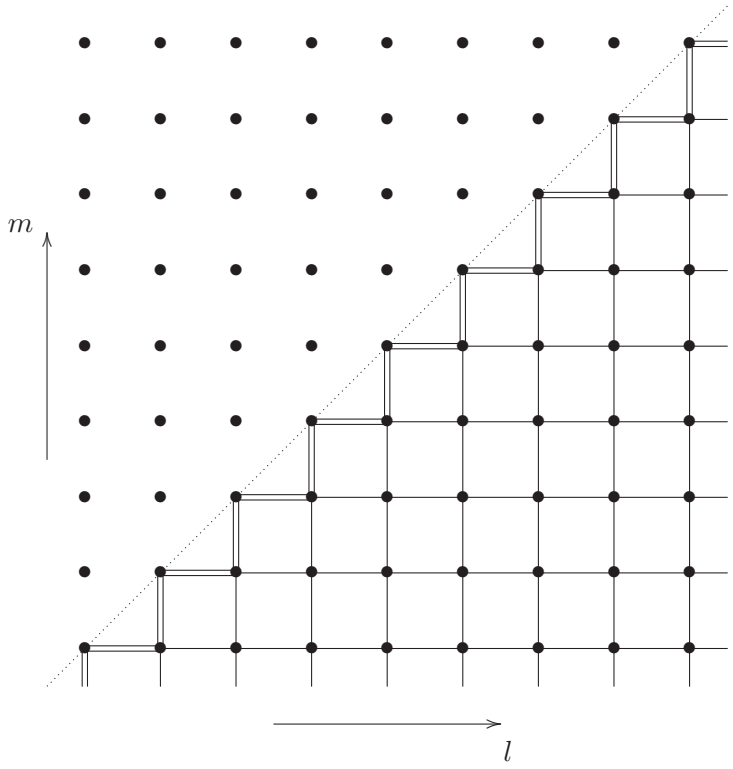

Figure 6.1: Schematic picture of the lattice Eq.(6.6). The lattice holds for the lower triangle $l \leq m$. The single bars "$-$" indicates hopping coefficient 1, while the double bars "$=$" indicates hopping coefficient $\sqrt{2}$.

We can calculate the Probability Distribution Function p_l (PDF) of $|\psi\rangle$ at lattice site l between 1 and L (the system size) with the formula

$$p_l \equiv \frac{1}{2}\left[\sum_{s=1}^{l} |\varphi_{s,l}|^2 + \sum_{s=l}^{L} |\varphi_{l,s}|^2\right] ; \tag{6.10}$$

and its participation number P

$$P \equiv \frac{1}{\sum_{l=1}^{L} p_i^2} \tag{6.11}$$

From (6.5) we can calculate the second moment m_2 of ψ. We first define the centers of mass $\bar{l}$ and $\bar{m}$

$$\bar{l} \equiv \sum_{l=1}^{L}\left[\sum_{m=l}^{L} l \cdot |\varphi_{l,m}|^2\right] , \quad \bar{m} := \sum_{l=1}^{L}\left[\sum_{m=l}^{L} m \cdot |\varphi_{l,m}|^2\right] . \tag{6.12}$$

It follows that

$$m_2^{(\psi)} := \sum_{l=1}^{L}\left[\sum_{m=l}^{L} [(l-\bar{l})^2 + (m-\bar{m})^2] \cdot |\varphi_{l,m}|^2\right] \tag{6.13}$$

We refer to Appendix A.3 for details. In the next subsection we discuss certain results of the two interacting particles problem, before to enter the problem in an Aubry-André chain in Sec.6.3.

6.3 Two Interacting Particles in an Aubry-André Chain

The Hamiltonian of the system is the Bose-Hubberd hamiltonian Eq.(6.1), defined with the quasiperiodic Aubry-André potential

$$\epsilon_l = \lambda \cos(2\pi(\alpha l + \beta)) \ . \tag{6.14}$$

The incommensurate parameter α is chosen as the golden mean $\alpha = (\sqrt{5}-1)/2$ and the phase shift β is irrelevant for the fate of the eigenstates, therefore it can be arbitrarily chosen in $[0, 2\pi]$. Recently Flach *et.al.* highlighted the existence of pairing bound states and consequent appearance of delocalization phenomena in the Aubry-André insulating regime of the single particle case [123]. The subsection Sec.6.3.1 refers then to the results reported in this paper.

6.3.1 Existence of Correlated Metallic States

In the non interacting case $U = 0$ with α chosen as the golden mean, the spectrum decomposes in five bands that are the products of the three bands of the single particle Aubry-André spectrum. The band structure is maintained also in presence of interaction $U \neq 0$. This follows since most of the states corresponds to the two particles situated in the lattice further than the localization volume of the single particle case. Therefore these states are practically unaffected by the increasing of the interaction constant. In Fig.(6.2) - left plot, we plot the participation number P versus the eigenvalues, and we clearly observe the five bands in the interacting case $U = 7.9$. Moreover, we notice that most of the states have low values of participation number, while certain ones exhibit a substantially higher P. In the right plot of Fig.(6.2) we plot the energy density p_l of two states, one localized (red), correspondent to a low value of the participation number of the left plot, and one extended (blue), correspondent to a high value instead. In [123], it has been shown that in this case $\{U, \lambda\} = (7.9, 2.5)$, the value of the highest participation number scales linearly with the system size L, which implies the appearance of delocalized states in the energy spectrum of the TIP within the single particle insulating regime. These states have been renamed *correlated metallic states*. The fact that these states occur only for certain values of the interaction strength U for given values of the potential strength λ in the phase space seems to indicates a resonance mechanism between renormalized states. We will discuss this issue more in depth in Sec.6.3.2.2.

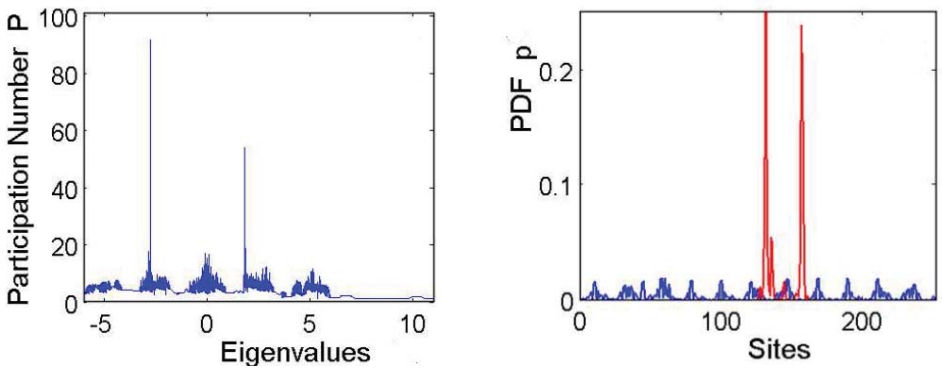

Figure 6.2: Left: Participation number P of the two interacting particles versus the respective eigenstates. Right: PDF distribution p_l of a localized state (red) and an extended one (blue). In this case, $\lambda = 2.5$, $U = 7.9$ and $\alpha = (\sqrt{5}-1)/2$. Figure taken from [123]

From the spectral analysis of the TIP, the time evolution has been computed for different values of the parameters $\{U, \lambda\}$. Initial state has been chosen as the two particles located at adjacent sites, and the Schrödinger equation Eq.(6.8) has been evolved until total time $t = 1.5 \cdot 10^4$. For each case $\{U, \lambda\}$ of the phase space, the wave packet second moment has been measured for sixty different initial positions of the particle, and the highest value of m_2 is plotted in Fig.6.3, left plot. We notice that, irrespective to the interaction strength U, for $\lambda \leq 2$ the TIP is in complete metallic regime. This follows from the fact that for $\lambda \leq 2$ every single particle state is extended. In the single particle insulating regime $\lambda > 2$, different regions of correlated metallic states can be observed. These regions correspond to values of $\{U, \lambda\}$ where correlated metallic eigenstates exist in the TIP energy spectrum. In Fig.6.3 - right plot, the time evolution of the distribution function p_l is computed for two cases: $U = 2$, which corresponds to insulator case and $U = 4.5$, which corresponds to the correlated metallic case. For both cases, $\lambda = 2.5$. These computation confirms that in the former case, the particles exhibit complete localization while in the latter delocalization appears.

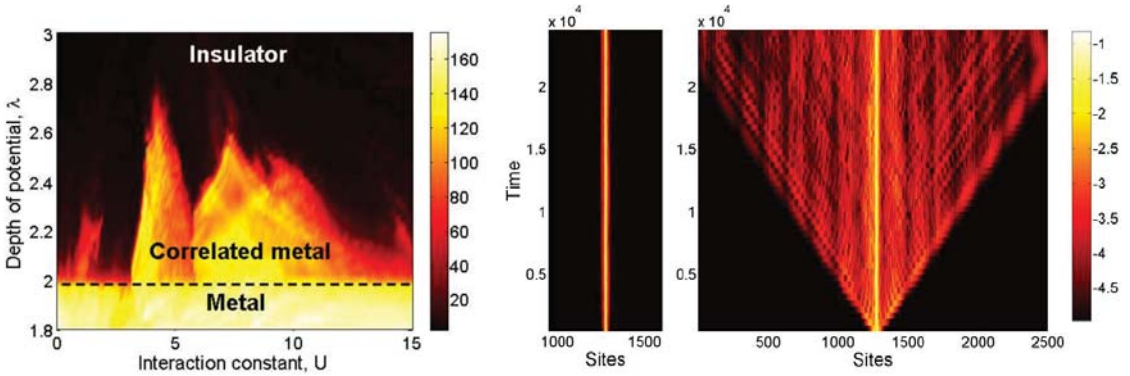

Figure 6.3: Left: Phase diagram of the square root of the second moment at time $t = 1.5 \cdot 10^4$ for a system size $N = 610$ sites. Right: Time evolution of the PDF distribution p_l for $\lambda = 2.5$ with $U = 2$ - insulator (left panel) and $U = 4.5$ - correlated metallic (right panel). For both figures, initial state with two particles located at adjacent sites and $\alpha = (\sqrt{5} - 1)/2$. Figures taken from [123].

These computations have clearly shown the existence of correlated metallic states in the energy spectrum within the insulating regime of the single particles $\lambda > 2$. The time evolution in correspondence of these states confirmed the wave packet spreading. However, the mechanism of the generation of these states in certain sub-regions of the phase space $\{U, \lambda\}$ is yet not clear. To this end, and to possibility generate them by design, we introduce the driving component in the interaction term. Our studies though have revealed to be not completely successful with respect to our original aim. However, they contributed on the understanding of the quasiperiodic case of the two interacting particle problem.

6.3.2 Driving the Interaction

We consider the Bose-Hubbard hamiltonian Eq.(6.1) in presence of a coherently driven interaction constant $U(t)$, defined as

$$U(t) = U_0(1 + \mu \cos(\omega t)) \ ; \tag{6.15}$$

where U_0 is the interaction strength of the undriven model, $0 < \mu \ll 1$ the driving strength and ω the driving frequency. The presence of the driving term does not break the expansion

of the one-dimensional Bose-Hubbard hamiltonian into a two dimensional lattice, Eq.(6.8). The lattice equation has the driven interaction acting on the diagonal.

$$i\frac{\partial}{\partial t}\varphi_{l,m} = (\epsilon_l + \epsilon_m + U(t)\delta_{l,m})\varphi_{l,m} + \varphi_{l-1,m} + \varphi_{l+1,m} + \varphi_{l,m-1} + \varphi_{l,m+1} \ . \tag{6.16}$$

We will expand this time-dependent model equation using the Floquet expansion [225,226], which yields to an effective time-independent three dimensional eigenvalue problem.

6.3.2.1 From Floquet to Wannier-Stark

Let's define the Floquet expansion for every lattice site (l, m) for a real value E

$$\varphi_{l,m} = \sum_{k=-\infty}^{+\infty} A_{l,m,k} e^{-i(E-\omega k)t} \tag{6.17}$$

The equation (6.16) becomes a three dimensional lattice

$$\begin{aligned} EA_{l,m,k,} = &(\epsilon_l + \epsilon_m + U_0\delta_{l,m} + \omega k)A_{l,m,k} \\ &+ A_{l+1,m,k} + A_{l-1,m,k} + A_{l,m+1,k} + A_{l,m-1,k} \\ &+ \frac{\mu U_0}{2}\delta_{l,m}(A_{l,m,k-1} + A_{l,m,k+1}) \end{aligned} \tag{6.18}$$

In absence of real hopping along l and m, we can solve the eigenvalue problem along the momentum direction k, which corresponds to the Wannier-Stark ladder [227] under an effective DC electric field ω. On the lattice diagonal, the hopping coefficient is $\mu U_0/2$, while off-diagonal the Wannier-Stark ladders have null hopping. The eigenfunctions are obtained using the Bessel function of the first kind $J_k(x)$ with fixed argument x, and their eigenvalues form equidistant spectra $E_{\nu,l,m} = \epsilon_l + \epsilon_m + U_0\delta_{l,m} + \omega\nu$ [228, 229].

$$B^{(\nu)}_{l,m,k} = J_{k-\nu}\left(\frac{\mu U_0}{\omega}\delta_{l,m}\right) , \qquad E_{\nu,l,m} = \epsilon_l + \epsilon_m + U_0\delta_{l,m} + \omega\nu \ . \tag{6.19}$$

We want to use this basis to define a coordinate rotation in the momentum space

$$A_{l,m,k,} = \sum_{\nu} c_{l,m,\nu} B^{(\nu)}_{l,m,k} \ . \tag{6.20}$$

This coordinate transformation rotates Eq.(6.18) into

$$\begin{aligned} Ec_{l,m,\nu} = &(\epsilon_l + \epsilon_m + U_0\delta_{l,m} - \omega\nu)c_{l,m,\nu} \\ &+ \sum_s \Big(J_s(z^-_{l,m})c_{l-1,m,\nu-s} + J_s(z^+_{l,m})c_{l+1,m,\nu-s} + \\ &\quad + J_s(x^-_{l,m})c_{l,m-1,\nu-s} + J_s(x^+_{l,m})c_{l,m+1,\nu-s}\Big) \end{aligned} \tag{6.21}$$

where

$$\begin{aligned} z^{\pm}_{l,m} &= \frac{\mu U_0}{\omega}(\delta_{l,m} + \delta_{l\pm1,m}) \\ x^{\pm}_{l,m} &= \frac{\mu U_0}{\omega}(\delta_{l,m} + \delta_{l,m\pm1}) \end{aligned} \tag{6.22}$$

We refer to Appendix C.3 for the details of the expansion. The resulting lattice has zero diagonal hoppings along the Fourier direction ν. Instead, each diagonal lattice site $c_{l,l,\nu}$ is connected to every first off-diagonal sites $c_{l\pm1,l\pm1,\nu-s}$ by the hopping coefficients $J_s(\Delta^{\pm}_{l,m})$,

with $\Delta = x, z$. The number of strong links (connectivity) with a given site at l, ν depends on the ratio of the difference in the new onsite energies $|\epsilon_l - \epsilon_{l\pm1} + s\omega|$ and the hopping strength $|J_s(\Delta_l^{\pm})|$. Strong links are then characterized by $|(\epsilon_l - \epsilon_{l\pm1} + s\omega)/J_s(\Delta_l^{\pm})| \leq 1$. These expansion, in analogy with the driven Anderson chains discussed in Sec.2.3, exhibit two distinct *single channel* and *multi-channel* regimes, according to the frequency values. In the former regime we expect that the driven model behaves as the undriven system. In the latter regime it is legitimate to expect an enhancement of the localization length as the frequency ω decays to zero, in analogy to the driven Anderson case presented in Sec.6.3.2. Then in particular, we want to see if the driving, for values of the frequency ω of the order of the gaps between the spectral bands, artificially generates the correlated metallic states within regions of the phase space Fig.6.3 - left plot, where families of these states do not exist.

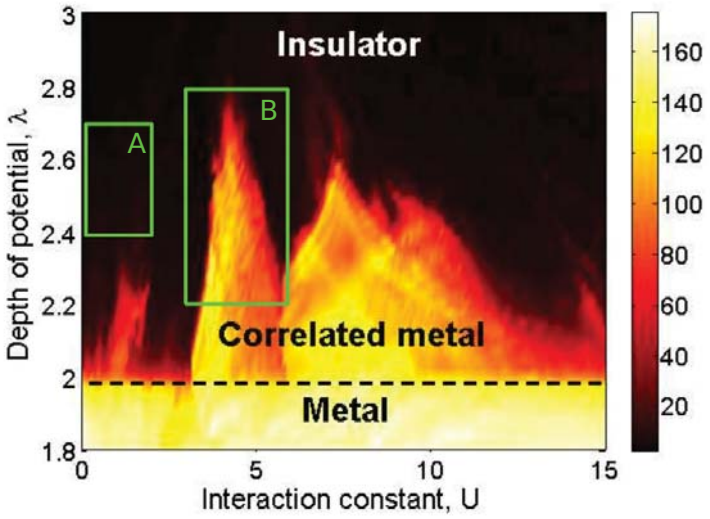

Figure 6.4: Phase diagram in Fig.6.3 - left plot, with our two regions of interest, highlighted in green boxes. Region $A \equiv [0, 2] \times [2.4, 2.7]$ and Region $B \equiv [3, 6] \times [2.2, 2.8]$.

We focus in two sub-regions of the parameter space $\{U, \lambda\}$, Fig.6.3 - left plot. Region A, defined as $A \equiv [0, 2] \times [2.4, 2.7]$, where complete localization holds in the undriven case. Region B, defined as $B \equiv [3, 6] \times [2.2, 2.8]$, where delocalization is observed, due to existence of correlated metallic states. Within region A, we aim to understand if the coherent driving could generate delocalization, either in the case of small frequency $\omega \longmapsto 0$ and in the case of resonant generation of correlated states. Within region B, we aim to understand the faith of the correlated states. Region A and B are shown in Fig.6.4. For both regions A and B, we compute the time evolution the two particles placed at adjacent sites in the center of the chain. For each computation performed, we first scan over the phase shift β of the Aubry-André potential (6.14)) in order to select the optimal one. Then, with the selected shift $\hat{\beta}$, we compute the time evolution longer in time. The computations then will be performed for given values (U_0, λ) within the respective regions, computing the time evolution of the wave packet spreading.

6.3.2.2 Region A

One of the motivation of the existence of resonant metallic states in the undriven case is rooted in the spectral structure given by the Aubry-André potential Eq.(6.14) in the undriven case. As seen in Fig.6.2, the spectrum is formed by some different minibands (five, for the choice of the golden ratio as the incommensurate parameter α in Eq.(6.14))

that are the products of the three single-particle spectral minibands. The renormalization of each bands is given by the averaged values of the overlap integrals I^0 (see Appendix C.2 for details). For the first sub-band, its value is $I^0 \approx 0.5$, while for the second is $I^0 \approx 0.3$ [123]. With the increase of the interaction constant U, certain renormalized states of the first band resonate with certain weakly renormalized states of the second band, generating the correlated metallic bound states. The width of the gaps between the bands is about two units, for $\lambda = 2.5$. Therefore, from the relation $I^0 U \approx 2$, the interaction strength U is expected to be $U \approx 4$ for the first overlap integral $I^0 \approx 0.5$, and $U \approx 6.7$ for the second one $I^0 \approx 0.3$. In Fig.6.3, for $\lambda = 2.5$ in correspondence of $U \approx 4$ and $U \approx 6.7$ we observe regions where exist correlated metallic states. These two regions are separated from a insulator gap.

The idea of the driving the interaction term - Eq.(6.15) - is to amplify the mechanism of formation of correlated metallic states that occurs in the undriven case, and possibly to generate families of these states in regions where these states are absent. Region $A \equiv [0, 2] \times [2.4, 2.7]$ has then been chosen since it is well into the insulator phase. In the case of a driven interaction Eq.(6.15) defined with $U_0 = 1$, we expect the frequency ω to satisfy the relation $I^0 \omega \approx 2$ and resonantly generate metallic states. Then, from the first overlap integral $I^0 \approx 0.5$ it follows a resonant frequency $\omega \approx 4$, and from the second overlap integral $I^0 \approx 0.3$ it follows a resonant frequency $\omega \approx 6.7$. In Fig.6.5 we show one case of the scan of the second moment m_2 at time $t = 10^3$ for different equispaced frequencies ω for $(U_0, \lambda) = (1.0, 2.5)$ with driving strength $\mu = 0.2$ (left plot) and $\mu = 0.4$ (right plot).

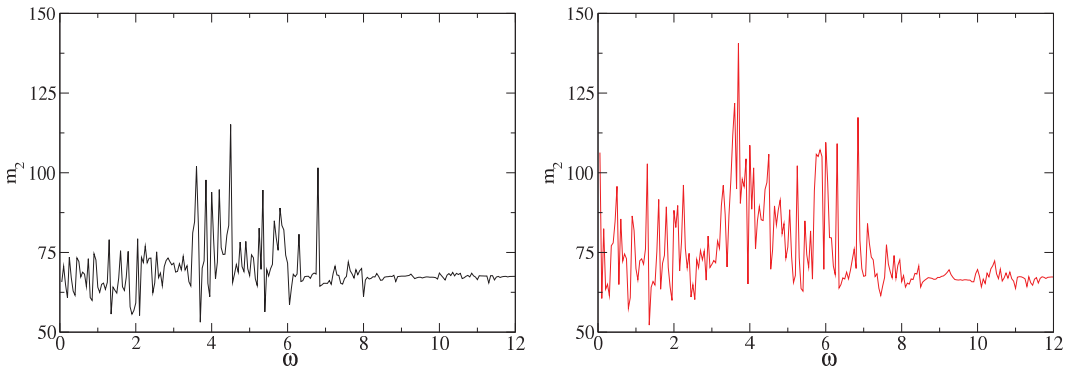

Figure 6.5: Left plot: second moment m_2 at time $t = 10^3$ versus the frequency ω for $\mu = 0.2$. Right plot: second moment m_2 at time $t = 10^3$ versus the frequency ω for $\mu = 0.4$. Both cases, $U_0 = 1.0$ and $\lambda = 2.5$. Omegastep $= 0.05$, system size $L = 2^8$.

At first, we can notice that in both plots of Fig.6.5, for frequencies $\omega \geq 10$, the second moment oscillations flatten down at $m_2 \approx 67.5$. This follows because, for high frequency values, the model enters the *single channel* regime, behaving as the undriven case. For frequencies $\omega \leq 10$, in both plots of Fig.6.5 we observe the highest fluctuations for frequency values around $3.5 \leq \omega \leq 5$ with also some peaks appearing for $\omega \approx 7$. Let's consider the highest peak observed in Fig.6.5, obtained for $\omega = 3.7$ and $\mu = 0.4$. In Fig.6.6 we show the time evolution of the second moment m_2 for a driving term defined with frequency $\omega = 3.7$ for either $\mu = 0.2$ and $\mu = 0.4$.

In Fig.6.6 - left plot, we can notice that the two curves of the time evolution of the second moment exhibit nearly analogous localization. In Fig.6.6 - right plot, we plot the energy density p_l for both $\mu = 0.2$ and $\mu = 0.4$ at time $t = 10^4$. The two cases show similar exponentially localized profiles. Several other simulation for different values (U, λ) in region A or for higher diving strength μ (not shown here for sake of space) exhibited the same

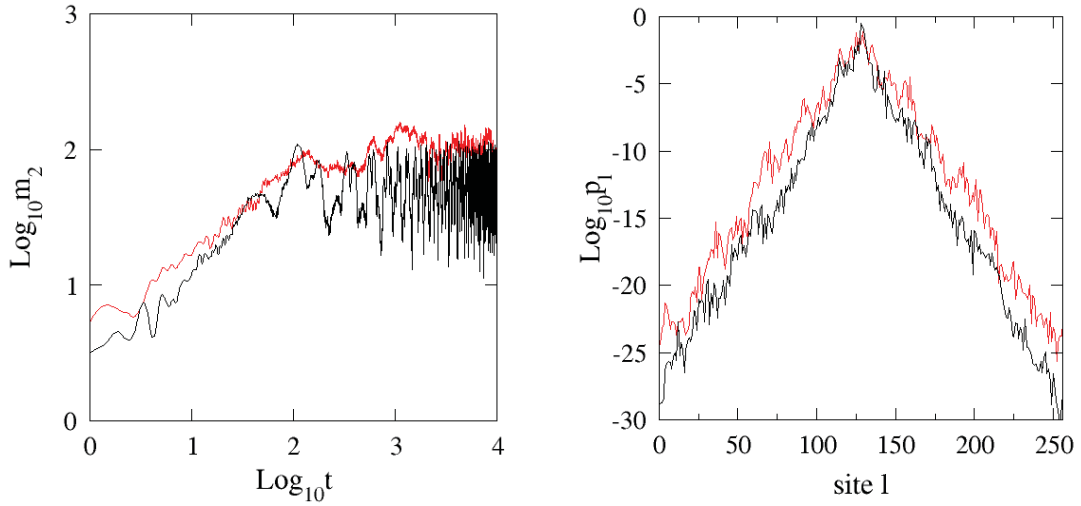

Figure 6.6: Left plot: time evolution of the second moment m_2 for $\mu = 0.2$ (black curve) and $\mu = 0.4$ (red curve). Right plot: energy density p_l versus lattice sites l at final time $t = 10^4$. Both cases, $\omega = 3.7$, $U_0 = 1.0$ and $\lambda = 2.5$. System size $L = 2^8$.

outcomes here exposed. It follows that the resonance mechanism (if exists) is anyway too weak to resonantly generate correlated metallic states. This numerically shows the lack of generation of correlated metallic states by this driving term.

In the case of small frequency ω, we enter multi-channel regime. We expect that the localization length of model increases as the frequency decays to zero $\omega \longmapsto 0$. In Fig.6.7 we show the time evolution of the second moment m_2 for the undriven case with $U_0 = 1.0$ and $\lambda = 2.5$, and two cases in presence of the driving with $\mu = 0.2$ with frequencies $\omega_1 = 5 \cdot 10^{-2}$ and $\omega_1 = 5 \cdot 10^{-5}$. We notice to the strong decrease of the frequency, it corresponds a weak increase of the second moment. This follows since the increase of the number of channels in the momentum space direction occurs only along the diagonal.

6.3.2.3 Region B

The region $B \equiv [3, 6] \times [2.2, 2.8]$ in Fig.6.4 contains one of the main area of the phase space (U, λ), where correlated metallic states exist in the undriven case. Our aim is the understanding of the effect the driving term Eq.(6.15) has on these correlated states. In particular, we are interested to see if this driving term leads to any coherent destruction of the tunneling.

The *coherent destruction of the tunneling* consists in the loss of spatial transport in the system due to the presence of external time-dependent driving, and it is an intriguing phenomenon in the study of driven quantum systems. Theoretically forecast in the nineties [263–265], it has been analytically discussed recently by Gong *et.al,* in [266], and experimentally observed [267, 268]. In particular, the coherent destruction of tunneling has been experimentally observed in many body systems, with noninteracting cold atoms in a double-well potential [269]. A possible realization of this phenomenon with many interacting particles has been proposed by Longhi in [270].

The region B includes the case $(U_0, \lambda) = (4.5, 2.5)$ that, as showed in Fig.6.3, there exists correlated metallic states in the undriven case [123]. In Fig.6.8 we show the second moment m_2 at time $t = 10^3$ versus the frequency ω, for two driving strengths $\mu = 0.2$ (left plot) and $\mu = 0.4$ (right plot). In both figures we observe that the second moment m_2 substantially decreases its value. On the left plot, for $\mu = 0.2$, the values of the second moment is

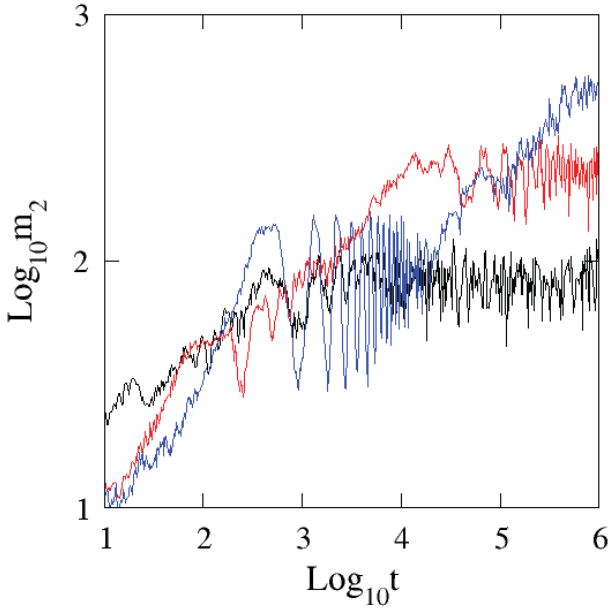

Figure 6.7: Time evolution of the second moment m_2 in multichannel regime for $U_0 = 1.0$, $\lambda = 2.5$ and $\mu = 0.2$. Frequency values: $\omega_1 = 5 \cdot 10^{-2}$ (red), $\omega_1 = 5 \cdot 10^{-5}$ (blue), undriven (black). System size $L = 2^8$.

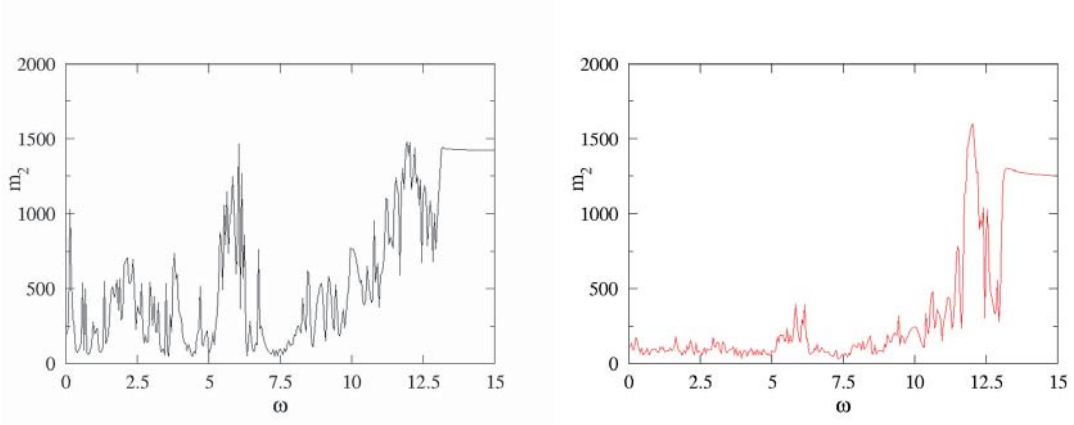

Figure 6.8: Left plot: second moment m_2 at time $t = 10^3$ versus the frequency ω for $\mu = 0.2$. Right plot: second moment m_2 at time $t = 10^3$ versus the frequency ω for $\mu = 0.4$. Both cases, $U_0 = 4.5$ and $\lambda = 2.5$. Omegastep $= 0.05$, system size $L = 2^8$.

generally lower than the undriven case $m_2 \approx 15 \times 10^3$, which hints to loss of delocalization. For frequency values $5 \leq \omega \leq 7$, the fluctuations of the second moment appears stronger, with peaks of the order of the unperturbed case. Likewise, we can observe an increase of the second moment m_2 for $11 \leq \omega \leq 12.5$, before the frequency gets to $\omega \geq 13$, where the second moment saturates around $m_2 \sim 10^3$. This follows because, for high frequency values, the model enters the *single channel* regime, behaving as in the undriven case. Analogous features can be observed in the right plot as well for $\mu = 0.4$, where the second moment flattens, up to $5 \leq \omega \leq 7$ where it exhibits weak fluctuations, and $11 \leq \omega \leq 12.5$ where instead fluctuations of the second moment are of the order of the undriven case $m_2 \sim 10^3$. We notice also that as the perturbation strength μ increases, the more the average values of the second moment decreases, as a signature that the destruction of tunneling is stronger.

We then focus on the left plot, with $\mu = 0.2$. In Fig.6.9 we show the time evolution of the second moment m_2 for the highest peaks observed in both regions of high fluctuations of the second moment, $\omega = 6.15$ for the first one ($5 \leq \omega \leq 7$) and $\omega = 12.3$ for the second one ($11 \leq \omega \leq 12.5$). Moreover, we compute the time evolution of the second moment for two local minimums $\omega = 4.5$ and $\omega = 7.7$. Then, in the right plot we plot the energy density function p_l at time $t = 10^4$ for two one peak ($\omega = 6.15$) and one local minima ($\omega = 4.5$)

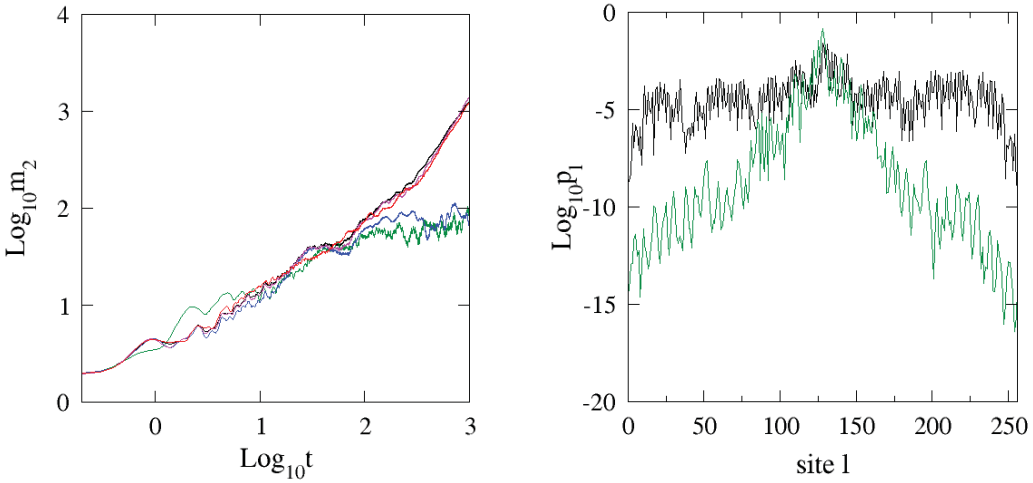

Figure 6.9: Left plot: time evolution of the second moment m_2 for $\omega = 6.15$ (black - local peak), $\omega = 12.3$ (red - local peak), $\omega = 4.5$ (green - local minimum) and $\omega = 7.7$ (blue - local minimum). The magenta curve corresponds to the undriven case. Right plot: energy density p_l versus lattice sites l at final time $t = 10^4$ for $\omega = 6.15$ (black - local peak) and $\omega = 4.5$ (green - local minimum). Both cases, $U_0 = 4.5$, $\lambda = 2.5$ and $\mu = 0.2$ and $L = 2^8$.

The curves of the time evolution correspondent to the two peaks $\omega = 6.15, 12.3$ behave as the undriven case and therefore exhibit delocalization. The time evolution correspondent to local minima $\omega = 4.5, 7.7$ instead exhibit localization, confirming the destruction of tunneling effect given by the driving term. From these figures we confirm how this coherent driving lift the presence of the correlated metallic states for large regions of the frequency domain. However, this effect vanishes in certain intervals, which might be connected to possible resonances.

6.4 Summary and Discussions

In this chapter we discussed preliminary studies done on the two interacting particle problem in a quasiperiodic chain in presence of driven interactions. From reviewing the undriven case of two particles in an Aubry-Andé chain, we have moved towards the analysis of the driven case, with the goal of understanding the generating mechanism of the groups of renormalized extended states. We studied the problem analytically, performing the Floquet analysis of the driven model Eq.(6.16), and numerically, studying the time evolution of wave packets. Even though we have observed hints of interesting phenomena, this class of driving does not generate families of extended states in regions of the model's phase space where these states do not exist. It follows that the generation of the correlated metallic states are yet unclear and, as a consequence, this project still lacks of conclusive results and it is currently ongoing. A better understanding could possibly arrive from a more careful analytical and numerical analysis of the undriven spectrum and the overlap integral in the mode representation of the equation, and discussing further the coherent destruction of

tunneling in combination with the Bessel function representation of the model described in Sec.C.3.

CHAPTER 7

Conclusions and Outlook

In these last decades, lattice structures have shown to be fundamental for the study of light, wave and particles propagation in periodic and aperiodic media, with the essential achievements of the theoretical prediction and the experimental realization of Bloch oscillations, Anderson localization and Aubry-André metal-insulator transition. Interests in these discrete systems is nowadays focused on the design of innovative lattice's spatial topology, for instance graphene, the implementation of several classes of spatial perturbations, time-dependent driving, and external fields. Lattices then confirmed to be ideal benchmarks for the study of emergent physical phenomena in condensed matter physics.

This thesis has been focused on the quasiperiodic Aubry-André-type of spatial perturbation of discrete systems, particularly one-dimensional chains. Localization phenomena in disordered and quasiperiodic topologies are longstanding problems in condensed matter, which yet posses a huge number of unsolved issues. In the case of the quasiperiodic lattices, these issues concern in particular the transition between metallic and insulating regimes in the energy spectrum. Our ultimate goal was to describe the transport features of certain quasieriodic lattices and their transitions by relating them the Aubry-André one-dimensional chain and its self-duality principle.

In order to achieve this goal, we initially focused on the one-dimensional Aubry-André chain and its energy spectrum, particularly on its self-similar nature. We constructed an iterative sequence of spatially periodic potentials with increasing period. The energy spectrum of a one-dimensional chain defined with this sequence of potential emulates the Aubry-André self similar structure. In the limit of infinite step, the potential turns quasiperiodic, the chain lacks of self duality principle and it exhibits an energy dependent transitions (mobility edges). We thus introduced a set of potentials that bonds the self-similarity of the energy spectrum of the chain, its quasiperiodicity and the transition between insulating and metallic phase.

After having established a connection between spectral self-similarity of a quasiperiodic chain and its phase transition, we shifted our studies to the Aubry-André perturbations of the flat-band topologies. It is well-known that spatial perturbations lift the spectral

singularities characteristic of these topologies, and they hybridize the flat-band states with the dispersive states. On the other hand, the rotations of these topologies into lattice of Fano defects generally holds also in presence of spatial perturbations. We combined the rotation of the topologies to the Aubry-André duality principle. In the very case of class $U = 1$ flat-band topologies, the combination of these two elements yielded to closed analytical forms of energy dependent phase transitions (mobility edges) in case of specific spatial correlations. In particular, we analytically showed the presence of singluarities, zeroes and divergencies in the mobility edge curves, prediction confirmed by numerical studies.

We then shifted focus into driven systems, namely two different one-dimensional chains driven in time. In the first case, we consider an Aubry-André chain and the driving consists in a weak external field periodic in time and quasiperiodic in space. The topological structure of the energy spectrum of the undriven Aubry-André model is closely related to the origin of the resonant metallic states within the model's insulating phase generated by drive. We found that for frequencies comparable to the model's main spectral gaps, the drive resonantly couples groups of localized eigenstates of the undriven model, generating groups of extended ones. Fact supported from the small detuning from the resonant frequencies returns these families of localized states to be decoupled and the delocalization gone. It follows that we found a simple but effective method to control the localization and generate extended states by design within the insulating regime of an Aubry-André chain.

The second case of the driven chains consists in a disordered chain in presence of a coherent quasiperiodic multi-frequency (color) driving in time acting on the spatial perturbation. By mean of Floquet and harmonic analysis, jointly with numerical methods, we highlighted presence of different regimes in the parameter space where the Anderson localization is unaffected, and regions where the localization lengths shows a substantial increase. Moreover, we showed that the localization length remains finite for any finite number of frequencies, and its divergence occurs in the limit of frequency going to zero. However, it is legitimate to expect that the localization length diverges as the number of colors diverges to infinity and the driving coherence is lost.

Finally, we explored the problem of two interacting particles in a one-dimensional Aubry-André chain. In this problem, groups of renormalized extended states exist within the insulating phase of the single particle for particular values of the interaction strength. We aimed to control the generation of families of correlated metallic states by a coherent drive of the interaction term. The scheme proposed did not generate new groups of renormalized extended states, leaving open the issue of generate them by design.

The theme underlying the thesis was the concept of *quasiperiocity*, and the main goal was the establishment of relations between the topological properties of the lattices, their energy spectrum with the model's localization feature. The examples considered exhibited different interesting effects related to the transition between metallic and insulating regimes. Thus, they showed that the interplay between lattice's topology, external driving and spatially quasiperiodic perturbation leads to interesting possible experimental developments of fine tuning of the metal-insulator transition in optical lattices.

In relation to experiments, after almost a decade of the experimental observation of Anderson localization [19] and Aubry-André metal-insulator transition [20], recently important examples of flat-band topologies (saw-tooth, Lieb) have been experimentally realized [160, 161, 271, 272], reporting the realization of the compact localized eigenmodes. Likewise, the recent years have witnessed advancements on the experimental realzation and control of the external driving of optical and photonic lattices [273, 274]. The combinations of these experimental results will possibly lead to the experimental realization of quasiperiodically perturbed flat-band topologies and driven quasiperiodic chains, the observation of the energy dependent mobility edge with their spectral singularities and di-

vergencies, as well as the realization of delocalization by design of particles within their insulating regimes. These could provide useful insights of transport phenomena of particles in quasiperiodic topologies, and the control of the transition between localized and metallic regimes. This would ultimately leads to possible advancements towards the synthesis of artificial semiconductors [275].

Even if these studies showed promising results, the link between the model topology, its spatial quasiperiodic perturbation, its spectral properties and the model's transport properties need more rigorous analytical argumentations. The Aubry-André model itself has shown in these years to be particularly inclined towards exact analytical proofs of its features. This strengthening could arise from the analysis of further examples of quasiperiodic topologies and the development of analytical tools (topological invariants, harmonic analysis, algebraic analysis), that would allow more systematic and extensive studies of the spectral decomposition of the lattices, their singularities, and the topology of the model spectrum after the introduction of the quasiperiodic potential. This could possibly also allow a more rigorous understanding of the role of many-body interaction and nonlinearity in quasiperiodic lattices.

APPENDIX A

Numerical Methods

The majority of the numerical work done in this thesis concerned the time integration of the Schrödinger equation Eq.(2.4), and the numerical diagonalization of associated time independent eigenvalue problem Eq.(2.6). In this appendix we introduce the numerical methods used and we present the parameters we use to characterize the eigenmodes.

A.1 Numerical Diagonalization

All the numerical simulations have been performed using initially C++, and then switching to Fortran90. Concerning the numerical solution of eigenvalue problems Eq.(2.6), in the case of C++, we have used the TNT diagonalization routine (http://math.nist.gov/tnt/). In the case of Fortran90, we have used the LAPACK routine (http://www.netlib.org/lapack/).

A.2 Wave Packet Dynamics

The computation of the time evolution of the cases of Schrödinger equation considered in this work have been performed numerically using symplectic integrators. These types integrators are numerical integration scheme for Hamiltonian systems, where each integration step from time t to time $t+\tau$ is performed using a canonical symplectic transformation.

For our cases, we use schemes that separate the Hamiltonian H in two integrable parts $H = A + \epsilon B$, each one with solutions e^{tL_A} and $e^{\epsilon t L_B}$. Then, we express the differential operator $e^{\tau L_H}$, which defines the formal solution of the differential equation $i\dot{\psi} = H\psi$, as a combinations of e^{tL_A} and $e^{\epsilon t L_B}$

$$e^{\tau L_H} = \prod_{i=1}^{s} e^{c_i \tau L_A} e^{\epsilon d_i \tau L_B} + O(\tau^{s+1}) \; ; \qquad \text{with} \quad \sum_{i=1}^{s} c_i = 1 \; , \quad \sum_{i=1}^{s} d_i = 1 \tag{A.1}$$

The higher the order s is, the better the precision and stability of the method are. However, higher order s costs in computational time. The scheme we have used for our cases of

Schrödinger equation is a third order $s = 3$ scheme, called $SBAB_2$. In Sec.A.2.1 we discuss this symplectic scheme, and in Sec.A.2.2 we discuss the modification performed to the $SBAB_2$ scheme in case of time-dependent hamiltonians.

A.2.1 SBAB$_2$

The $SABA_2$ integration scheme is obtained from Eq.(A.1) where $s = 3$. The integrator then is

$$SABA_2 = e^{\epsilon d_1 \tau L_B} e^{c_2 \tau L_A} e^{\epsilon d_2 \tau L_B} e^{c_2 \tau L_A} e^{\epsilon d_1 \tau L_B} \ ; \tag{A.2}$$

with $c_2 = \frac{1}{2}$, $d_1 = \frac{1}{6}$ and $d_2 = \frac{2}{3}$. In the case Eq.(2.4)

$$i\frac{\partial}{\partial t}\psi_l = \epsilon_l \psi_l + \psi_{l-1} + \psi_{l+1} \ , \tag{A.3}$$

the hamiltonian A and B are ($\epsilon = 1$)

$$A = \sum_l \left[\psi^*_{l+1}\psi_l + \psi_{l+1}\psi^*_l\right] \ ; \qquad B = \sum_l \epsilon_l |\psi_l|^2 \ . \tag{A.4}$$

The differential operators e^{tL_A} and $e^{t\epsilon L_B}$ are

$$\psi_l(t+\tau) = e^{tL_A}\psi_l(t) = \begin{cases} \varphi_q(t) & = \sum_m \psi_m(t) e^{i2\pi q(m-1)/N} \ . \\ \varphi_q(t+\tau) & = \varphi_q(t) e^{i2\cos(2\pi(q-1/N))\tau} \ , \\ \psi_l(t+\tau) & = \frac{1}{N}\sum_q \varphi_q(t+\tau) e^{-i2\pi l(q-1)/N} \ . \end{cases} \tag{A.5}$$

$$\psi_l(t+\tau) = e^{tL_B}\psi_l(t) = e^{-i\epsilon_l \tau}\psi_l(t) \ . \tag{A.6}$$

A.2.2 Time Dependent Hamiltonian

To take properly into consideration the presence of time-dependent terms $V_l(t)$ in the hamiltonian equation

$$H(t) = H_0 + V_l(t) \ ; \tag{A.7}$$

we integrate the time independent part H_0 using the scheme indicated above, and manually integrate the time-dependent component. We show here the case of the driven Aubry-André case Sec.5.2. The cases of driven Anderson Sec.5.3 and driven two interacting particles Sec.6.3.2 are very similar to the case discussed.

The hamiltonian of the system Eq.(5.2) is

$$\begin{aligned} i\frac{d\psi_l}{dt} &= \psi_{l+1} + \psi_{l-1} + V_1 \cos(2\pi\alpha l + \delta)\psi_l \\ &\quad + V_2 \cos(2\pi\beta l + \Omega t)\psi_l \ . \end{aligned} \tag{A.8}$$

The time dependent component $V_l(t)$ yields an integral from time t to time $t+\tau$ as

$$\psi_l(t+\tau) = e^{i\int_t^{t+\tau} V_l(r)dr}\psi_l(t) \ . \tag{A.9}$$

The integral lying at the exponent has solution

$$\begin{aligned} \int_t^{t+\tau} V_l(r)dr = .V_2 \int_t^{t+\tau} \cos(2\pi\beta l + \Omega r)dr &= \frac{V_2}{\Omega}\sin(2\pi\beta l + \Omega r)\Big|_t^{t+\tau} \\ &= \frac{V_2}{\Omega}\Big[\sin(2\pi\beta l + \Omega(t+\tau)) - \sin(2\pi\beta l + \Omega(t))\Big] \\ &= \frac{2V_2}{\Omega}\sin\left(\frac{\Omega\tau}{2}\right)\cos\left[(2\pi\beta l + \Omega\Big(t+\frac{\tau}{2}\Big)\right] \ . \end{aligned} \tag{A.10}$$

In Eq.(A.6), the differential operator e^{tL_B} becomes

$$\psi_l(t+\tau) = e^{tL_B}\psi_l(t) = e^{-i[\epsilon_l\tau + W_l(t,\tau)]}\psi_l(t) \ . \tag{A.11}$$

for $W_l(t,\tau)$ defined as

$$W_l(t,\tau) \equiv \frac{2V_2}{\Omega}\sin\left(\frac{\Omega\tau}{2}\right)\cos\left[(2\pi\beta l + \Omega\Big(t+\frac{\tau}{2}\Big)\right] \ . \tag{A.12}$$

A.3 Mode's Characterization

In this section, we introduce some measures we have used to quantify the localization features of the mode $\psi \equiv \{\psi_l\}_{l\in\mathbb{Z}}$. Without loss of generality, we consider ψ to be one-dimensional and of unitary norm $\mathcal{N} = 1$ (norm defined as)

$$\mathcal{N} = \sum_l |\psi_l|^2 \ . \tag{A.13}$$

We address the case of the mode's exponential localization, which indicate that the mode's amplitude $|\psi_|$ is non negligible within a finite subset of the lattice, and its tails decay exponentially as

$$|\psi_l| \sim e^{-|l|/\xi(E)} \ ; \qquad |l| \longmapsto +\infty \ ; \tag{A.14}$$

for E the mode's energy. The decay rate $\xi(E)$ of the mode is called *localization length*, while the subset of the spatial domain between the two tails, where mode's amplitude $|\psi_|$ is non negligible, is called *localization volume*. From Eq.(A.14), it follows that the smaller the localization length $\xi(E)$ is, the faster the decay. In one-dimensional chains, an iterative scheme can be used to approximate the localization length $\xi(E)$. We first observe that, if the mode decays exponentially as Eq.(A.14), for large enough lattice site l it holds that

$$R_l = \left|\frac{\psi_{l+1}}{\psi_l}\right| = \frac{A_{l+1}}{A_l} \sim e^{\frac{1}{\xi(E)}} \ . \tag{A.15}$$

with the amplitude-phase expansion $\psi_l = A_l e^{iEt}$, Eq.(2.5). The natural logarithm of Eq.(A.15) lead us to obtain the inverse of the localization length $\xi^{-1}(E)$. We obtain the sequence R_l recursively for an initial value $R_0 = 1$ from the eigenvalue problem associated to the one-dimensional tight-binding Eq.(2.4). Eq.(2.6) can be rewritten as

$$A_{l+1} = (\epsilon_l - E)A_l - A_{l-1} \ ; \tag{A.16}$$

which, dividing by A_l, it is equivalent to

$$R_l = (\epsilon_l - E) - \frac{1}{R_{l-1}} \ ; \tag{A.17}$$

where $R_l = A_{l+1}/A_l$. We then approximate the inverse of the localization length $\xi^{-1}(E)$ by the formula

$$\xi^{-1}(E) = \lim_{M\to+\infty}\frac{1}{M}\sum_{n=1}^{M}\ln|R_l| \tag{A.18}$$

Numerically the recursion does not go infinity $M \longmapsto +\infty$. Even if for large M this expression is self-averaging, it can be helpful to introduce further averages $\langle\cdot\rangle$, for example over the disorder realization for onsite energy ϵ_l considered as an uncorrelated sequence uniformly distributed over a bounded set (Anderson case). This yields to

$$\xi^{-1}(E) = \lim_{M\to+\infty}\frac{1}{M}\left\langle\sum_{n=1}^{M}\ln\left|\frac{A_{l+1}}{A_l}\right|\right\rangle. \tag{A.19}$$

This approach becomes impractical for higher-dimensional lattices or more complicated topologies. The flat-band lattices are a separate case, since this recursive technique is made possible because of the rotation of the models in lattices of Fano defect, as described in Eq.(4.18)

Next to quantify the decay rate of the localized mode $\psi \equiv \{\psi_l\}_{l\in\mathbb{Z}}$, we can define the following measures [84]:

- the *participation number* P describes the number of sites of non-trivial amplitude. It is defined as
$$P = \frac{1}{\sum_l |\psi_l|^4} \ . \tag{A.20}$$
$P = 1$ indicates a mode localized in one site, while if the participation number the $P \sim N$ scales linearly with the chosen system size N, it indicates an extended mode.

- the *second moment* m_2 estimates the squared distance between the mode's tails. It is defined as
$$m_2 = \sum_l \Big[\sum_k k|\psi_k|^2 - l \Big]^2 |\psi_l|^2 \ . \tag{A.21}$$
A large value of second moment indicates that there exists strongly excited sites far away from each other., however, the strongly excited sites can be very sparse.

APPENDIX B

Quasiperiodic Driving of Disordered Chains

In this appendix we discuss some concepts and analytical results we have been using in Sec.5.3 for the analysis of the Anderson model in presence of quasiperiodic multi-frequency driving. In Sec.B.1 aspects of multi-frequency perturbation are discussed and in Sec.B.2 we explain in details the Floquet expansion and the rotation in a basis of Bessel function done in Sec.5.3.2 and Sec.5.3.3 on the driven one-dimensional Anderson model.

B.1 Multi-Frequency Perturbation

In this section we introduce the concept of quasiperiodicity in time and we review elements of the Floquet theory and Fourier analysis of multi-frequency dynamical systems, in relation to 5.3. As introduced in 2.4, we recall the definition

Definition. *Let $\varphi : \mathbb{R} \longrightarrow \mathbb{R}$ be a real continuous one-dimensional function. For φ being quasiperiodic implies that there exists continuous function $F : \mathbb{R}^D \longrightarrow \mathbb{R}$ with $D \geq 2$ periodic in every component with period 2π such that*

$$\varphi(t) = F(\omega_1 t, \dots, \omega_D t) \ , \quad t \in \mathbb{R} \ , \tag{B.1}$$

for D frequencies $\Omega = (\omega_1, \dots, \omega_D)$ incommensurate between each other

$$\mathbf{k} \cdot \Omega = k_1\omega_1 + \cdots + k_D\omega_D \neq 0 \ , \quad \forall \mathbf{k} \in \mathbb{Z}^D \ , \ \ \mathbf{k} \neq 0 \ . \tag{B.2}$$

The periodicity in each component makes the domain $\mathbb{R}^D$ of the function F to become a D dimensional torus $\mathbb{T}^D = \mathbb{R}^D/(2\pi\mathbb{Z})^D$. The trajectory described by the function $\gamma : \mathbb{R} \to \mathbb{T}^D$, $\gamma(t) = (\omega_1 t, \dots, \omega_D t)$ along the manifold $\mathbb{T}^D$ forms a closed loop if Eq.(B.2) does not hold and the frequencies ω are commensurate. Instead for incommensurate frequencies, the trajectory fills densely the manifold. It follows that for every $x_0 \in \mathbb{T}^D$, $x_0 = \gamma(0)$ and for every $\delta \neq 0$ small, there exists a t_δ such that $x = \gamma(t_\delta) \in U^\delta_{x_0}$ with $U^\delta_{x_0}$ a punctured

neighborhood of x_0, $U^{\delta}_{x_0} = B(x_0, \delta[\setminus \{x_0\}$. By translation invariance, for any $\delta \neq 0$ small this feature holds for every $x_0 = \gamma(t_0)$ with the same t_δ. By the continuity of F, it follows that for every t_0 and for every $\varepsilon \neq 0$ small there exists $\delta \ll 1$ and t_δ such that

$$|\varphi(t_0 + t_\delta) - \varphi(t_0)| \leq \varepsilon \ . \tag{B.3}$$

This property is in analogy with the property of spatial quasiperiodicity for discrete sequences reported in Eq.(2.14).

The incommensurate condition of the frequencies Eq.(B.2) is the origin of the feature Eq.(B.3). Such condition also modifies mathematical objects we have used on the analysis of a single frequency driven Anderson chain Sec.5.3, such as Floquet expansion and Fourier series. The so-called *many-modes Floquet expansion* exists for Hamiltonian function H which time dependence is described as Eq.(B.1), (B.2). A solution of the time evolution equation $i\dot{\Psi} = H\Psi$ can then be expanded as

$$\Psi(t) = u(t)e^{-iEt} \ . \tag{B.4}$$

for the quasienergy E and the component $u(t)$, which shares the time dependence with the Hamiltonian H, can be expanded in a *generalized Fourier series* written as

$$u(t) = \sum_{k_1} \sum_{k_2} \cdots \sum_{k_D} A_{k_1,k_2,\ldots,k_d} e^{ik_1\omega_1 t} e^{ik_2\omega_2 t} \cdots e^{ik_D\omega_D t} \ . \tag{B.5}$$

Each series correspond to one of the frequency of Ω. Using the vector notation for the index $\mathbf{k} \in \mathbb{Z}^D$, the expansion can be condensed in

$$u(t) = \sum_{\mathbf{k}} A_{\mathbf{k}} e^{i\mathbf{k}\cdot\Omega t} \ . \tag{B.6}$$

In our case, for an Hamiltonian H defined as Eq.(5.8), the Floquet and the Fourier transformation combined yield to an expansion

$$\psi_l(t) = \sum_{\mathbf{k}} A_{l,\mathbf{k}} e^{-i[(E-\mathbf{k}\cdot\Omega)t - \mathbf{k}\cdot\Phi_l]} \tag{B.7}$$

where Φ_l is the vector of $\Phi_l = (\phi^1_l, \ldots, \phi^D_l) \in \ ]-\pi, \pi[^D$ for every lattice site $l \in \mathbb{Z}$.

B.2 Floquet Analysis

In this section we analyze in details the Floquet expansion and the representation in Bessel function coordinate of the Anderson chain in presence of a multicolor quasiperiodic driving Eq.(5.3.2.3). In Sec.B.2.1 we discuss the single color case, in Sec.B.2.2 the general case.

B.2.1 Single Color

We focus on the one color case $D = 1$ using references [228, 229]. The D color case is a generalization of these calculations. The one-dimensional time-dependent model Eq.(5.10) is mapped to a time independent two-dimensional eigenvalue problem Eq.(5.14) via the Floquet expansion Eq.(5.11)

$$\psi_l(t) = \sum_{k} A_{l,k} e^{-i[(E-k\omega)t - k\phi_l]} \ . \tag{B.8}$$

With

$$\mu\epsilon_l \cos(\omega t + \phi_l)\psi_l = \frac{\mu\epsilon_l}{2} \sum_k \left[A_{l,k-1} + A_{l,k+1}\right] e^{-i[(E-k\omega)t - k\phi_l]} \tag{B.9}$$

and

$$\begin{aligned}\lambda(\psi_{l+1} + \psi_{l-1}) = \lambda \sum_k \Big[& A_{l-1,k} e^{-i[(E-k\omega)t - k\phi_{l-1}]} \\ & + A_{l-1,k} e^{-i[(E-k\omega)t - k\phi_{l-1}]}\Big] \\ - \lambda \sum_k \Big[& A_{l-1,k} e^{-ik(\phi_l - \phi_{l-1})} e^{-i[(E-k\omega)t - k\phi_l]} \\ & + A_{l+1,k} e^{-ik(\phi_l - \phi_{l+1})} e^{-i[(E-k\omega)t - k\phi_l]}\Big]\end{aligned} \tag{B.10}$$

we define the hopping coefficients $\xi^{\pm}_{l,k}$ as

$$\xi^{\pm}_{l,k} = e^{-ik(\phi_l - \phi_{l\pm1})} \tag{B.11}$$

to arrive at

$$\begin{aligned}&\sum_k (E - k\omega) A_{l,k} e^{-i[(E-k\omega)t - k\phi_l]} = \\ &= \sum_k \Big[\epsilon_l A_{l,k} + \frac{\mu\epsilon_l}{2}(A_{l,k-1} + A_{l,k+1}) \\ &\quad - \lambda\big(\xi^-_{l,k} A_{l-1,k} + \xi^+_{l,k} A_{l+1,k}\big)\Big] e^{-i[(E-k\omega)t - k\phi_l]}\end{aligned} \tag{B.12}$$

which finally yields the two dimensional eigenvalue problem of Eq.(5.14)

$$\begin{aligned}E A_{l,k} = (\epsilon_l + k\omega) A_{l,k} - \lambda(\xi^-_{l,k} A_{l-1,k} + \xi^+_{l,k} A_{l+1,k}) \\ + \frac{\mu\epsilon_l}{2}(A_{l,k-1} + A_{l,k+1})\ .\end{aligned} \tag{B.13}$$

This is then transformed using Eq.(5.13):

$$A_{l,k} = \sum_\nu c_{l,\nu} B^{(\nu)}_{l,k}\ , \qquad B^{(\nu)}_{l,k} = J_{k-\nu}\left(\frac{\mu\epsilon_l}{\omega}\right)\ . \tag{B.14}$$

The basis $\mathcal{B} = \{B^{(\nu)}_{l,k}\}_\nu$ diagonalizes the eigenvalue problem in the Fourier direction k with eigenvalues $\epsilon_\nu = \omega\nu$. It follows that

$$\begin{aligned}&k\omega A_{l,k} + \frac{\mu\epsilon_l}{2}(A_{l,k-1} + A_{l,k+1}) = \\ &= \sum_\nu c_{l,\nu}\left[k\omega B^{(\nu)}_{l,k} + \frac{\mu\epsilon_l}{2}\left(B^{(\nu)}_{l,k-1} + B^{(\nu)}_{l,k+1}\right)\right] \\ &= \sum_\nu \omega\nu\ c_{l,\nu} B^{(\nu)}_{l,k}\ .\end{aligned} \tag{B.15}$$

The eigenvalue problem Eq.(B.13) in the new basis $\mathcal{B}$ reads

$$\begin{aligned}E \sum_\nu c_{l,\nu} B^{(\nu)}_{l,k} = \sum_\nu \Big[&(\epsilon_l + \omega\nu) c_{l,\nu} B^{(\nu)}_{l,k} \\ &- \lambda\big(\xi^-_{l,k} c_{l-1,\nu} B^{(\nu)}_{l-1,k} + \xi^+_{l,k} c_{l+1,\nu} B^{(\nu)}_{l+1,k}\big)\Big]\ .\end{aligned} \tag{B.16}$$

We multiply both sides of Eq.(B.16) with a second Bessel function $B_{l,k}^{(\nu_2)}$ of index ν_2 and then sum over k. Using the Bessel functions orthonormality relation [228, 229]

$$\sum_k B_{l,k}^{(\nu)} B_{l,k}^{(\nu_2)} = \sum_k J_{k-\nu}\left(\frac{\mu\epsilon_l}{\omega}\right) J_{k-\nu_2}\left(\frac{\mu\epsilon_l}{\omega}\right) = \delta_{\nu,\nu_2} \tag{B.17}$$

in Eq.(B.16) we obtain

$$\begin{aligned} E\sum_k\sum_\nu c_{l,\nu} B_{l,k}^{(\nu)} B_{l,k}^{(\nu_2)} &= E c_{l,\nu} \ , \\ \sum_k\sum_\nu (\epsilon_l + \omega\nu) c_{l,\nu} B_{l,k}^{(\nu)} B_{l,k}^{(\nu_2)} &= (\epsilon_l + \omega\nu) c_{l,\nu} \ . \end{aligned} \tag{B.18}$$

The matrix elements (hopping) along the real direction l become

$$\begin{aligned} &\sum_k\sum_\nu \xi_{l,k}^{\pm} c_{l\pm1,\nu} B_{l\pm1,k}^{(\nu)} B_{l,k}^{(\nu_2)} = \\ &= \sum_\nu c_{l\pm1,\nu}\Big(\sum_k \xi_{l,k}^{\pm} B_{l\pm1,k}^{(\nu)} B_{l,k}^{(\nu_2)}\Big) \ . \end{aligned} \tag{B.19}$$

Using Graf's generalization of Neumann's addition theorem [228, 229]

$$\sum_k e^{ik\theta} J_{\nu+k}(x) J_k(y) = \left(\frac{x - ye^{-i\theta}}{x - ye^{i\theta}}\right)^{\frac{\nu}{2}} J_\nu\Big(\sqrt{x^2 + y^2 - 2xy\cos\theta}\Big) \ . \tag{B.20}$$

and defining the random phase difference

$$\theta_l^{\pm} = \phi_l - \phi_{l\pm1} \ , \tag{B.21}$$

Eq.(B.19) is modified as

$$\sum_k\sum_\nu \xi_{l,k}^{\pm} c_{l\pm1,\nu} B_{l\pm1,k}^{(\nu)} B_{l,k}^{(\nu_2)} = \sum_s (\sigma_l^{\pm})^s J_s(\Delta_l^{\pm}) c_{l\pm1,\nu-s} \tag{B.22}$$

where

$$\begin{aligned} \sigma_l^{\pm} &= \left(\frac{\epsilon_l - e^{-i\theta_l^{\pm}}\epsilon_{l\pm1}}{\epsilon_l - e^{i\theta_l^{\pm}}\epsilon_{l\pm1}}\right)^{\frac{1}{2}} \ , \\ \Delta_l^{\pm} &= \frac{\mu}{\omega}\sqrt{\epsilon_l^2 + \epsilon_{l\pm1}^2 - 2\epsilon_l\epsilon_{l\pm1}\cos\theta_l^{\pm}} \ . \end{aligned} \tag{B.23}$$

Since the complex coefficient $\sigma_l^{\pm}$ has absolute value equal to unity, we rewrite it as

$$\sigma_l^{\pm} = \mathrm{e}^{i\varphi_l^{\pm}} \ , \qquad \tan\varphi_l^{\pm} = -\frac{\epsilon_{l\pm1}\sin\theta_l^{\pm}}{\epsilon_l - \epsilon_{l\pm1}\cos\theta_l^{\pm}} \ . \tag{B.24}$$

The final eigenvalue problem becomes (Eq.(5.17))

$$\begin{aligned} E c_{l,\nu} &= (\epsilon_l + \omega\nu) c_{l,\nu} \\ -\lambda\sum_s &\Big[\mathrm{e}^{is\varphi_l^-} J_s(\Delta_l^-) c_{l-1,\nu-s} + \mathrm{e}^{is\varphi_l^+} J_s(\Delta_l^+) c_{l+1,\nu-s}\Big] \ . \end{aligned} \tag{B.25}$$

B.2.2 General Case

Let's recall the general case of the driven model Eq.(5.8)

$$i\dot{\psi}_l = \epsilon_l\Big[1 + \sum_{i=1}^{D} \mu_i cos(\omega_i t + \phi_l^i)\Big]\psi_l - \lambda(\psi_{l+1} + \psi_{l-1}) \ . \tag{B.26}$$

We introduce the vectors

$$\begin{aligned} \mathbf{k} =& (k_1, \dots, k_D) \in \mathbb{Z}^D \ ; \\ \Phi_l =& (\phi_l^1, \dots, \phi_l^D) \in \ ]-\pi, \pi[^D \ , \quad l \in \mathbb{Z} \ ; \\ \Omega =& (\omega_1, \dots, \omega_D) \in \mathbb{R}^D \ . \end{aligned} \tag{B.27}$$

Moreover, we define $\mathbf{e_i}$ as the i-th vector of the canonical basis of $\mathbb{Z}^D$. The frequencies ω_i can then be rewritten as $\omega_i = \mathbf{e_i} \cdot \Omega$. The Floquet expansion is

$$\psi_l(t) = \sum_{\mathbf{k}} A_{l,\mathbf{k}} e^{-i[(E - \mathbf{k}\cdot\Omega)t - \mathbf{k}\cdot\Phi_l]} \tag{B.28}$$

Let's start with the driving term of Eq.(B.26). Each term of the sum over i from one to D results

$$\begin{aligned} \mu_i\epsilon_l \cos(\omega_i t + \phi_l^i)\psi_l &= \frac{\mu_i\epsilon_l}{2} \sum_{\mathbf{k}} A_{l,\mathbf{k}} \Big[e^{i(\omega_i t + \phi_l^i)} + e^{-i(\omega_i t + \phi_l^i)}\Big] e^{-i[(E - \mathbf{k}\cdot\Omega)t - \mathbf{k}\cdot\Phi_l]} \\ &= \frac{\mu_i\epsilon_l}{2} \sum_{\mathbf{k}} A_{l,\mathbf{k}} \Big[e^{-i[(E - (\mathbf{k}+\mathbf{e_i})\cdot\Omega)t - (\mathbf{k}+\mathbf{e_i})\cdot\Phi_l]} \\ &\qquad + e^{-i[(E - (\mathbf{k}-\mathbf{e_i})\cdot\Omega)t - (\mathbf{k}-\mathbf{e_i})\cdot\Phi_l]}\Big] \\ &= \frac{\mu_i\epsilon_l}{2} \sum_{\mathbf{k}} \Big[A_{l,\mathbf{k}-\mathbf{e_i}} + A_{l,\mathbf{k}+\mathbf{e_i}}\Big] e^{-i[(E - \mathbf{k}\cdot\Omega)t - \mathbf{k}\cdot\Phi_l]} \ . \end{aligned} \tag{B.29}$$

The hopping terms of Eq.(B.26) turns in

$$\begin{aligned} \lambda(\psi_{l+1} + \psi_{l-1}) = \lambda \sum_{\mathbf{k}} &\Big[A_{l+1,\mathbf{k}} e^{-i[(E - \mathbf{k}\cdot\Omega)t - \mathbf{k}\cdot\Phi_{l+1}]} \\ &\quad + A_{l-1,\mathbf{k}} e^{-i[(E - \mathbf{k}\cdot\Omega)t - \mathbf{k}\cdot\Phi_{l-1}]}\Big] \\ - \lambda \sum_{\mathbf{k}} &\Big[A_{l+1,\mathbf{k}} e^{-i\mathbf{k}\cdot(\Phi_l - \Phi_{l+1})} e^{-i[(E - \mathbf{k}\cdot\Omega)t - \mathbf{k}\cdot\Phi_l]} \\ &\quad + A_{l-1,\mathbf{k}} e^{-i\mathbf{k}\cdot(\Phi_l - \Phi_{l-1})} e^{-i[(E - \mathbf{k}\cdot\Omega)t - \mathbf{k}\cdot\Phi_l]}\Big] \ . \end{aligned} \tag{B.30}$$

Defining the complex hopping coefficients $\xi^{\pm}_{n,\mathbf{k}}$ as Eq.(5.15)

$$\xi^{\pm}_{l,\mathbf{k}} = e^{-i\mathbf{k}\cdot(\Phi_l - \Phi_{l\pm1})} = \prod_{i=1}^{D} e^{-ik_i(\phi_l^i - \phi_{l\pm1}^i)} = \prod_{i=1}^{D} \xi^{i,\pm}_{l,k_i} \ . \tag{B.31}$$

Eq.(B.26) becomes

$$\begin{aligned} &\sum_{\mathbf{k}} (E - \mathbf{k}\cdot\Omega) A_{l,\mathbf{k}} e^{-i[(E - \mathbf{k}\cdot\Omega)t - \mathbf{k}\cdot\Phi_l]} = \\ &= \sum_{\mathbf{k}} \Big[\epsilon_l A_{l,\mathbf{k}} + \sum_{i=1}^{D} \frac{\mu_i\epsilon_l}{2}\Big(A_{l,\mathbf{k}-\mathbf{e_i}} + A_{l,\mathbf{k}+\mathbf{e_i}}\Big) \\ &\qquad - \lambda\Big(\xi^{-}_{l,\mathbf{k}} A_{l-1,\mathbf{k}} + \xi^{+}_{l,\mathbf{k}} A_{l+1,\mathbf{k}}\Big)\Big] e^{-i[(E - \mathbf{k}\cdot\Omega)t - \mathbf{k}\cdot\Phi_l]} \end{aligned} \tag{B.32}$$

which yield to the $D+1$ dimensional eigenvalue problem in Eq.(5.14)

$$\begin{aligned} EA_{l,\mathbf{k}} = (\epsilon_l + \mathbf{k}\cdot\Omega)A_{l,\mathbf{k}} - \lambda\Big(\xi^-_{l,\mathbf{k}}A_{l-1,\mathbf{k}} + \xi^+_{l,\mathbf{k}}A_{l+1,\mathbf{k}}\Big) \\ + \sum_{i=1}^{D}\frac{\mu_i\epsilon_l}{2}\Big(A_{l,\mathbf{k}-\mathbf{e_i}} + A_{l,\mathbf{k}+\mathbf{e_i}}\Big)\ , \end{aligned} \tag{B.33}$$

We define ν as the index vector

$$\mathbf{v} = (\nu_1, \ldots, \nu_D) \in \mathbb{Z}^D\ . \tag{B.34}$$

The rotation in the momentum space is then defined

$$\begin{aligned} A_{l,\mathbf{k}} &= \sum_{\mathbf{v}} c_{l,\mathbf{v}}\mathcal{D}^{(\mathbf{v})}_{l,\mathbf{k}}\ ; \\ \mathcal{D}^{(\mathbf{v})}_{l,\mathbf{k}} &= \prod_{i=1}^{D} B^{i,(\nu_i)}_{l,k_i} = \prod_{i=1}^{D} J_{k_i-\nu_i}\left(\frac{\mu_i\epsilon_l}{\omega_i}\right)\ . \end{aligned} \tag{B.35}$$

where, for every i, the Bessel function $B^{i,(\nu_i)}_{l,k_i}$ diagonalize the Wannier-Stark ladder in the momentum direction k_i with eigenvalues $\epsilon^{\nu_i} = \omega\nu_i$

$$\begin{aligned} &\mathbf{k}\cdot\Omega A_{l,\mathbf{k}} + \sum_{i=1}^{D}\frac{\mu_i\epsilon_l}{2}\Big(A_{l,\mathbf{k}-\mathbf{e_i}} + A_{l,\mathbf{k}+\mathbf{e_i}}\Big) = \\ &= \sum_{i=1}^{D}\left[k_i\omega_i A_{l,\mathbf{k}} + \frac{\mu_i\epsilon_l}{2}\Big(A_{l,\mathbf{k}-\mathbf{e_i}} + A_{l,\mathbf{k}+\mathbf{e_i}}\Big)\right] \\ &= \sum_{i=1}^{D}\sum_{\mathbf{v}} c_{l,\mathbf{v}}\left[k_i\omega_i\mathcal{D}^{(\mathbf{v})}_{l,\mathbf{k}} + \frac{\mu_i\epsilon_l}{2}\Big(\mathcal{D}^{(\mathbf{v})}_{l,\mathbf{k}-\mathbf{e_i}} + \mathcal{D}^{(\mathbf{v})}_{l,\mathbf{k}+\mathbf{e_i}}\Big)\right] \\ &= \sum_{\mathbf{v}} c_{l,\mathbf{v}}\left[\sum_{i=1}^{D}\left(\prod_{j\neq i} B^{j,(\nu_j)}_{l,k_j}\right)\right. \\ &\qquad \left.\left(k_i\omega_i B^{i,(\nu_i)}_{l,k_i} + \frac{\mu_i\epsilon_l}{2}\Big(B^{i,(\nu_i)}_{l,k_i-1} + B^{i,(\nu_i)}_{l,k_i+1}\Big)\right)\right] \\ &= \sum_{\mathbf{v}} c_{l,\mathbf{v}}\left[\sum_{i=1}^{D}\left(\prod_{j\neq i} B^{j,(\nu_j)}_{l,k_j}\right)\omega_i\nu_i B^{i,(\nu_i)}_{l,k_i}\right] \\ &= \sum_{\mathbf{v}} c_{l,\mathbf{v}}\mathcal{D}^{(\mathbf{v})}_{l,\mathbf{k}}\left[\sum_{i=1}^{D}\omega_i\nu_i\right] \\ &= \sum_{\mathbf{v}} \Omega\cdot\mathbf{v}\ c_{l,\mathbf{v}}\mathcal{D}^{(\mathbf{v})}_{l,\mathbf{k}} \end{aligned} \tag{B.36}$$

Eq.(B.33) in the new basis $\mathcal{B}$ reads

$$\begin{aligned} E\sum_{\mathbf{v}} c_{l,\mathbf{v}}\mathcal{D}^{(\mathbf{v})}_{l,\mathbf{k}} = \sum_{\mathbf{v}}\Big[(\epsilon_l + \Omega\cdot\mathbf{v})c_{l,\mathbf{v}}\mathcal{D}^{(\mathbf{v})}_{l,\mathbf{k}} \\ - \lambda(\xi^-_{l,\mathbf{k}}c_{l-1,\mathbf{v}}\mathcal{D}^{(\mathbf{v})}_{l-1,\mathbf{k}} + \xi^+_{l,\mathbf{k}}c_{l+1,\mathbf{v}}\mathcal{D}^{(\mathbf{v})}_{l+1,\mathbf{k}})\Big]\ . \end{aligned} \tag{B.37}$$

We then multiply Eq.(B.37) for a second Bessel function product $\mathcal{D}^{(\mathbf{n})}_{l,\mathbf{k}}$ of index $\mathbf{n} = (\eta_1, \ldots, \eta_D) \in \mathbb{Z}^D$ and then sum over $\mathbf{k}$. Let's first analyze the Bessel function factor $\mathcal{D}^{(\mathbf{v})}_{l,\mathbf{k}}\mathcal{D}^{(\mathbf{n})}_{l,\mathbf{k}}$. Recalling the Bessel function's orthonormality relation

$$\sum_{k_i} B^{i,(\nu_i)}_{l,k_i}B^{i,(\eta_i)}_{l,k_i} = \sum_{k} J_{k_i-\nu_i}\left(\frac{\mu_i\epsilon_l}{\omega_i}\right)J_{k_i-\eta_i}\left(\frac{\mu_i\epsilon_l}{\omega_i}\right) = \delta_{\nu_i,\eta_i} \tag{B.38}$$

we obtain

$$\begin{aligned}
&\sum_{\mathbf{k}} \mathcal{D}^{(\mathbf{v})}_{l,\mathbf{k}} \mathcal{D}^{(\mathbf{n})}_{l,\mathbf{k}} = \sum_{\mathbf{k}} \left[\prod_{i=1}^{D} B^{i,(\nu_i)}_{l,k_i} B^{i,(\eta_i)}_{l,k_i} \right] = \\
&= \sum_{k_1} B^{1,(\nu_1)}_{l,k_1} B^{1,(\eta_1)}_{l,k_1} \left[\sum_{k_2} \cdots \sum_{k_D} \left(B^{D,(\nu_D)}_{l,k_D} B^{D,(\eta_D)}_{l,k_D} \right) \right] \\
&= \sum_{k_1} \left[\sum_{k_2} \cdots \sum_{k_{D-1}} \left(B^{D-1,(\nu_{D-1})}_{l,k_{D-1}} B^{D-1,(\eta_{D-1})}_{l,k_{D-1}} \right) \right] \delta_{\nu_D,\eta_D} \\
&= \sum_{k_1} \left[\sum_{k_2} \cdots \sum_{k_m} \left(B^{m,(\nu_m)}_{l,k_m} B^{m,(\eta_m)}_{l,k_m} \right) \right] \left(\prod_{i=m+1}^{D} \delta_{\nu_i,\eta_i} \right) \\
&= \cdots = \prod_{i=1}^{D} \delta_{\nu_i,\eta_i} = \delta_{\mathbf{v},\mathbf{n}}
\end{aligned} \tag{B.39}$$

It therefore follows in Eq.(B.37)

$$\begin{aligned}
E \sum_{\mathbf{k}} \sum_{\mathbf{v}} c_{l,\mathbf{v}} \mathcal{D}^{(\mathbf{v})}_{l,\mathbf{k}} \mathcal{D}^{(\mathbf{n})}_{l,\mathbf{k}} &= E c_{l,\mathbf{v}} \ ; \\
\sum_{\mathbf{k}} \sum_{\mathbf{v}} (\epsilon_l + \Omega \cdot \mathbf{v}) c_{l,\mathbf{v}} \mathcal{D}^{(\mathbf{v})}_{l,\mathbf{k}} \mathcal{D}^{(\mathbf{n})}_{l,\mathbf{k}} &= (\epsilon_l + \Omega \cdot \mathbf{v}) c_{l,\mathbf{v}} \ .
\end{aligned} \tag{B.40}$$

In the hopping terms of Eq.(B.37), the Bessel function factor Eq.(B.39) includes the complex factor Eq.(B.31). By Graf's theorem Eq.(B.20) and recalling the definition of the complex coefficients of the hopping Eq.(B.31), the product then turns

$$\begin{aligned}
&\sum_{\mathbf{k}} \xi^{\pm}_{l,\mathbf{k}} \mathcal{D}^{(\mathbf{v})}_{l,\mathbf{k}} \mathcal{D}^{(\mathbf{n})}_{l,\mathbf{k}} = \\
&= \sum_{k_1} \left[\sum_{k_2} \cdots \sum_{k_D} \left(\xi^{D,\pm}_{l,k_D} B^{D,(\nu_D)}_{l,k_D} B^{D,(\eta_D)}_{l,k_D} \right) \right] \\
&= \sum_{k_1} \left[\sum_{k_2} \cdots \sum_{k_{D-1}} \left(\xi^{D-1,\pm}_{l,k_{D-1}} B^{D-1,(\nu_{D-1})}_{l,k_{D-1}} B^{D-1,(\eta_{D-1})}_{l,k_{D-1}} \right) \right. \\
&\qquad \left. \left(\sum_{s} \left(\sigma^{\pm}_{l,D} \right)^{s} J_s\left(\Delta^{\pm}_{l,D} \right) \right) \right] \\
&= \sum_{k_1} \left[\sum_{k_2} \cdots \sum_{k_m} \left(\xi^{m,\pm}_{l,k_m} B^{m,(\nu_m)}_{l,k_m} B^{m,(\eta_m)}_{l,k_m} \right) \right] \\
&\qquad \left[\prod_{i=m+1}^{D} \left(\sum_{s_i} \left(\sigma^{\pm}_{l,i} \right)^{s_i} J_{s_i}\left(\Delta^{\pm}_{l,i} \right) \right) \right] \\
&= \prod_{i=1}^{D} \left(\sum_{s_i} \left(\sigma^{\pm}_{l,i} \right)^{s_i} J_{s_i}\left(\Delta^{\pm}_{l,i} \right) \right)
\end{aligned} \tag{B.41}$$

where

$$\begin{aligned}
\sigma^{\pm}_{l,i} &= \left(\frac{\epsilon_l - e^{i\theta^{\pm}_{l,i}} \epsilon_{l\pm1}}{\epsilon_l - e^{-i\theta^{\pm}_{l,i}} \epsilon_{l\pm1}} \right)^{\frac{1}{2}} \\
\Delta^{\pm}_{l,i} &= \frac{\mu_i}{\omega_i} \sqrt{\epsilon_l^2 + \epsilon_{l\pm1}^2 - 2\epsilon_l \epsilon_{l\pm1} \cos\theta^{\pm}_{l,i}}
\end{aligned} \tag{B.42}$$

Defining the integer vector $\mathbf{s} = (s_1, \ldots, s_D) \in \mathbb{Z}^D$, the hopping terms along the real direction l become

$$\begin{aligned} &\sum_{\mathbf{k}} \sum_{\mathbf{v}} \xi^{\pm}_{l\pm1,\mathbf{k}} c_{l\pm1,\mathbf{v}} \mathcal{D}^{(\mathbf{v})}_{l\pm1,\mathbf{k}} \mathcal{D}^{(\mathbf{n})}_{l,\mathbf{k}} = \\ &= \sum_{\mathbf{s}} \left(\prod_{i=1}^{D} \left(\sigma^{\pm}_{l,i}\right)^{s_i} J_{s_i}\left(\Delta^{\pm}_{l,i}\right) \right) c_{l\pm1,\mathbf{v}} \end{aligned} \tag{B.43}$$

Defining the complex coefficient

$$\Gamma^{\pm}_{l,\mathbf{s}} = \prod_{i=1}^{D} \left(\sigma^{\pm}_{l,i}\right)^{s_i} , \quad \mathbf{s} \in \mathbb{Z}^D \tag{B.44}$$

The eigenvalue problem Eq.(B.37) reads as Eq.(5.33)

$$\begin{aligned} E c_{l,\mathbf{v}} = &(\epsilon_l + \Omega \cdot \mathbf{v}) c_{l,\mathbf{v}} \\ &- \lambda \sum_{\mathbf{s}} \Bigg[\Gamma^{-}_{l,\mathbf{s}} \prod_{i=1}^{D} J_{s_i}\left(\Delta^{-}_{l,i}\right) c_{l-1,\mathbf{v}-\mathbf{s}} \\ &\qquad + \Gamma^{+}_{l,\mathbf{s}} \prod_{i=1}^{D} J_{s_i}\left(\Delta^{+}_{l,i}\right) c_{l+1,\mathbf{v}-\mathbf{s}} \Bigg] \end{aligned} \tag{B.45}$$

APPENDIX C

The Two Interacting Particles Problem - Technical Issues

In this appendix we discuss three technical aspects of the two interacting particle problem. The first consists in the mapping of the one dimensional quantum problem expressed in the Fock basis into a two dimensional linear lattice. Then we recall the definition of overlap integral between single particle modes due to the interaction term. The third one consists in the details of the expansion of the two dimensional time dependent problem into a three dimensional time independent problem using the Bessel function representation.

C.1 Mapping

The Bose-Hubbard hamiltonian Eq.(6.1) consists in two part: $\mathcal{H}_0$ which describes the dynamic of each single particle, and $\mathcal{H}_1$, which describes the particle-particle interaction.

$$\mathcal{H} = \sum_n \left[\epsilon_n \hat{b}_n^+ \hat{b}_n + \hat{b}_{n+1}^+ \hat{b}_n + \hat{b}_{n+1} \hat{b}_n^+\right] + \frac{U}{2} \sum_l \hat{b}_n^+ \hat{b}_n^+ \hat{b}_n \hat{b}_n \equiv \mathcal{H}_0 + \mathcal{H}_1 \ , \tag{C.1}$$

We recall the basis $|l, m\rangle$ defined in Eq.(6.4) for two indistinguishable particles

$$|l, m\rangle := \frac{\hat{b}_l^+ \hat{b}_m^+ |0\rangle}{\sqrt{1 + \delta_{l,m}}} \ , \qquad l \leq m \ . \tag{C.2}$$

In the basis a state ψ can be expanded in

$$\psi = \sum_l \sum_{m \geq l} \varphi_{l,m} |l, m\rangle \ . \tag{C.3}$$

This basis maps the Hamiltonian quantum model into a two dimensional lattice Eq.(6.8). Let's start from $\mathcal{H}_0$, computing the onsite energy term on the general basis term $|l, m\rangle$ for

$l \leq m$.

$$\begin{aligned}\sum_n \epsilon_n \hat{b}_n^+ \hat{b}_n |l,m\rangle &= \epsilon_l \hat{b}_l^+ \hat{b}_l |l,m\rangle + \epsilon_m \hat{b}_m^+ \hat{b}_m |l,m\rangle \\ &= (\epsilon_l + \epsilon_m)|l,m\rangle \ .\end{aligned} \tag{C.4}$$

Let's consider now the first of the hopping terms. First, the off-diagonal case $l \leq m+1$

$$\begin{aligned}\sum_n \hat{b}_{n+1}^+ \hat{b}_n |l,m\rangle &= \hat{b}_{l+1}^+ \hat{b}_l |l,m\rangle + \hat{b}_{m+1}^+ \hat{b}_m |l,m\rangle \qquad l \leq m+1 \\ &= |l+1,m\rangle + |l,m+1\rangle \ .\end{aligned} \tag{C.5}$$

For the diagonal case $l = m$

$$\begin{aligned}\sum_n \hat{b}_{n+1}^+ \hat{b}_n |l,l\rangle = \hat{b}_{l+1}^+ \hat{b}_l |l,l\rangle &= \frac{1}{\sqrt{2}} \hat{b}_{l+1}^+ \hat{b}_l \hat{b}_l^+ \hat{b}_l^+ |0\rangle \qquad l = m \\ &= \frac{1}{\sqrt{2}} \hat{b}_{l+1}^+ (1 - \hat{b}_l^+ \hat{b}_l) \hat{b}_l^+ |0\rangle \\ &= \frac{1}{\sqrt{2}} \hat{b}_{l+1}^+ \hat{b}_l^+ |0\rangle + \frac{1}{\sqrt{2}} \hat{b}_{l+1}^+ \hat{b}_l^+ (1 - \hat{b}_l^+ \hat{b}_l)|0\rangle \\ &= \frac{1}{\sqrt{2}} |l, l+1\rangle + \frac{1}{\sqrt{2}} \hat{b}_{l+1}^+ \hat{b}_l^+ |0\rangle + \frac{1}{\sqrt{2}} \hat{b}_{l+1}^+ \hat{b}_l^+ \hat{b}_l^+ \hat{b}_l |0\rangle \\ &= \sqrt{2} |l, l+1\rangle.\end{aligned} \tag{C.6}$$

Likewise it follows for the complex conjugate term of the hopping that

$$\begin{aligned}\sum_n \hat{b}_{n+1} \hat{b}_n^+ |l,m\rangle &= |l-1,m\rangle + |l,m-1\rangle \ , \qquad l \leq m+1 \ ; \\ \sum_n \hat{b}_{n+1} \hat{b}_n^+ |l,l\rangle &= \sqrt{2}|l-1,l\rangle \qquad\qquad\qquad\quad l = m \ ,\end{aligned} \tag{C.7}$$

The general term $\langle l', m'|\mathcal{H}_0|l, m\rangle$ for l, l', m, m' with $l \leq m$ and $l' \leq m'$ follows

$$\langle l', m'|\mathcal{H}_0|l, m\rangle = \begin{cases} 1 & \text{if } l < m+1, (l' \pm 1 = l \ ; m' = m) \\ 1 & \text{if } l < m+1, (l' = l \ ; m' \pm 1 = m) \\ \sqrt{2} & \text{if } l = m+1, (l' - 1 = l \ ; m' = m) \\ \sqrt{2} & \text{if } l = m+1, (l' = l \ ; m' + 1 = m) \\ 1 & \text{if } l = m+1, (l' + 1 = l \ ; m' = m) \\ 1 & \text{if } l = m+1, (l' = l \ ; m' - 1 = m) \\ \sqrt{2} & \text{if } l = m, (l' + 1 = l \ ; m' = m) \\ \sqrt{2} & \text{if } l = m, (l' = l \ ; m' - 1 = m) \end{cases} \tag{C.8}$$

which yields to a set of equations that describes one half of a two-dimensional lattice $l \leq m$ (see Fig.(6.1)) in Sec.6.2)

$$\begin{cases} i\dot{\psi}_{l,m} & = (\epsilon_l + \epsilon_m)\psi_{l,m} + \psi_{l-1,m} + \psi_{l+1,m} + \psi_{l,m-1} + \psi_{l,m+1} \ , & l < m-1 \\ i\dot{\psi}_{l,l+1} & = (\epsilon_l + \epsilon_{l+1})\psi_{l,l+1} + \psi_{l,l+2} + \psi_{l-1,l+1} + \sqrt{2}\psi_{l,l} + \sqrt{2}\psi_{l+1,l+1} \ , & l = m-1 \\ i\dot{\psi}_{l,l} & = 2\epsilon_l \psi_{l,l} + \sqrt{2}\psi_{l+1,l} + \sqrt{2}\psi_{l-1,l} \ , & l = m \end{cases} \tag{C.9}$$

Unfolding the triangular structure combined with the transformation

$$\begin{cases} \varphi_{l,l} = \sqrt{2}\psi_{l,l} \ , & l = m \ ; \\ \varphi_{l,m} = \psi_{l,m} \ , & l \neq m \ . \end{cases} \tag{C.10}$$

lead to

$$i\dot{\varphi}_{l,m} = (\epsilon_l + \epsilon_m)\varphi_{l,m} + \varphi_{l+1,m} + \varphi_{l-1,m} + \varphi_{l,m+1} + \varphi_{l,m-1} \ . \tag{C.11}$$

Including the interaction hamiltonian $\mathcal{H}_1$ implies the presence of an extra term onsite term in Eq.(C.11).

$$\frac{U}{2}\sum_l \hat{b}_n^+\hat{b}_n^+\hat{b}_n\hat{b}_n|\mathfrak{l},m\rangle = \frac{U}{2}\sqrt{2}|l,l\rangle \ . \tag{C.12}$$

The general term $\langle l',m'|\mathcal{H}_1|\mathfrak{l},m\rangle$ for l,l',m,m' follows

$$\langle l',m'|\mathcal{H}_1|\mathfrak{l},m\rangle = \frac{U}{2}\sqrt{2}\sqrt{2} = U \ . \tag{C.13}$$

In Eq.(C.11), the interaction hamiltonian $\mathcal{H}_1$ generates a diagonal terms $U\delta_{l,m}$. Defining the onsite term

$$\epsilon_{l,m} = \epsilon_l + \epsilon_m + U\delta_{l,m} \ ; \tag{C.14}$$

it follows Eq.(6.8)

$$i\dot{\varphi}_{l,m} = \epsilon_{l,m}\varphi_{l,m} + \varphi_{l+1,m} + \varphi_{l-1,m} + \varphi_{l,m+1} + \varphi_{l,m-1} \ . \tag{C.15}$$

In Sec.6.2, for sake of space we report this equivalent version of the Bose-Hubbard model Eq.(6.1). The triangular version is more cumbersome, however convenient for numerical purposes, since it allows to decrease the total number of CPU operations and, therefore the CPU time.

C.2 Overlap Integral

Let's consider two eigenmodes of the two non-interacting particle problem A_k^μ and A_l^ν with $\mu \leq \nu$

$$|\mu,\nu\rangle = \frac{1}{\sqrt{1+\delta_{\mu,\nu}}}\sum_{k,l} A_k^\mu A_l^\nu \hat{b}_k^+\hat{b}_l^+|0\rangle \ . \tag{C.16}$$

We can expand an eigenstate $|\psi(t)\rangle$ as

$$|\psi(t)\rangle = \sum_{\mu\leq\nu}\sum_\nu \phi_{\mu,\nu}|\mu,\nu\rangle \ . \tag{C.17}$$

and, in presence of interaction U, the time evolution equation of the coefficients $\phi_{\mu,\nu}$ is

$$i\dot{\phi}_{\mu,\nu} = \epsilon_{\mu,\nu}\phi_{\mu,\nu} + U\sum_{\mu'\leq\nu'}\sum_{\nu'} I_{\mu\nu,\mu'\nu'}\phi_{\mu',\nu'} \ . \tag{C.18}$$

The terms $\epsilon_{\mu,\nu}$ (renormalized energies) $I_{\mu\nu,\mu'\nu'}$ (overlapping integrals) are obtained with the following formlua

$$\begin{aligned} \epsilon_{\mu,\nu} &= (E_\mu + E_\nu) + UI^0_{\mu\nu} \ ; \\ I^0_{\mu\nu} &= \frac{2}{1+\delta_{\mu,\nu}}\sum_j (A_j^\mu A_j^\nu)^2 \ ; \\ I_{\mu\nu,\mu'\nu'} &= \frac{2}{\sqrt{(1+\delta_{\mu,\nu})(1+\delta_{\mu,\nu})}}\sum_j A_j^\mu A_j^\nu A_j^{\mu'} A_j^{\nu'} \ . \end{aligned} \tag{C.19}$$

The values of the overlapping integrals describe the renormalization strength of each spectral bands.

C.3 Floquet Analysis

Equation (6.1) can be mapped in the two dimensional linear lattice of equation

$$i\dot{\varphi}_{l,m} = (\epsilon_l + \epsilon_m + U(t)\delta_{l,m})\varphi_{l,m} + \varphi_{l-1,m} + \varphi_{l+1,m} + \varphi_{l,m-1} + \varphi_{l,m+1} \ . \tag{C.20}$$

with

$$U(t) = U_0(1 + \mu\cos(\omega t)) \ . \tag{C.21}$$

We define a Fourier expansion in time defined for every lattice site (n, m) for a real value E

$$\varphi_{l,m} = \sum_{k=-\infty}^{+\infty} A_{l,m,k} e^{-i(E-\omega k)t} \tag{C.22}$$

The equation (C.20) becomes

$$\begin{aligned}\sum_{k=-\infty}^{+\infty} (E-\omega k) A_{l,m,k} e^{-i(E-\omega k)t} = &\sum_{k=-\infty}^{+\infty} \Big[(\epsilon_l + \epsilon_m + U_0\delta_{l,m})A_{l,m,k}\Big] e^{-i(E-\omega k)t} \\ &+ \sum_{k=-\infty}^{+\infty} \Big[A_{l+1,m,k} + A_{l-1,m,k} + A_{l,m+1,k} + A_{l,m-1,k}\Big] e^{-i(E-\omega k)t} \\ &+ \sum_{k=-\infty}^{+\infty} \frac{\mu U_0}{2}\Big[A_{n,m,k-1} + A_{n,m,k+1}\Big] e^{-i(E-\omega k)t} \ ;\end{aligned} \tag{C.23}$$

which give a three dimensional eigenvalue problem

$$\begin{aligned}E A_{l,m,k,} = &(\epsilon_l + \epsilon_m + U_0\delta_{l,m} + \omega k) A_{l,m,k} \\ &+ A_{l+1,m,k} + A_{l-1,m,k} + A_{l,m+1,k} + A_{l,m-1,k} \\ &+ \frac{\mu U_0}{2}\delta_{l,m}(A_{l,m,k-1} + A_{l,m,k+1}) \ .\end{aligned} \tag{C.24}$$

Along k - second line - there is a Wannier-Stark ladder with dc field ω and hopping coefficient $(\mu U_0/2)\delta_{l,m}$. Therefore, off diagonal the Stark ladder has zero hopping.

For given (l, m),the family of Bessel function of first kind constitutes a basis of eigenvectors of the Wannier-Stark ladder along k. Therefore, we define the set $\{B^{(\nu)}_{l,m,k}\}_\nu$ along the lattice in k defined as

$$B^{(\nu)}_{l,m,k} = J_{k-\nu}\left(\frac{\mu U_0}{\omega}\delta_{l,m}\right) , \qquad E_{\nu,l,m} = \epsilon_l + \epsilon_m + U_0\delta_{l,m} + \omega\nu \ . \tag{C.25}$$

where, for each ν, $\mathcal{E}^{(\nu)}$ is the associated eigenvalue. For every (n, m) these Bessel functions $\{B^{(\nu)}_{n,m}\}_\nu$ diagonalize the Wannier-Stark ladder along k (second line of the equation (C.24)). We want to again use these two sets $\{\{B^{(\nu)}_n\}_n\}_\nu$ to expand $\{A_{n,m}\}_{n,m}$ along k

$$A_{l,m,k,} = \sum_\nu c_{l,m,\nu} B^{(\nu)}_{l,m,k} \ . \tag{C.26}$$

Equation (C.24) now reads

$$\begin{aligned} E\sum_{\nu} c_{l,m,\nu}B^{(\nu)}_{l,m,k} &= \sum_{\nu}\Big[(\epsilon_l+\epsilon_m+U_0\delta_{l,m}+\omega k)c_{l,m,\nu}B^{(\nu)}_{l,m,k}\Big] \\ &+\sum_{\nu}\Big[c_{l+1,m,\nu}B^{(\nu)}_{l+1,m,k}+c_{l-1,m,\nu}B^{(\nu)}_{l-1,m,k}+ \\ &\qquad +c_{l,m+1,\nu}B^{(\nu)}_{l,m+1,k}+c_{l,m-1,\nu}B^{(\nu)}_{l,m-1,k}\Big] \\ &+\sum_{\nu}\frac{\mu U_0}{2}\delta_{l,m}\Big[c_{l,m,\nu}B^{(\nu)}_{l,m,k-1}+c_{l,m,\nu}B^{(\nu)}_{l,m,k+1}\Big]\ . \end{aligned} \tag{C.27}$$

Considering the Stark Ladder along the momentum direction k, we have

$$\begin{aligned} &\sum_{\nu} c_{l,m,\nu}\Big[\omega k B^{(\nu)}_{l,m,k}+\frac{\mu U_0}{2}\delta_{l,m}(B^{(\nu)}_{l,m,k-1}+B^{(\nu)}_{l,m,k+1})\Big] \\ &=-\sum_{\nu} c_{l,m,\nu}\omega\nu B^{(\nu)}_{l,m,k} \end{aligned} \tag{C.28}$$

Therefore, equation (C.27) reads

$$\begin{aligned} E\sum_{\nu} c_{l,m,\nu}B^{(\nu)}_{l,m,k} &= \sum_{\nu}\Big[(\epsilon_l+\epsilon_m+U_0\delta_{l,m}-\omega\nu)c_{l,m,\nu}B^{(\nu)}_{l,m,k}\Big] \\ &+\sum_{\nu}\Big[c_{l+1,m,\nu}B^{(\nu)}_{l+1,m,k}+c_{l-1,m,\nu}B^{(\nu)}_{l-1,m,k}+ \\ &\qquad +c_{l,m+1,\nu}B^{(\nu)}_{l,m+1,k}+c_{l,m-1,\nu}B^{(\nu)}_{l,m-1,k}\Big] \end{aligned} \tag{C.29}$$

We use the orthonormality of the Bessel function along the lattice direction k.

$$\sum_{k} B^{(\nu)}_{l,m,k}B^{(\nu_2)}_{l,m,k}=\sum_{k} J_{k-\nu}\Big(\frac{\mu U_0}{\omega}\delta_{l,m}\Big)J_{k-\nu_2}\Big(\frac{\mu U_0}{\omega}\delta_{l,m}\Big)=\delta_{\nu,\nu_2} \tag{C.30}$$

Therefore first we multiply by $B^{(\nu_2)}_{l,m,k}$ for an integer ν_2. Then we first sum over the lattice index k and then over the Bessel function index ν_2. Let's consider the left side of equation (C.29)

$$\begin{aligned} E\sum_{\nu_2}\sum_{k}\sum_{\nu} c_{l,m,\nu}B^{(\nu)}_{l,m,k}\cdot B^{(\nu_2)}_{l,m,k} &= E\sum_{\nu} c_{l,m,\nu}\Big[\sum_{\nu_2}\sum_{k} B^{(\nu)}_{l,m,k}B^{(\nu_2)}_{l,m,k}\Big] \\ &= E\sum_{\nu} c_{l,m,\nu}\sum_{\nu_2}\delta_{\nu,\nu_2} \\ &= E\sum_{\nu} c_{l,m,\nu} \end{aligned} \tag{C.31}$$

Likewise for the onsite energy

$$\begin{aligned} &\sum_{\nu_2}\sum_{k}\sum_{\nu}(\epsilon_l+\epsilon_m+U_0\delta_{l,m}-\omega\nu)c_{l,m,\nu}B^{(\nu)}_{l,m,k}\cdot B^{(\nu_2)}_{l,m,k}= \\ &=\sum_{\nu}(\epsilon_l+\epsilon_m+U_0\delta_{l,m}-\omega\nu)c_{l,m,\nu}\Big[\sum_{\nu_2}\sum_{k} B^{(\nu)}_{l,m,k}B^{(\nu_2)}_{l,m,k}\Big] \\ &=\sum_{\nu}(\epsilon_l+\epsilon_m+U_0\delta_{l,m}-\omega\nu)c_{l,m,\nu} \end{aligned} \tag{C.32}$$

The hopping term reads

$$\begin{aligned}
&\sum_{\nu_2}\sum_{k}\sum_{\nu}\Big[c_{l\pm1,m,\nu}B^{(\nu)}_{l\pm1,m,k}+c_{l,m\pm1,\nu}B^{(\nu)}_{l,m\pm1,k}\Big]\cdot B^{(\nu_2)}_{l,k}\\
&=\sum_{\nu}\Bigg[c_{l\pm1,m,\nu}\Big(\sum_{\nu_2}\sum_{k}B^{(\nu)}_{l\pm1,m,k}B^{(\nu_2)}_{l,m,k}\Big)\\
&\qquad+c_{l,m\pm1,\nu}\Big(\sum_{\nu_2}\sum_{k}B^{(\nu)}_{l,m\pm1,k}B^{(\nu_2)}_{l,m,k}\Big)\Bigg]
\end{aligned}\tag{C.33}$$

Within the sum in round brackets along the first real coordinate l we have

$$\begin{aligned}
&\sum_{k}B^{(\nu)}_{l\pm1,m,k}B^{(\nu_2)}_{l,m,k}=\sum_{k}J_{k-\nu}\Big(\frac{\mu U_0}{\omega}\delta_{l\pm1,m}\Big)J_{k-\nu_2}\Big(\frac{\mu U_0}{\omega}\delta_{l,m}\Big)\\
&=\sum_{k}J_{k-(\nu-\nu_2)}\Big(\frac{\mu U_0}{\omega}\delta_{l\pm1,m}\Big)J_{k}\Big(\frac{\mu U_0}{\omega}\delta_{l,m}\Big)
\end{aligned}\tag{C.34}$$

We rewrite the Eq.(C.34) along the coordinate l using the Neumann's Addition Theorem (Abramopwitz and Stetgun)

$$\sum_{n}J_{l\pm\nu}(x)J_l(y)=J_\nu(x\mp y)\tag{C.35}$$

It follows that

$$\begin{aligned}
&\sum_{k}J_{k-(\nu-\nu_2)}\Big(\frac{\mu U_0}{\omega}\delta_{l\pm1,m}\Big)J_{k}\Big(\frac{\mu U_0}{\omega}\delta_{l,m}\Big)\\
&=J_{\nu-\nu_2}\Big(\frac{\mu U_0}{\omega}\delta_{l\pm1,m}+\frac{\mu U_0}{\omega}\delta_{l,m}\Big)\\
&=J_{\nu-\nu_2}\Big(\frac{\mu U_0}{\omega}(\delta_{l\pm1,m}+\delta_{l,m})\Big)\\
&=J_{\nu-\nu_2}(z^{\pm}_{l,m})\ .
\end{aligned}\tag{C.36}$$

with

$$z^{\pm}_{l,m}=\frac{\mu U_0}{\omega}(\delta_{l,m}+\delta_{l\pm1,m})\tag{C.37}$$

This simplification holds also for the second real coordinate m. Eq.(C.33) becomes

$$\begin{aligned}
&\sum_{\nu_2}\sum_{k}\sum_{\nu}\Big[c_{l\pm1,m,\nu}B^{(\nu)}_{l\pm1,m,k}+c_{l,m\pm1,\nu}B^{(\nu)}_{l,m\pm1,k}\Big]\cdot B^{(\nu_2)}_{l,k}\\
&=\sum_{\nu}\sum_{\nu_2}\Big[J_{\nu-\nu_2}(z^{-}_{l,m})c_{l-1,m,\nu}+J_{\nu-\nu_2}(z^{+}_{l,m})c_{l+1,m,\nu}+\\
&\qquad+J_{\nu-\nu_2}(x^{-}_{l,m})c_{l,m-1,\nu}+J_{\nu-\nu_2}(x^{+}_{l,m})c_{l,m+1,\nu}\Big]\ ,
\end{aligned}\tag{C.38}$$

where

$$\begin{aligned}
z^{\pm}_{l,m}&=\frac{\mu U_0}{\omega}(\delta_{l,m}+\delta_{l\pm1,m})\\
x^{\pm}_{l,m}&=\frac{\mu U_0}{\omega}(\delta_{l,m}+\delta_{l,m\pm1})
\end{aligned}\tag{C.39}$$

Since for an integer s it holds

$$\nu-\nu_2=s\quad\Leftrightarrow\quad\nu_2=\nu-s\ ,\tag{C.40}$$

it follow that

$$\begin{aligned}
&\sum_{\nu_2}\sum_{k}\sum_{\nu}\left[c_{l\pm1,m,\nu}B^{(\nu)}_{l\pm1,m,k}+c_{l,m\pm1,\nu}B^{(\nu)}_{l,m\pm1,k}\right]\cdot B^{(\nu_2)}_{l,k}\\
&=\sum_{\nu}\sum_{s}\left(J_s(z^-_{l,m})c_{l-1,m,\nu-s}+J_s(z^+_{l,m})c_{l+1,m,\nu-s}+\right.\\
&\qquad\left.+J_s(x^-_{l,m})c_{l,m-1,\nu-s}+J_s(x^+_{l,m})c_{l,m+1,\nu-s}\right)\ ,
\end{aligned}\tag{C.41}$$

Equation (C.29) now reads

$$\begin{aligned}
E\sum_{\nu}c_{l,m,\nu}&=\sum_{\nu}(\epsilon_l+\epsilon_m+U_0\delta_{l,m}-\omega\nu)c_{n,m,\nu}\\
&+\sum_{\nu}\sum_{s}\Big(J_s(z^-_{l,m})c_{l-1,m,\nu-s}+J_s(z^+_{l,m})c_{l+1,m,\nu-s}+\\
&\qquad+J_s(x^-_{l,m})c_{l,m-1,\nu-s}+J_s(x^+_{l,m})c_{l,m+1,\nu-s}\Big)
\end{aligned}\tag{C.42}$$

which gives an eigenvalue problem in the momentum space

$$\begin{aligned}
Ec_{l,m,\nu}&=(\epsilon_l+\epsilon_m+U_0\delta_{l,m}-\omega\nu)c_{l,m,\nu}\\
&+\sum_{s}\Big(J_s(z^-_{l,m})c_{l-1,m,\nu-s}+J_s(z^+_{l,m})c_{l+1,m,\nu-s}+\\
&\qquad+J_s(x^-_{l,m})c_{l,m-1,\nu-s}+J_s(x^+_{l,m})c_{l,m+1,\nu-s}\Big)\ ;
\end{aligned}\tag{C.43}$$

where

$$\begin{aligned}
z^{\pm}_{l,m}&=\frac{\mu U_0}{\omega}(\delta_{l,m}+\delta_{l\pm1,m})\\
x^{\pm}_{l,m}&=\frac{\mu U_0}{\omega}(\delta_{l,m}+\delta_{l,m\pm1})\ .
\end{aligned}\tag{C.44}$$

which correspond to the eigenvalue problem Eq.(6.21).

Bibliography

[1] I. Newton, *Philosophi Naturalis Principia Mathematica*, (1687).

[2] P. W. Anderson, *Absence of diffusion in certain random lattices*, Phys. Rev. **109**, 1492 (1958).

[3] W.J. de Haas, J.H. de Boer and G.J. van den Berg, *The electrical resistance of gold, copper and lead at low temperatures*, Physica **1**, 1115 (1934).

[4] G.J. Van den Berg, *Progress in low temperature physics*, **4**, 194, Gorter editor, North Holland, Amsterdam, (1964).

[5] J. Kondo, *Resistance minimum in dilute magnetic alloys*, Progress of Theoretical Physics, **32**, 37 (1964).

[6] E. Abrahams, P. W. Anderson, D. C. Licciardello, and T. V. Ramakrishnan, *Scaling theory of localization: bsence of quantum diffusion in two dimensions*, Phys. Rev. Lett. **42**, 673 (1979).

[7] B.R. Bulka, B. Kramer and A. MacKinnon, *Mobility edge in the three dimensional anderson model*, Zeitschrift für Physik B Condensed Matter, **60**, 1, 13-17 (1985).

[8] D. Basko, I. Aleiner and B. Altshuler, *Metal-insulator transition in a weakly interacting many-electron system with localized single-particle states*, Ann. Phys. **321**, 1126 (2006).

[9] C. Monthus and T. Garel, *Many-body localization transition in a lattice model of interacting fermions: Statistics of renormalized hoppings in configuration space*, Phys. Rev. B **81**, 134202 (2010).

[10] D.O. Krimer, R. Khomeriki and S. Flach, *Two interacting particles in a random potential*, Pis'ma v ZhETF **94**, 438 (2011); JETP Letters **94**, 406 (2011).

[11] M. Schreiber, S.S. Hodgman, P. Bordia, H.P. Lüschen, M.H. Fischer, R. Vosk, E. Altman, U. Schneider, I. Bloch, *Observation of many-body localization of interacting fermions in a quasirandom optical lattice*, Science **21** Vol. 349, Issue 6250, 842 (2015).

[12] D.O. Krimer and S.Flach, *Interaction-induced connectivity of disordered two-particle states* , Phys. Rev. B **91**, 100201(R) (2015).

[13] S. Flach, D. Krimer and Ch. Skokos, *Universal spreading of wavepackets in disordered nonlinear systems* , Phys. Rev. Lett. **102**, 024101 (2009); Phys. Rev. Lett. **102**, 209903 (2009).

[14] Ch. Skokos, D.O. Krimer, S. Komineas and S. Flach, *Delocalization of wave packets in disordered nonlinear chains* , Phys. Rev. E **79**, 056211 (2009).

[15] T.V. Laptyeva, J.D. Bodyfelt, D.O. Krimer, Ch. Skokos and S. Flach, *The crossover from strong to weak chaos for nonlinear waves in disordered systems* , EPL **91**, 30001 (2010).

[16] T.V. Laptyeva, J.D. Bodyfelt and S. Flach, *Universal subdiffusion of nonlinear waves in two dimensions with disorder*, EPL **98**, 60002 (2012).

[17] T.V. Laptyeva, J.D. Bodyfelt and S. Flach, *Do nonlinear waves in random media follow nonlinear diffusion equations?* , Physica D **1**, 256 (2013).

[18] Ch. Skokos, I. Gkolias and S. Flach, *Nonequilibrium chaos of disordered nonlinear waves* , Phys. Rev. Lett. **111**, 064101 (2013).

[19] J. Billy, V. Josse, Z. Zuo, A. Bernard, B. Hambrecht, P. Lugan, D. Clément, L. Sanchez-Palencia, P. Bouyer and A. Aspect, *Direct observation of Anderson localization of matter waves in a controlled disorder*, Nature **453**, 891-894 (2008).

[20] G. Roati, C. D. Errico, L. Fallani, M. Fatttori, C. Fort, M. Zaccanti, G. Modugno, M. Modugno and M. Inguscio, *Anderson localization of a non-interacting Bose-Einstein condensate.*, Nature **453**, 895 (2008).

[21] D.S. Wiersma, P. Bartolini, A. Lagendijk, and R. Righini, *Localization of light in a disordered medium*, Nature **390**, 671 (1997).

[22] F. Scheffold, R. Lenke, R. Tweer and G. Maret, *Localization or classical diffusion of light?*, Nature **398**, 206 (1999).

[23] M. Storzer, P. Gross, C.M. Aegerter and G. Maret, *Observation of the critical regime near Anderson localization of light*, Phys. Rev. Lett. **96**, 063904 (2006).

[24] T. Schwartz, G. Bartal, S. Fishman and M. Segev, *Transport and Anderson localization in disordered two-dimensional photonic lattices.*, Nature **446**, 52 (2007).

[25] Y. Lahini, A. Avidan, F. Pozzi, M. Sorel, R. Morandotti, D.N. Christodoulides and Y. Silberberg, *Anderson localization and nonlinearity in one-dimensional disordered photonic lattices*, Phys. Rev. Lett. **100**, 013906 (2008).

[26] R. Dalichaouch, J.P. Armstrong, S. Schultz, P.M. Platzman and S.L. McCall, *Microwave localization by two-dimensional random scattering*, Nature **354**, 53 (1991).

[27] A.A. Chabanov, M. Stoytchev A.Z. Genack, *Statistical signatures of photon localization*, Nature **404**, 850 (2000).

[28] R.L. Weaver, *Anderson localization of ultrasound*, Wave Motion **12**, 129 (1990).

[29] E. Akkermans and G. Montambaux, *Mesoscopic physics of electrons and photons*, (Cambridge Univ. Press, Cambridge, UK, 2006).

[30] V. Milner and A.Z. Genack, *Photon localization laser: low-threshold lasing in a random amplifying layered medium via wave localization*, Phys. Rev. Lett. **94**, 073901 (2005).

[31] K.L. Van der Molen, R.W. Tjerkstra, A.P. Mosk and A. Lagendijk, *Spatial extent of random laser modes*, Phys. Rev. Lett. **98**, 143901 (2007).

[32] J. Fallert, R.J.B. Dietz, J. Sartor, D. Schneider, C. Klingshirn and H. Kalt, *Co-existence of strongly and weakly localized random laser modes*, Nature Photon. **3**, 279 (2009).

[33] P. Stano and P. Jacquod, *Suppression of interactions in multimode random lasers in the Anderson localized regime*, Nature Photonics **7**, 66 (2013).

[34] J. Floss, S. Fishman and I.Sh. Averbukh, *Anderson localization in laser-kicked molecules*, Phys. Rev. A **88**, 023426 (2013).

[35] C. Lecaplain, P. Grelu and S. Wabnitz, *Dynamics of the transition from polarization disorder to antiphase polarization domains in vector fiber lasers*, Phys. Rev. A **89**, 063812 (2014).

[36] P.L. Christiansen, J.C. Eilbeck, R.D. Parmetier, *Future directions of nonlinear dynamics in physical and biological systems*, Springer, Science Vol **213** (1993)

[37] G. Vattay, S. Kauffman and S. Niiranen, *Quantum biology on the edge of quantum chaos*, PLoS one **9** (3), e89017 (2014).

[38] V.N. Prigodin and K.B. Efetov, *Localization transition in a random network of metallic wires: a model for highly conducting polymers*, Phys. Rev. Lett. **70**, 2932 (1993).

[39] T. Strudley, T. Zehender, C. Blejean, E.P.A.M. Bakkers and O.L. Muskens, *Mesoscopic light transport by very strong collective multiple scattering in nanowire mats*, Nature Photonics **7**, 413 (2013).

[40] S. Mookherjea, J.R. Ong, X. Luo and L. Guo-Qiang, *Electronic control of optical Anderson localization modes*, Nature Nanotechnology **9**, 365-371 (2014).

[41] S.H. Choi, K.M. Byun KM and Y.L. Kim, *Excitation of multiple resonances in 1D Anderson localized systems for efficient light amplification* , Opt Lett. **40** (5), 847 (2015).

[42] F. Izrailev and A. A. Krokhin, *Localization and the mobility edge in one-dimensional potentials with correlated disorder*, Phys. Rev. Lett. **82**, 4062 (1999).

[43] A. Croy, P. Cain and M. Schreiber, *Anderson localization in 1D systems with correlated disorder*, Eur. Phys. J. B **82** 107 (2011).

[44] E. Fratini and S. Pilati, *Anderson localization in optical lattices with correlated disorder*, Phys. Rev. A **92**, 063621 (2015).

[45] D. Mogilevtsev, F.A. Pinheiro, R.R. dos Santos, S.B. Cavalcanti and L.E. Oliveira, *Light propagation and Anderson localization in disordered superlattices containing dispersive metamaterials: effects of correlated disorder*, Phys. Rev. B **84**, 094204 (2011).

[46] T.A.L. Ziman, *Localization with off-diagonal disorder: a qualitative theory*, Phys. Rev. B **26**, 7066 (1982).

[47] U. Krey, *Anderson localization in different one-dimensional systems with off-diagonal disorder and spin-dependence*, Zeitschrift für Physik B Condensed Matter **54**, 1, 1-9 (1983).

[48] P. Biswas, P. Cain, R.A. Römer and M. Schreiber, *Off-diagonal disorder in the Anderson model of localization*, Phys. Stat. Sol. B **218**, 205 (2000).

[49] E. Schrödinger, Annalen der Physik **384**, (4) 361 (1926); Annalen der Physik **384**, (4) 489 (1926); Annalen der Physik **385**, (13) 437 (1926); Annalen der Physik **386**, (18) 109 (1926).

[50] D.W. Ward and S. Volkmer, *How to derive the Schrödinger equation*, arXiv:physics/0610121v1 (2006).

[51] Yu. S. Kivshar and G. P. Agrawal, *Optical Solitons: From Fibers to Photonic Crystals*, Academic Press, Amsterdam, (2003).

[52] E. Fermi, J. Pasta, and S. Ulam, LA-1940 internal report, 1955. *Studies on nonlinear problems I*, Reprinted in the Collect Papers of E. Fermi, Vol. II, University of Chicago Press and Accademia Nazionale dei Lincei, 978, (1965).

[53] F. M. Izrailev and B. V. Chirikov, *Statistical properties of a non-linear string"*, Sov. Phys. Dokl. **11**, 30 (1966).

[54] L. Casetti, M. Cerruti-Sola, M. Pettini, and E. G. D. Cohen, *The Fermi-Pasta-Ulam problem revisited: stochasticity thresholds in nonlinear Hamiltonian systems*, Phys. Rev. E **55**, 6566 (1997).

[55] S. Flach, O.I. Kanakov, M.V. Ivanchenko and K.G. Mishagin, *q-breathers in FPU lattices - scaling and properties for large systems*, Int. J. Mod. Phys. B **21**, 3925 (2007).

[56] A. Ponno, H. Christodoulidi, Ch. Skokos and S. Flach, *The two-stage dynamics in the Fermi-Pasta-Ulam problem: from regular to diffusive behavior* , Chaos **21**, 043127 (2011).

[57] T.V. Laptyeva, S. Flach and K. Kladko, *The weak password problem: chaos, criticality, and encrypted p-CAPTCHAs* , EPL **95**, 50007 (2011).

[58] M. Peyrard and A.R. Bishop, *Statistical mechanics of a nonlinear model for DNA denaturation*, Phys. Rev. Lett. **62**, 2755,(1989).

[59] L.V. Yakushevich, *Nonlinear DNA dynamics: a new model*, Phys. Rev. A **136**, 413 (1989).

[60] L.V. Yakushevich, *Nonlinear Physics of DNA*, Wiley Series in Nonlinear Science, John Wiley, Chichester (1998).

[61] S. Zdravkovic, M.V. Sataric, *Nonlinear Schrödinger equation and DNA dynamics*, Phys. Lett. A **373**, 126 (2008).

[62] S. Zdravkovic, M.V. Sataric, *Parameter selection in a Peyrard-Bishop-Dauxois for DNA dynamics*, Phys. Lett. A **373**, 2739 (2009).

[63] S. Zdravkovic, *Helicoidal Peyrard-Bishop model of DNA dynamics*, J. of Nonlin. Math. Phys. **18**, 463 (2011).

[64] J. Zhang, Z. Zhang and P. Tong, *Effects of delayed nonlinear response on wave packet dynamics in one-dimensional generalized Fibonacci chains*, Physica B **421**, 18 (2013).

[65] E.L. Albuquerque, U.L. Fulco, V.N. Freire, W.W.S. Caetano, M.L. Lyra, F.A.B.F. de Moura, *DNA-based nanobiostructured devices: the role of quasiperiodicity and correlation effects*, Phys. Rep. **535**, 139-209 (2014).

[66] C. Kittel, *Quantum theory of solids*, Wiley, New York (1963).

[67] R. Hunsperger, *Integrated optics, theory and technology*, Springer (1982).

[68] S. Longhi, *Aharonov-Bohm photonic cages in waveguide and coupled resonator lattices by synthetic magnetic fields* , Opt. Lett. **39** (20), 5892-5895 (2014)

[69] N.V. Alexeeva, I.V. Barashenkov, K. Rayanov and S. Flach, *Actively coupled optical waveguides* , Phys. Rev. A **89**, 013848 (2014).

[70] P. Millar, J.S. Aitchinson, J.U. Kang, G.I. Stegeman, A. Villeneuve, G.T. Kennedy and W. Sibbett, *Nonlinear waveguide arrays in AlGaAs*, J. Opt. Phys. Soc. Am. B **14** (11), 3224 (1997).

[71] A.S. Desyatnikov, D.N. Neshev, R. Fischer, W. Krolikowski, N. Sagemerten, D. Träger, C. Denz, A. Dreischuh and Y. S. Kivshar, Proc. SPIE **6023**, Tenth International Conference on Nonlinear Optics of Liquid and Photorefractive Crystals,(2006).

[72] C. Denz, S. Flach, Sergej and Y.S. Kivshar, *Nonlinearities in periodic structures and metamaterials*, Springer Series in Optical Science **150** (2010).

[73] I. Bloch, *Ultracold quantum gases in optical lattices*, Nature Physics **1**, 23 (2005).

[74] T. Lepetit, *Optical physics: magnetic appeal in strained lattice*, Nature Photonics **7**, 86 (2013).

[75] I. Bloch, *Quantum coherence and entanglement with ultracold atoms in optical lattices*, Nature **453**, 1016 (2008).

[76] G. Grüner, *The dynamics of charge-density waves*, Rev. Mod. Phys. **60**, 1129 (1988).

[77] D.S.Fisher, M.P.A. Fisher and D.A. Huse, *Thermal fluctuations, quenched disorder, phase transitions, and transport in type-II superconductors*, Phys. Rev. B **43**, 130 (1991).

[78] L. Balents and M.P.A. Fisher, *Temporal order in dirty driven periodic media*, Phys. Rev. Lett. **75**, 4270 (1995).

[79] A.C. Hewson *The Kondo problem to heavy fermions*, New York: Cambridge University Press (1993).

[80] R. Landauer, *Spatial variation of currents and fields due to localized scatterers in metallic conduction*, IBM Journal of Research and Development **1**, 223 (1957).

[81] S. Datta, *Electronic Transport in Mesoscopic Systems*, Cambridge University Press, Cambridge, (1995)

[82] Y.V. Nazarov, Ya.M. Blanter, *Quantum transport: introduction to nanoscience*, Cambridge University Press, **29**, (2009).

[83] B. Kramer and A. MacKinnon, *Localization: theory and experiments*, Rep. Prog. Phys. **56**, 1469 (1993).

[84] D.O. Krimer and S. Flach, Statistics of wave interactions in nonlinear disordered systems, Phys. Rev. E **82**, 046221 (2010).

[85] P. G. Harper, *Single band motion of conduction electrons in a uniform magnetic field*, Proc. Phys. Soc. A,**68**, 874 (1955).

[86] S. Aubry and G. Andre, *Analiticity breaking and Anderson localization in incommensurate lattices*, Ann. Israel Phys. Soc., **3**, Hilger, Bristol, 133 (1980).

[87] D. Shechtman, I. Blech, D. Gratias and J. W. Cahn, *Metallic phase with long-range orientational order and no translational symmetry*, Phys. Rev. Lett. **53**, 1951 (1984).

[88] D. Shechtman, *The icosahedral quasiperiodic phase*, Physica Scripta **49**,49-53 (1988)

[89] M. Engel, P.F. Damasceno, C.L. Phillips, S.C. Glotzer, *Computational self-assembly of a one-component icosahedral quasicrystal*, Nature Materials **14**, 109 (2015).

[90] R. Penrose, *The role of aesthetics in pure and applied mathematical research*, Bulletin of the Institute of Mathematics and Its Applications **10**, No. 2, 266 (1974).

[91] F.M. Dekking, *On repetitions of blocks in binary sequences*, J. Combin, Theory Ser. A **27**, 292 (1976).

[92] F.M. Dekking, *Transcendence du nombre de Thue-Morse*, C.R.Acad.Sci.deParis **285**,157 (1977).

[93] G. Christol, T. Kamae, M. Mendes-France and G. Rauzy, *Suites algebrique, automates et substitutions*, Bull.Soc.Math.(France) **108**, 401 (1980).

[94] A.Cobham, *On the base-dependence of sets of numbers recognizable by finite automata*, Math.Syst.Theory **3**, 186 (1969).

[95] A. Cobham, *Uniform tag sequences*, Math.Syst.Theory **6**, 164 (1972).

[96] G.T. Herman, G. Hozenberg, *Developmental systems and languages*, North-Holland,Amsterdam, (1975).

[97] A.N. Kolmogorov, *On the conservation of conditionally periodic motions under small perturbation of the Hamiltonian*, Dokl. Akad. Nauk SSSR **98**, 525-530 (1954) (in Russian) [English translation LNP **93** 51-56 (1979)]

[98] J. Pöschel, *A lecture on the classical KAM-theorem*, Proceedings of Symposia in Pure Mathematics (AMS) **69**, 707 (2001).

[99] B.B. Mandelbrot, *The Fractal Geometry of Nature*, Freeman, New York (1982).

[100] R. Merlin, K. Bajema, R. Clarke, F.-Y. Juang and P.K. Bhattacharya, *Quasiperiodic GaAs-AlAs heterostructures*, Phys. Rev. Lett. **55** 1768 (1985).

[101] M.W.C. Dharma-Wardana, A.H. MacDonald, D.J. Lockwood, J.-M. Baribeau and D.C. Houghton, *Raman scattering in Fibonacci superlattices*, Phys. Rev. Lett. **58**, 1761 (1987).

[102] D.J. Lockwood, M.W.C. Dharma-Wardana, G.C. Aers and J.-M. Baribeau, *Substrate and capping layer effects on the phonon-spectrum of ultrathin superlattices*, Appl. Phys. Lett. **52**, 2040 (1988).

[103] M. Queffelec, *Substitution dynamical systems - spectral analysis*, Lecture Notes in Mathematics **1294**, Springer-Verlag (2010).

[104] J. Brillhart and P. Morton, *A Case study in mathematical research: the Golay-Rudin-Shapiro sequence*, The American Mathematical Monthly, **103**, 854 (1996).

[105] A. Avila, S. Jitomirskaya, *The ten Martini problem*, Annals of Mathematics **170** , 303 (2009).

[106] S. Ya. Jitomirskaya, I. V. Krasovsky, *Continuity of the measure of the spectrum for discrete quasiperiodic operators*, Math. Res. Lett. **9**, 413 (2002).

[107] C. Tang, M. Kohmoto, *Global scaling properties of the spectrum for a quasiperiodic schrödinger equation*, Phys. Rev. B, **34**, 2041 (1986).

[108] J. Bell and R.B. Stinchcombe, *Hierarchical clustering in the spectra of incommensurate systems*, J.Phys. A **20**, L739 (1987).

[109] T. Geisel, R. Ketzmerick and G. Petschel, *New class of level statistics in quantum systems with unbounded diffusion*, Phys. Rev. Lett. **69**, 1651 (1991).

[110] Y. Last, *Zero measure spectrum for the almost Mathieu operator*, Commun. Math. Phys. **164**, 421-432 (1994).

[111] M. Wilkinson and E.J. Austin, *Spectral dimension and dynamics for Harper equation*, Phys. Rev. B **50**, 1420 (1994).

[112] A. Avila, *The absolutely continuous spectrum of the almost Mathieu operator*, arXiv:0810.2965 (2008).

[113] S. Ya. Jitomirskaya, *Metal-insulator transition for the almost Mathieu operator*, Ann. of Math. **150** 1159 (1999).

[114] A. Gordon, S. Ya. Jitomirskaya, Y. Last and B. Simon, *Duality and singular continuous spectrum in the almost Mathieu equation*, Acta Math **178**, 169 (1997).

[115] C. Aulbach, A. Wobst, G.L. Ingold, P. Hänggi and I. Varga, *Phase-space visualization of a metal-insulator transition*, New J. Phys. **6**, 70 (2004).

[116] A. Haro, J. Piug, *A Thouless formula and Aubry duality for long-range Schrödinger skew-products*, Nonlinearity **26**, 1163 (2013).

[117] H. Hiramoto, M. Kohmoto, *Scaling analysis of quasiperiodic systems: generalized Harper model*, Phys. Rev. B **40**, 8225 (1989).

[118] D.J. Boers, B. Goedeke, D. Hinrichs, M. Holthaus, *Mobility edges in bichromatic optical lattices*, Phys. Rev. A **75**, 063404 (2007).

[119] M. Kohmoto, L. P. Kadanoff and C. Tang, *Localization problem in one dimension: mapping and escape*, Phys. Rev. Lett. **50**, 1870 (1983).

[120] S. Ostlund, R. Pandit, D. Rand, H. J. Schellnhuber and E. D. Siggia, *One-dimensional Schrödinger equation with an almost periodic potential*, Phys. Rev. Lett. **50**, 1873 (1983).

[121] D. R. Grempell, S. Fishman and R. Prange, *Localization in an incommensurate potential: an exactly solvable model*, Phys. Rev. Lett. **49**, 833 (1982).

[122] D. R. Grempell, S. Fishman and R. Prange, *Quantum dynamics of a nonintegrable system*, Phys. Rev. A, **29**, 1639 (1984).

[123] S. Flach, M. Ivanchenko, R. Khomeriki, *Correlated metallic two particle bound states in quasiperiodic chains* , EPL **98**, 66002 (2012).

[124] Y. Lahini, R. Pugatch, F. Pozzi, M. Sorel, R. Morandotti, N. Davidson, and Y. Silberberg, *Observation of a localization transition in quasiperiodic photonic lattices*, Phys. Rev. Lett.**103**, 013901 (2009).

[125] G. Roati, M. Zaccanti, C. D Errico, J. Catani, M. Modugno, A. Simoni, M. Inguscio, and G. Modugno, *K39 Bose-Einstein condensate with tunable interactions*, Phys. Rev. Lett. **99**, 010403 (2007).

[126] M. Fattori, C. D Errico, G. Roati, M. Zaccanti, M. Jona-Lasinio, M. Modugno, M. Inguscio and G. Modugno, *Atom interferometry with a weakly interacting Bose-Einstein condensate*, Phys. Rev. Lett. **100**, 080405 (2008).

[127] M. Larcher, F. Dalfovo and M. Modugno, *Effects of interaction on the diffusion of atomic matter waves in one-dimensional quasiperiodic potentials*, Phys. Rev. A **80**, 053606 (2009).

[128] H. Hiramoto, S. Abe, *Dynamics of an electron in quasiperiodic systems. Harper model*, J. Phys. Soc. Jpn **57**, 1365 (1988).

[129] B. Mandelbrot, *How Long is the Coast of Britain? Statistical Self-Similarity and Fractional Dimension*, Science. **156** (3775): 636–638 (1967).

[130] R. Ketzmerick, G. Petschel and T. Geisel, *Slow decay of temporal correlations in quantum systems with Cantor spectra*, Phys. Rev. Lett. **69**, 695 (1992).

[131] K. Rayanov, G. Radon, S. Flach, *Decohering localized waves*, Phys. Rev. E **88**, 012901 (2013).

[132] N. Levenberg, G. Martin, A. Shields and S. Zdravkovska, *Factorizations of Lebesgue measure via convolutions*, Proc. Am. Math. Soc. **104**, 419 (1988).

[133] L. Bos and B. Pavlov, *Absolute continuity of convolutions of singular measures and new branches of spectrum of Liouvillians and few body Hamiltonians*, Chapman & Hall/CRC **399**, Boca Raton, FL, 308 (1999).

[134] M. Goda, S. Nishino, and H. Matsuda, *Inverse Anderson transition caused by flat-bands*, Phys. Rev. Lett. **96**, 126401 (2006).

[135] S. D. Huber and E. Altman, *Bose condensation in flat-bands*, Phys. Rev. B **82**, 184502 (2010);

[136] D. Green, L. Santos, and C. Chamon, *Isolated flat-bands and spin 1 conical bands in two-dimensional lattices*, Phys. Rev. B **82**, 075104 (2010).

[137] M. Hyrkäs, V. Apaja and M. Manninen, *Many-particle dynamics of bosons and fermions in quasi-one-dimensional flat-band lattices*, Phys. Rev. A **87**, 023614 (2013).

[138] E. J. Bergholtz and Z. Lu, Topological flat-band models and fractional Chern insulators, Int. J. Mod. Phys. B **27**, 1330017 (2013).

[139] A. Parameswaran, R. Roy, and S. L. Sondhi, Fractional quantum Hall physics in topological flat-bands, Comptes Rendus Physique, **14**, 816 (2013).

[140] O. Derzhko and J. Richter, *Universal low-temperature behavior of frustrated quantum antiferromagnets in the vicinity of the saturation field*, Eur. Phys. J. B **52**, 23 (2006);

[141] O. Derzhko, J. Richter, A. Honecker, M. Maksymenko and R. Moessner, *Low-temperature properties of the Hubbard model on highly frustrated one-dimensional lattices*, Phys. Rev. B **81**, 014421 (2010).

[142] D. Leykam, S. Flach, O. Bahat-Treidel and A.S. Desyatnikov, *Flat-band states: disorder and nonlinearity*, Phys. Rev. B **88**, 224203 (2013).

[143] J. Vidal, B. Douçot, R. Mosseri and P. Butaud, *Interaction induced delocalization for two particles in a periodic potential*, Phys. Rev. Lett. **85**, 3906 (2000).

[144] J. Vidal, B. Douçot, R. Mosseri and P. Butaud, *Disorder and interactions in Aharonov-Bohm cages*, Phys. Rev. B, **64**, 155306 (2001).

[145] G. Cuniberti, L. Craco, D. Porath and C. Dekker, *Backbone-induced semiconducting behavior in short DNA wires*, Phys. Rev. B, **65**, 241314(R) (2002).

[146] C.T. Shih, S. Roche and R.A. Römer, Phys. Rev. Lett., **100**, 018105 (2008).

[147] S. Sil, S.K. Maiti and A. Chakrabarti, *Point-mutation effects on charge-transport properties of the tumor-suppressor gene p53*, Phys. Rev. Lett. **101**, 076803 (2008).

[148] C.T. Shih, S.A. Wells, C.L. Hsu, Y.Y. Cheng and R. Römer, *The interplay of mutations and electronic properties in disease-related genes*, Sci. Rep., **2** 272 (2012).

[149] F. Bloch, J. Dalibard and W. Zwerger, *Many-body physics with ultracold gases*, Rev. Mod. Phys. **80**, 885 (2005).

[150] D.N. Christodoulides, F. Lederer and D. Silberberg, *Discretizing light behaviour in linear and nonlinear waveguide lattices*, Nature **424**, 817 (2003).

[151] N. Masumoto, N. Kim, T. Burnes, K. Kusudo, A. Loeffler, S. Hoefling, A. Forchel and Y. Yamamoto, *Exciton-polariton condensates with flat-bands in a two-dimensional kagome lattice*, New. J. Phys. **14**, 065002 (2012).

[152] G.B. Jo, J. Guzman, C.K. Thomas, P. Hosur, A. Vishwanath and D.M. Stamper-Kurn, *Ultracold atoms in a tunable optical Kagome lattice*, Phys. Rev. Lett. **108**, 045305 (2012).

[153] M. Aidelsburger, M. Lohse, C. Schweizer, M. Atala, J.T. Barreiro, S. Nascimbene, N.R. Cooper, I. Bloch and N. Goldman, *Measuring the Chern number of Hofstadter bands with ultracold bosonic atoms*, Nature **465**, 162 (2015).

[154] K. Kim, M.S. Chang, S. Korenblit, R. Islam, E.E. Edwards, J.K. Freericks, G.D. Lin, L.M. Duan and C. Monroe, *Quantum simulation of frustrated Ising spins with trapped ions*, Nature **465**, 590 (2010).

[155] M Sigrist and T.M. Rice, *Unusual paramagnetic phenomena in granular high-temperature superconductors - A consequence of d-wave pairing?*, Rev. Mod. Phys. **67**, 503 (1995).

[156] B. Doucot and J. Vidal, Pairing of cooper pairs in a fully frustrated Josephson-junction chain, Phys. Rev. Lett. **88**, 227005 (2002).

[157] M.V. Feigel'man, L.B. Ioffe, V.B. Geshkenbein, P. Dayal and G. Blatter, *Superconducting tetrahedral quantum bits*, Phys. Rev. Lett. **92**, 098301 (2004).

[158] Y. Nakata, T. Okada, T. Nakanishi an M. Kitano, *Observation of flat-band for terahertz spoof plasmons in a metallic kagome lattice*, Phys. Rev. B **85**, 205128 (2012).

[159] M. Nixon, E. Ronen, A.A. Friesem and N. Davidson, *Observing geometric frustration with thousands of coupled lasers*, Phys. Rev. Lett. **110**, 184102 (2013).

[160] D. Guzmán-Silva, C. Meijá-Cortés, M. A. Bandres, M. C. Rechtsman, S. Weimann, S. Nolte, M. Segev, A. Szameit, and R. A. Vicencio, *Experimental observation of bulk and edge transport in photonic Lieb lattices*, New. J. Phys. **16**, 063061 (2014).

[161] R.A. Vicencio, C. Cantillano, L. Morales-Inostroza, B. Real, C. Mejita-Cortes, S. Weimann, A. Sazameit and M.I. Molina, *Observation of localized states in Lieb photonic lattices*, Phys. Rev. Lett. **114**, 245503 (2015).

[162] S. Flach, D. Leykam, J.D. Bodyfelt, P. Matthies, and A.S. Desyatnikov, *Detangling flat-bands into Fano lattices*, Europhys. Lett. **105**, 30001 (2014); ibid, **106**, 19901 (2014).

[163] J.E. Avron, R. Seiler and B. Simon, *Homotopy and quantization in condensed matter physics*, Phys. Rev. Lett. **51**, 51 (1983).

[164] M. Kohmoto, *Topological invariant and the quantization of the Hall conductance*, Ann. Phys. (Berlin) **160**, 343 (1985).

[165] M.Z. Hasan and C. Lane, *Colloquium: topological insulators*, Rev. Mod. Phys. **82**, 3045 (2010).

[166] D. Xiao, M.C. Chan and Q. Niu, *Berry phase effects on electronic properties*, Rev. Mod. Phys., **82**, 1959 (2010).

[167] Y. Ando, *Topological insulator materials*, J. Phys. Soc. Japan **82**, 102001 (2013).

[168] F.D.M. Haldane, *Model for a quantum Hall effect without Landau levels: condensed-matter realization of the parity anomaly*, Phys. Rev. Lett., **61**, 2015 (1988).

[169] L. Chen, T. Mazaheri, A. Seideland X. Tang, *The impossibility of exactly flat non-trivial Chern bands in strictly local periodic tight binding models*, Journal of Phys. A, **47**, 152001 (2014).

[170] E. Kapit and E. Müller, *Exact parent hamiltonian for the quantum Hall states in a lattice*, Phys. Rev. Lett., **105**, 215303 (2010).

[171] H. Atakisi and M.Ö. Oktel, *Landau levels in lattices with long-range hopping*, Phys. Rev. A, **88**, 033612 (2013).

[172] T. Scaffidi and S.H. Simon, *Exact solutions of fractional Chern insulators: Interacting particles in the Hofstadter model at finite size*, Phys. Rev. B, **90**, 115132 (2014).

[173] R.E. Peierls, *Zur Theorie des Diamagnetismus von Leitungselektronen*, Z. Phys. **80** , 763 (1933).

[174] A.E. Miroshnichenko, S.Flach, and Y.S. Kivshar *Fano resonances in nanoscale structures*, Rev. Mod. Phys. **82**, 2257 (2010).

[175] A. Honecker, F. Mila, and M. Troyer, *Magnetization plateaux and jumps in a class of frustrated ladders: A simple route to a complex behaviour*, Euro. Phys. J. B **15**, 227 (2000);

[176] T. Hakobyan, J.H. Hetherington, and M. Roger, *Phase diagram of the frustrated two-leg ladder model*, Phys. Rev. B **63**, 144433 (2001);

[177] F. Casola, T. Shiroka, A. Feiguin, S. Wang, M. S. Grbic, M. Horvatic, S. Krämer, S. Mukhopadhyay, K. Conder, C. Berthier, H.-R. Ott, H. M. Ronnow, Ch. Rüegg, and J. Mesot, *Field-Induced Quantum Soliton Lattice in a Frustrated Two-Leg Spin-1/2 Ladder*, Phys. Rev. Lett. **110**, 187201 (2013);

[178] T. Sugimoto, M. Mori, T. Tohyama, and S. Maekawa, *Spin-spin correlation enhanced by impurities in a frustrated two-leg spin ladder*, JPS Conf. Proc. **3**, 014016 (2014).

[179] We have varied this cutoff value up to $\xi \leq N$, and it does not change the spectra drastically.

[180] J.D. Bodyfelt, D. Leykam, C. Danieli, X. Yu and S. Flach, *Flat-bands under correlated perturbations* Phys. Rev. Lett. **113**, 236403 (2014).

[181] S. Ganeshan, J.H. Pixley and S. Das Sarma, *Nearest Neighbor Tight Binding Models with an Exact Mobility Edge in One Dimension*, Phys. Rev. Lett. **114**, 146601 (2015).

[182] With a similar argument discussed in Sec.4.4.1, in this antisymmetry all the eigenstates are expelled from the flat-band energy $E = t$.

[183] L.A. Ponomarenko, A. K. Geim, A. A. Zhukov, R. Jalil, S. V. Morozov, K.S. Novoselov, I. V. Grigorieva, E. H. Hill, V.V. Cheianov, V. I. Falko, K. Watanabe,T. Taniguchi and R.V. Gorbachev, *Tunable metal-insulator transition in double-layer graphene heterostructures*, Nat. Phys. **7**, 958 (2011).

[184] B. Radisavljevic and A. Kis, *Mobility engineering and a metaliinsulator transition in monolayer MoS2*, Nat. Mat. **12**, 815 (2013).

[185] J. Givernaud, C. Champeaux, A. Catherinot, A. Pothier, P. Blondy, and A. Crunteanu, *Tunable band stop filters based on metal-insulator transition in vanadium dioxide thin films* , IEEE MTT-S Intl., 1103 (2008);

[186] F. Fan, Y. Hou, Z. Jiang, X. Wang, and S. Chang, *Terahertz modulator based on insulator-metal transition in photonic crystal waveguide* , Appl. Opt. **51**, 4589 (2012).

[187] S. Denisov, S. Flach and P. Hänggi, *Tunable transport with broken space-time symmetries*, Phys. Rep. **538**, 77 (2014).

[188] J. Dalibard, F. Gerbier, G. Juleniunas and P. Öhberg, *Colloquium: Artificial gauge potentials for neutral atoms*, Rev. Mod. Phys. **83**, 1523 (2011).

[189] N. Goldman, G. Juleniunas, P. Öhberg and I.B. Spielman, *Light induced gauge fields for ultracold atoms*, Rep. Progr. Phys. **77**, 126401 (2014).

[190] H. Zhai, *Spin-orbit coupled quantum gases*, Int. J. Mod. Phys. B **26**, 1230001 (2012).

[191] N. Goldman and J. Dalibard, *Periodically driven quantum systems: effective hamiltonians and engineered gauge fields*, Phys. Rev. X **4**, 031027 (2014).

[192] A. Hemmerich, *Effective time-independent description of optical lattices with periodic driving*, Phys. Rev. A **81**, 063626 (2010).

[193] A. Eckardt, P Hauke, P. Soltan-Panahi, C. Becker, K. Sengstock and M. Lewenstein, *Frustrated quantum antiferromagnetism with ultracold bosons in a triangular lattice*, Europhys. Lett. **89**, 10010 (2010).

[194] C.E. Creffeld and F. Sols, *Directed transport in driven optical lattices by gauge generation*, Phys. Rev. A **84**, 023630 (2011)

[195] J. Struck, C. Ölschläger, R. Le Targat, P. Soltan-Panahi, A. Eckart, M. Lewenstein, P. Windpassinger and K. Sengstock, *Quantum simulation of frustrated classical magnetism in triangular optical lattices*, Science **333**, 996 (2011).

[196] J. Struck, M. Weinberg, C. Ö lschlä ger, P. Windpassinger, J. Simonet, K. Sengstock, P. Hö ppner, P. Hauke, A. Eckart, M. Lewenstein and L. Mathey, *Engineering Ising-XY spin-models in a triangular lattice using tunable artificial gauge fields*, Nat. Phys. **9**, 738 (2013).

[197] L. Jiang, T. Kitagawa, J. Alicea, A. R. Akhmerov, D. Pekker, G. Refael, J. Ignacio Cirac, E. Demler, M. D. Lukin, and P. Zoller, *Majorana fermions in equilibrium and in driven cold-atom quantum wires*, Phys. Rev. Lett. **106**, 220402 (2011).

[198] G. Liu, N. Hao, S.-L. Zhu, and W. M. Liu, *Topological superfluid transition induced by a periodically driven optical lattice*, Phys. Rev. A **86**, 013639 (2012).

[199] Q.-J. Tong, J.-H. An, J. Gong, H.-G. Luo, and C. H. Oh, *Generating many Majorana modes via periodic driving: A superconductor model*, Phys. Rev. B **87**, 201109 (2013).

[200] M. Thakurathi, A. A. Patel, D. Sen, and A. Dutta, *Floquet generation of Majorana end modes and topological invariants*, Phys. Rev. B **88**, 155133 (2013).

[201] K. Drese and M. Holthaus, *Exploring a metal-insulator transition with ultracold atoms in standing light waves?*, Phys. Rev. Lett. **78**, 2932 (1997).

[202] H. Yamada, K. S.Ikeda, *Dynamical delocalization in one-dimensional disordered systems with oscillatory perturbation*, Phys. Rev E **59**, 5214 (1999).

[203] H. Yamada, K. S. Ikeda, and M. Goda, *Quantum diffusion in a coherently time-varying one-dimensional disordered system*, Phys. Lett. A **182**, 77 (1993).

[204] H. Yamada, and K. S. Ikeda, *Anomalous diffusion and scaling behavior of dynamically perturbed one-dimensional disordered quantum systems*, Phys. Lett. A **248**, 179 (1998).

[205] L. Hufnagel, M. Weiss, A. Iomin, R. Ketzmerick, S. Fishman, T. Geisel, *Metal-insulator transitions in the cyclotron resonance of periodic semiconductor nanostructures due to avoided band crossings*, Phys. Rev.B **62** 15348 (2000).

[206] R. Lima, D. Shepelyansky, *Fast delocalization in a model of quantum kicked rotator*, Phys. Rev. Lett. **67**, 1377 (1991).

[207] A R. Kolovsky, G. Mantica, *The driven Harper model*, Phys. Rev. B **86**, 054306 (2012).

[208] G Ritt, C Geckeler, T Salger, G Cennini, M Weitz, *Fourier synthesis of optical potentials for atomic quantum gases*, Phys. Rev. A, **74**, 063622 (2006).

[209] M. Modugno, *Exponential localization in one-dimensional quasi-periodic optical lattices*, New J. Phys **11**, 033023 (2009).

[210] E.U. Dinaburg, Ya.G. Sinai, *The one-dimensional Schrödinger equation with a quasiperiodic potential*, Functional Analysis and its Applications **9**, 279 (1975) .

[211] G. Roux, T. Barthel, I. P. McCulloch, C. Kollath, U. Schollwöck, T. Giamarchi, *Quasiperiodic Bose-Hubbard model and localization in one-dimensional cold atomic gases*, Phys. Rev. A **78**, 023628 (2008).

[212] J. Chabe, G. Lemarie, B. Gremaud, D. Delande, P. Szriftgiser and J.-C. Garreau, *Experimental observation of the Anderson metal-insulator transition with atomic matter waves*, Phys. Rev. Lett. **101**, 255702 (2008).

[213] J. Bellissard, B.Simon, *Cantor spectrum for the almost Mathieu equation*, Journal of Functional Analysis **48**, 408-419 (1982).

[214] S. Denisov, L. Morales-Molina and S. Flach, *Quantum resonances and rectification of driven cold atoms in optical lattices*, EPL **79**, 10007 (2007); S. Denisov, L. Morales-Molina, S. Flach and P. Hänggi, *Periodically driven quantum ratchets: symmetries and resonances*, Phys. Rev. A **75**, 063424, (2007).

[215] F. Wegner, *Inverse participation ratio in 2+ϵ dimensions*, Z. Phys. B **36**, 209 (1980).

[216] J. Laskar, and P. Robutel, *High order symplectic integrators for perturbed Hamiltonian systems*, Celest. Mech. Dyn. Astron. **80**, 39 (2001).

[217] H. Yoshida, *Construction of higher order symplectic integrators*, Phys. Lett. A **150**, 262 (1990); H. Yoshida, *Recent progress in the theory and application of symplectic integrators*, Cel. Mech. Dyn. Astr. **56**, 27 (1993);

[218] E. Gerlach, S. Eggl, Ch. Skokos, J.D. Bodyfelt and G. Papamikos, Proc. of 10th HSTAM Intnl. Congress on Mechanics, arXiv:1306.0627 (2013);

[219] Ch. Skokos, E. Gerlach, J.D. Bodyfelt, G. Papamikos and S. Eggl, *High order three part split symplectic integrators: efficient techniques for the long time simulation of the disordered discrete nonlinear Schrödinger equation* , Phys. Lett. A **378**, 1809 (2014).

[220] E. Gerlach, J. Meichsner and Ch. Skokos, *On the symplectic integration of the discrete nonlinear Schrödinger equation with disorder*, arXiv:1512.07778 (2015).

[221] D.F. Martinez, and R.A. Molina, *Delocalization induced by low-frequency driving in disordered tight-binding lattices*, Phys. Rev. B **73**, 073104 (2006).

[222] V.A. Gopar and R.A. Molina, *Controlling conductance statistics of quantum wires by driving ac fields*, Phys. Rev. B **81**, 195415 (2010).

[223] T. Kitagawa,T. Oka, and E. Demler, *Photo control of transport properties in a disordered wire: average conductance, conductance statistics, and time-reversal symmetry*, Ann. Phys. **327**, 1868 (2012).

[224] T. Nakanishi, T. Ohtsuki, and T. Kawarabayashi, *Dephasing by time-dependent random potentials*, J. Phys. Soc. Jpn. **66**, 949 (1997).

[225] G. Floquet, *Sur les equations differentielles lineaires a coefficients periodiques*, Annales scientifiques De l'ENS, **12**, second edition, 47 (1883).

[226] J. H. Shirley, *Solution of the Schrödinger equation with a hamiltonian periodic in time*, Phys. Rev. **138**, B979 (1965).

[227] H. Fukuyama, R. A. Bari, and H. C. Fogedby, *Tightly bound electrons in a uniform electric field*, Phys. Rev. B **8**, 5579 (1973).

[228] G.N. Watson, *A treatise on the theory of Bessel function*, Cambridge University press (1922).

[229] M. Abramowitz and I. A. Stegun, *Handbook of Mathematical Functions*, Dover Publications Inc., New York (1972).

[230] D. O. Krimer, R. Khomeriki and S. Flach, *Delocalization and spreading in a nonlinear Stark ladder*, Phys. Rev. E **80**, 036201 (2009).

[231] O. N. Dorokhov, *Multichanel localization and magnetic impurities*, Solid State Commun. **46**, 605 (1983).

[232] P. A. Mello, P. Pereyra and N. Kummar, *Macroscopic approach to multichannel disordered conductors*, Ann. Phys. **181**, 290 (1988).

[233] S. Kim, S. Ostlund and G. Yu, *Fourier analysis of multi-frequency dynamical systems* Physica D **31** 117-126 (1988).

[234] A. Soffer and W.M. Wang, *Anderson localization for time periodic random Schrödinger operators*, Commun. Part. Diff. Eq. **28**, 333 (2003).

[235] J. Bourgain,and W.M. Wang, *Anderson localization for time quasiperiodic random Schrödinger and wave equations*, Commun. Math. Phys. **248**, 429 (2004).

[236] R. Abou-Chacra, P.W. Anderson and D.J. Thouless, *A selfconsistent theory of localization*, J. of Phys. C **6**, 1734 (1973);

[237] B.L. Altshuler and A.G. Aronov, *Electron-electron interactions in disordered systems*, Efros and Pollak editors, Amsterdam: North Holland, Amsterdam (1985);

[238] K.B. Efetov, *Density-density correlator in a model of a disordered metal on a Bethe lattice*, JETP **65**, 360; ibid. **66**, 634 (1987);

[239] T. Giamarchi and H.J. Schulz, *Anderson localization and interactions in one-dimensional metals*, Phys. Rev. B **37**, 325 (1988).

[240] I.L. Aleiner, B.L. Altshuler and G.V. Shlyapnikov, *A finite-temperature phase transition for disordered weakly interacting bosons in one dimension*, Nat. Phys.**6**, 900 (2010).

[241] Y. Imry, *Coherent propagation of two interacting particles in a random potential*, Europhys. Lett. **30**, 405 (1995).

[242] K. Frahm, A. Müller-Groeling, J.-L. Pichard, and D. Weinmann, *Scaling in interaction-assisted coherent transport*, Europhys. Lett. **31**, 169 (1995).

[243] F. von Oppen, T. Wettig and J. Müller, *Interaction-induced delocalization of two particles in a random potential: scaling properties*, Phys. Rev. Lett. **76**, 491 (1996).

[244] R A. Römer and M. Schreiber, *No enhancement of the localization length for two interacting particles in a random potential*, Phys. Rev. Lett. **78**, 515 (1997).

[245] R A. Römer, M. Schreiber and T. Vojta, *Two interacting particles in a random potential: numerical calculations of the interaction matrix elements*, Phys. Status Solidi **211**, 681 (1999).

[246] K. M. Frahm, *Interaction induced delocalization of two particles: large system size calculations and dependence on interaction strength*, Eur. Phys. J. B **10**, 371 (1999).

[247] S. De Toro Arias, X. Waintal and J.-L. Pichard, *Two interacting particles in a disordered chain III: Dynamical aspects of the interplay disorder-interaction*, Eur. Phys. J. B **10**, 149 (1999).

[248] M.V. Ivanchenko, T. V. Laptyeva and S. Flach, *Quantum chaotic sub diffusion in random potentials*, Phys. Rev. B. **89**, 060301(R) (2014).

[249] M. Raczkowski and F.F. Assaad, *Dimensional-crossover driven Mott transition in the frustrated Hubbard model*, Phys. Rev. Lett. **109**, 126404 (2012).

[250] J. Imriška, M. Iazzi, L. Wang, E. Gull, D. Greif, T. Uehlinger, G. Jotzu, L. Tarruell, T. Esslinger and M. Troyer, *Thermodynamics and magnetic properties of the anisotropic 3D Hubbard model*, Phys. Rev. Lett. **112**, 115301 (2014); Erratum: Phys. Rev. Lett. **112**, 159903 (2014).

[251] J. Schönmeier-Kromer and L. Pollet, *Ground-state phase diagram of the two-dimensional Bose-Hubbard model with anisotropic hopping*, Phys. Rev. A **89**, 023605 (2014).

[252] H.M. Cataldo and D.M. Jezek, *Bose-Hubbard model in a ring-shaped optical lattice with high filling factors*, Phys. Rev. A **84**, 013602 (2011).

[253] X.H. Zhang, S.P. Kou, *Mott insulator in a generalized Bose-Hubbard model with topologically nontrivial flat-band*, Int. J. Mod. Phys. B 27, 1250214 (2013)

[254] D. L. Shepelyansky, *Coherent propagation of two interacting particles in a random potential*, Phys. Rev. Lett. **73**, 2607 (1994).

[255] J.B. Sokoloff, *Unusual band structure, wave functions and electrical conductance in crystals with incommensurate periodic potentials*, Phys. Rep. **126**, 189 (1985).

[256] A. Barelli, J. Bellissard, P. Jacquod, and D.L.Shepelyansky, *Double butterfly spectrum for two interacting particles in the Harper model*, Phys. Rev. Lett. **77**, 4752 (1996).

[257] D.L. Shepelyansky, *Two interacting particles in the Harper model*, Phys. Rev. B **54**, 14896 (1996).

[258] S.N. Evangelou and D.E. Katsanos, *Two interacting electrons in a quasiperiodic chain*, Phys. Rev. B **56**, 12797 (1997).

[259] A. Eilmes, U. Grimm, R.A. Römer and M. Schreiber, *Two interacting particles at a metal-insulator transition*, Eur. Phys. J. B **8**, 547 (1999).

[260] G. Dufour and G. Orso, *Anderson localization of pairs in bichromatic optical lattices*, Phys. Rev. Lett. **109**, 155306 (2012).

[261] K.M. Frahm and D.L. Shepeliansky, *Delocalization of two interacting particles in the 2D Harper model*, Eur. Phys. J. B **89**, 8 (2016).

[262] V.P. Michal, B.L. Altshuler and G.V. Shlyapnikov, *Delocalization of weakly interacting bosons in a 1D quasiperiodic potential*, Phys. Rev. Lett. **113**, 045304 (2014).

[263] F. Grossmann, T. Dittrich, P. Jung and P. Hänggi, *Coherent destruction of tunneling*, Phys. Rev. Lett. bf 67, 516 (1991).

[264] F. Grossmann and P. H"änggi, *Localization in a driven two-level dynamics*, Europhys. Lett. **81**, 571 (1992).

[265] M. Grifoni and P.Hänggi, *Driven quantum tunneling*, Phys. Rep. **304**, 229 (1998).

[266] J. Gong, L. Morales-Molina and P. Hänggi, *Many-body coherent destruction of tunneling*, Phys. Rev. Lett. **103**, 133002 (2009).

[267] G. Della Valle, M. Ornigotti, E. Cianci, V. Foglietti, P. Laporta and S. Longhi, *Visualization of coherent destruction of tunneling in an optical double well system*, Phys. Rev. Lett. **98**, 263601 (2007).

[268] H. Lignier, C. Sias, D. Ciampini, Y. Singh, A. Zenesini, O. Morsch and E. Arimondo, *Dynamical control of matter-wave tunneling in periodic potentials*, Phys. Rev. Lett. **99**, 220403 (2007).

[269] E. Kierig, U. Schnorrberger, A. Schietinger, J. Tomkovic and M. K. Oberthaler, *Single-particle tunneling in strongly driven double-well potentials*, Phys. Rev. Lett. **100**, 190405 (2008).

[270] S. Longhi, *Many-body coherent destruction of tunneling in photonic lattices*, Phys. Rev. A **83**, 034102 (2011).

[271] R. Vicencio and A. Szameit, *Observation of linear properties in a Sawtooth photonic lattice*, Advanced Photonic, OSA Technical Digest (online), JTu3A.59 (2014).

[272] S. Mukherjee, A. Spracklen, D. Choudhury, N. Goldman, P. Öhberg, E. Andersson, and R.R. Thomson, *Observation of a localized flat-band state in a photonic Lieb lattice*, Phys. Rev. Lett. **114**, 245504 (2015).

[273] G. Jotzu, M. Messer, R. Desbuquois, M. Lebrat, T. Uehlinger, D. Greif and T. Esslinger, *Experimental realisation of the topological Haldane model*, Nature **515**, 237 (2014).

[274] Y.-L. Xu, W.S. Fegadolli, L. Gan, M.-H. Lu, X.-P. Liu, Z.-Y. Li, A. Scherer and Y.-F. Chen, *Experimental realization of Bloch oscillations in a parity-time synthetic silicon photonic lattice*, Nature Communications **7**, 11319 (2016).

[275] C.H. Ahn, K. Senthil, H.K. Cho and S.Y. Lee, *Artificial semiconductor/insulator superlattice channel structure for high-performance oxide thin-film transistors*, Scientific Reports **3**, 2737 (2013).

APPENDIX D

Statements of Contribution to Doctoral Thesis Containing Publications

MASSEY UNIVERSITY
GRADUATE RESEARCH SCHOOL

STATEMENT OF CONTRIBUTION TO DOCTORAL THESIS CONTAINING PUBLICATIONS

(To appear at the end of each thesis chapter/section/appendix submitted as an article/paper or collected as an appendix at the end of the thesis)

We, the candidate and the candidate's Principal Supervisor, certify that all co-authors have consented to their work being included in the thesis and they have accepted the candidate's contribution as indicated below in the *Statement of Originality*.

Name of Candidate: Carlo Danieli

Name/Title of Principal Supervisor: Prof. Sergej Flach

Name of Published Research Output and full reference:

H. Hatami, C. Danieli, J. D. Bodyfelt and S. Flach, Quasiperiodic driving of Anderson localized waves in one dimension, Physical Review E 93, 062205 (2016).

In which Chapter is the Published Work: Chapter 5

Please indicate either:

- The percentage of the Published Work that was contributed by the candidate: 40%
  and / or
- Describe the contribution that the candidate has made to the Published Work:

Candidate's Signature

23/06/2016

Date

Principal Supervisor's signature

23/06/2016

Date

MASSEY UNIVERSITY
GRADUATE RESEARCH SCHOOL

STATEMENT OF CONTRIBUTION TO DOCTORAL THESIS CONTAINING PUBLICATIONS

(To appear at the end of each thesis chapter/section/appendix submitted as an article/paper or collected as an appendix at the end of the thesis)

We, the candidate and the candidate's Principal Supervisor, certify that all co-authors have consented to their work being included in the thesis and they have accepted the candidate's contribution as indicated below in the *Statement of Originality*.

Name of Candidate: Carlo Danieli

Name/Title of Principal Supervisor: Prof. Sergej Flach

Name of Published Research Output and full reference:

C. Danieli, J. D. Bodyfelt and S. Flach, Flatband Engineering of Mobility Edges, Phys. Rev. B 91, 235134 (2015).

In which Chapter is the Published Work: Chapter 4

Please indicate either:

- The percentage of the Published Work that was contributed by the candidate: 80%
  and / or
- Describe the contribution that the candidate has made to the Published Work:

Candidate's Signature

23/06/2016

Date

Principal Supervisor's signature

23/06/2016

Date

MASSEY UNIVERSITY
GRADUATE RESEARCH SCHOOL

STATEMENT OF CONTRIBUTION TO DOCTORAL THESIS CONTAINING PUBLICATIONS

(To appear at the end of each thesis chapter/section/appendix submitted as an article/paper or collected as an appendix at the end of the thesis)

We, the candidate and the candidate's Principal Supervisor, certify that all co-authors have consented to their work being included in the thesis and they have accepted the candidate's contribution as indicated below in the *Statement of Originality*.

Name of Candidate: Carlo Danieli

Name/Title of Principal Supervisor: Prof. Sergej Flach

Name of Published Research Output and full reference:

C. Danieli, K. Rayanov, B. Pavlov, G. Martin and S.Flach, Approximating Metal-Insulator Transitions, Int. Journal of Mod. Phys. B 29, 1550036 (2015).

In which Chapter is the Published Work: Chapter 3

Please indicate either:

- The percentage of the Published Work that was contributed by the candidate: 70%
  and / or
- Describe the contribution that the candidate has made to the Published Work:

Candidate's Signature

23/06/2016

Date

Principal Supervisor's signature

23/06/2016

Date

MASSEY UNIVERSITY
GRADUATE RESEARCH SCHOOL

STATEMENT OF CONTRIBUTION TO DOCTORAL THESIS CONTAINING PUBLICATIONS

(To appear at the end of each thesis chapter/section/appendix submitted as an article/paper or collected as an appendix at the end of the thesis)

We, the candidate and the candidate's Principal Supervisor, certify that all co-authors have consented to their work being included in the thesis and they have accepted the candidate's contribution as indicated below in the *Statement of Originality*.

Name of Candidate: Carlo Danieli

Name/Title of Principal Supervisor: Prof. Sergej Flach

Name of Published Research Output and full reference:

J. D. Bodyfelt, D. Leykam, C. Danieli, X. Yu and S.Flach, Flat bands under correlated perturbations, Phys. Rev. Lett. 113, 236403 (2014).

In which Chapter is the Published Work: Chapter 4

Please indicate either:

- The percentage of the Published Work that was contributed by the candidate: 30

  and / or
- Describe the contribution that the candidate has made to the Published Work:

Candidate's Signature

23/06/2016

Date

Principal Supervisor's signature

23/06/2016

Date

MASSEY UNIVERSITY
GRADUATE RESEARCH SCHOOL

STATEMENT OF CONTRIBUTION TO DOCTORAL THESIS CONTAINING PUBLICATIONS

(To appear at the end of each thesis chapter/section/appendix submitted as an article/paper or collected as an appendix at the end of the thesis)

We, the candidate and the candidate's Principal Supervisor, certify that all co-authors have consented to their work being included in the thesis and they have accepted the candidate's contribution as indicated below in the *Statement of Originality*.

Name of Candidate: Carlo Danieli

Name/Title of Principal Supervisor: Prof. Sergej Flach

Name of Published Research Output and full reference:

L.Morales-Molina, E.Doerner, C.Danieli and S.Flach, Resonant metallic states in driven quasiperiodic lattices: Aubry-Andre localization by design, Phys. Rev. A 90, 043630 (2014).

In which Chapter is the Published Work: Chapter 5

Please indicate either:

- The percentage of the Published Work that was contributed by the candidate: 30%

  and / or

- Describe the contribution that the candidate has made to the Published Work:

  The candidate extended and finalized a project previously started from S. Flach and L.Morales-Molina

Candidate's Signature

23/06/2016

Date

Principal Supervisor's signature

23/06/2016

Date